Doctor of Philosophy

A Study on Ignition delay and Lift-off Length under GCI Condition for Gasoline-Biodiesel Blends

The Graduate School

of the University of Ulsan

Department of Mechanical Engineering

Vu Dinh Nam

A Study on Ignition delay and Lift-off Length under GCI Condition for Gasoline-Biodiesel Blends

Supervisor: Prof. Lim, Ock Taeck

A Dissertation

Submitted to
The Graduate School of the University of Ulsan
In partial Fulfillment of the Requirements
for the Degree of
Doctor of Philosophy

by

Vu Dinh Nam

Department of Mechanical Engineering
University of Ulsan, Republic of Korea

November 2019

A Study on Ignition delay and Lift-off Length under GCI Condition for Gasoline-Biodiesel Blends

This certifies that the dissertation
of Vu Dinh Nam is approved.

Committee Chair	**Prof. Park, Kyu Yeol**
Committee Member	**Prof. Shin, Jichul**
Committee Member	**Dr. Lee, Young Jae**
Committee Member	**Asst. Prof. Chang, Kyoung Sik**
Committee Member	**Prof. Lim, Ock Taeck**

Department of Mechanical Engineering
University of Ulsan
December 2019

ABSTRACT

A Study on Ignition delay and Lift-off Length under GCI Condition for Gasoline-Biodiesel Blends

Department of Mechanical Engineering
Vu Dinh Nam

In the last few decades, the gasoline compression ignition engines show better thermal efficiency than gasoline spark-ignited combustion and approaches diesel compression-ignited combustion, as well as lower emissions of hazardous air pollutants such as nitrous oxide and particulate matter. In GCI engines fueled with gasoline biodiesel blended fuels also shown the promise to reduce soot emission significantly while maintaining high engine efficiency. The GB blends is injected at initially to obtain the same combustion phasing as with diesel fuel. The mixing process of fuel and air is improved due to extra time, so combustion occurs with much greater mixing compared to diesel fuel. However, there are few studies concerning gasoline-biodiesel blended fuels, and the spray combustion characteristics and pollutant formation mechanisms have yet to be well understood. Especially, the ignition delay and lift-off length are governing factors that impact on the combustion phasing in the engine cycle, the degree of fuel vapor/air pre-mixing required to produce the first mixture, pollutant formation, and most notably NOx and PM. This dissertation allows to understand the effects of gasoline biodiesel ratio, injection conditions, and operating conditions on its ignition delay and combustion characteristics by the optical investigation. That is important to utilize gasoline biodiesel blended fuels with higher combustion efficiency and environmental benefits.

In this work, the constant volume combustion chamber and rapid compression expansion machine were successfully established with validated safety and consistency to simulate the high-pressure and high-temperature environment in diesel engines. Both provide optical accessibility and the ability to control the ambient temperature and ambient oxygen

concentration and allow for the study of spray combustion with optical diagnostic techniques. Also, a gasoline-biodiesel reaction mechanism was developed to predict the chemical ignition delay of the blended fuels. The reaction mechanism with 4285 species and 15246 reactions was validated and implemented using the CHEMKIN PRO software.

Firstly, the fuel samples were four GB blends including GB20, GB40, GB60 and GB80 corresponding to 20 %, 40 %, 60 %, and 80 % volumetric biodiesel respectively, neat gasoline, and neat biodiesel. Fuel samples were injected into the CVCC to combust using a single-hole research-grade injector. Natural soot luminous images from the combustible flame were captured by a CMOS camera to determine the ignition delay and the flame lift-off length. A self-written LabVIEW code was made to separate and smoothen the flame from background noise in the image processing. Based on experimental data, the moderate biodiesel addition (less than 20%) can improve the ability of cold-engine starting, also solve engine misfire under low-load condition due to its flammability while maintaining advantages of gasoline with great volatility and high ignition delay which significantly enhance the mixture formation process.

Secondly, the gasoline was blended with biodiesel at 5%, 10%, 15%, and 20% by volume, and then tested in a rapid compression expansion machine at a compression ratio of 11 and a temperature range of 700-850 K to observe the auto-ignition delay phenomenon under engine-like conditions. The experimental conditions are focused on improving the auto-ignition characteristic of gasoline direct-injection compression ignition combustion strategies under low load and cold start. These results revealed that a higher biodiesel fraction helps to obtain shorter ignition delay, which reduces the requirement of intake temperature. The blended fuel with 20% biodiesel showed the lowest ambient temperature at the injection timing requirement and was 80 K lower than gasoline. The combustion duration and pressure peak of every blended fuel were similar to each other after increasing the biodiesel fraction.

Thirdly, a comprehensive study was performed and focused on the ignition characteristics of the GB20 in a constant volume chamber under a wide range of experimental conditions simulating engine operating conditions: gas density (5 kg/m^3 and 15 kg/m^3), ambient temperature (800 K-1200 K), oxygen content (10 % - 21 %), various injection pressures (30 MPa - 130 MPa), and injection durations (400 μs – 3500 μs). As a result, the ignition delay and ignition distance heavily depend on the operating conditions. The increase of ambient temperature, ambient gas density, or oxygen concentration significantly decreases the ignition

delay and ignition distance. The injection parameters, including the injection pressure and injection duration, also influence the air-fuel mixing process, thus changing the local ambient temperature and local air-fuel ratio, resulting in increasing/decreasing the ignition delay and ignition distance. Besides, this experimental study provides experimental data for the mapping of ignition delay; it is vitally important to control the internal combustion engines for obtaining high performance with gasoline biodiesel blended fuels. The ignition delay data is also the primary metric for development, calibration, and validation of CFD models for the GCI engine with GB20. The ignition delay measurement from the RCEM is longer than CVCC for the GB20 fuel due to impingement in RCEM, existence of NOx due to pre-combustion in CVCC, and higher flow rate of fuel is cooling down injection location in the RCEM.

Finally, the measured auto-ignition delay was compared to a simulated result that is predicted by the CHEMKIN-PRO software to validate the accuracy of the ignition delay for the gasoline-biodiesel blended fuel to better understand the fuel ignition characteristics. These results revealed that a higher biodiesel fraction helps to obtain shorter chemical ignition delay, which reduces the auto-ignition delay, thus the requirement of the lower intake temperature.

Keywords: Gasoline-biodiesel, Ignition pressure, Ignition duration, RCEM, CVCC, Temperature, Oxygen concentration, Lift-off length, Ignition delay.

ACKNOWLEDGEMENT

First and foremost, I would like to thank my advisor, Professor Ocktaeck Lim, for his guidance and support. His fruitful comments during our research progress meeting helped me a lot to prepare my experimental laboratory and were always available to troubleshoot problems in the lab. I much appreciate working with him during this research. I greatly appreciate working with him during this research. I would also like to express my thanks to the Graduate School of Mechanical and Automotive Engineering, University of Ulsan.

My sincere thanks go to all members of Smart Powertrain Laboratory. I will always appreciate your valuable support during my experimental setup. Many special thanks go to members of the Department of Automotive Engineering for their excellent co-operation, inspirations, and supports during this study. Special thanks go to Hung Yen University of Technology and Education for providing me the opportunity, approval, and support to pursue my Ph.D. at the University of Ulsan.

I acknowledge my sincere indebtedness and gratitude to my parents for their love, dream, and sacrifice throughout my life. I am also grateful to my wife and daughter for their sacrifice, patience, and understanding that was inevitable to make this work possible. I cannot find the appropriate words that could adequately describe my appreciation for their devotion, support, and faith in my ability to attain my goals.

Table of contents

Table of contents v

List of tables ix

List of figures x

Abbreviation and nomenclatures xiii

1 Introduction 1

1.1 Motivation 1

1.2 Approach 4

1.3 Objective 7

1.4 Thesis outline 8

2 Literature review 11

2.1 GCI engine technology 11

2.1.1 GCI technology 11

2.1.2 Opportunities and challenges associated with GCI 13

2.2 Effect of various control strategies on GCI engine 14

2.2.1 Injection strategy 14

2.2.2 Fuel ignition quality 15

2.2.3 EGR strategy 16

2.3 Ignition delay and lift-off length 16

2.3.1 Ignition delay 17

2.3.2 Measurement of ignition delay 19

2.3.3 Factors affecting ignition delay 22

2.3.4 Lift-off length 24

2.3.5 ID and LOL effect on compression ignition combustion 26

2.4 Fuel 29

2.4.1 Current transport fuels 29

2.4.2 Alternatives to conventional fuels 30

2.4.3 Biodiesel fuel 32
2.5 Summary 33
3 Experiment setup and methodology 35
3.1 CVCC System 35
3.1.1 Constant Volume Combustion Chamber 35
3.1.2 Supply and Exhaust System 40
3.2 RCEM System 40
3.3 Data acquisition and control system 41
3.3.1 Control system 42
3.3.2 Data acquisition system 43
3.3.3 Control program 44
3.4 Fuel supply system 49
3.5 Pressure trace 50
3.6 Optical diagnostic system 51
3.7 Image processing 51
4 Effect of biodiesel addition on auto ignition delay and lift of length under low-temperature condition 54
4.1 Introduction 54
4.2 Experimental methods 57
4.3 Optical arrangement and ignition calculation 58
4.3.1 Optical arrangement 58
4.3.2 Definition of ignition delay 58
4.3.3 Evaluation of the flame lift-off length 60
4.4 Image processing 61
4.5 Fuel and test condition 62
4.6 Ignition Delay Results 64
4.7 Lift-off length results 69

4.8 Summary 71
5 Effect of small amount of biodiesel on auto ignition and combustion characteristics under engine-like conditions 73
5.1 Introduction 73
5.2 Experimental methods 75
5.3 Ignition delay calculation 76
5.4 Chemical kinetics calculations and validation 78
5.4.1 Chemical kinetics calculations 78
5.4.2 Validation 79
5.5 Pressure trace 81
5.6 Heat release rate 82
5.7 Ignition behavior 84
5.8 Simulation and comparison to the experimental investigation 86
5.8.1 Effects of the biodiesel fraction on the chemical delay of the blended fuel 86
5.8.2 Experimental and predicted chemical ignition delay for the blended fuel at the RCEM condition 87
5.9 Summary 90
6 Effects of the operation parameters on ignition characteristics of GB20 in a constant volume chamber 91
6.1 Optical arrangement 91
6.2 Effect of injection pressure and injection duration 92
6.2.1 Ignition delay 94
6.2.2 Lift-off length 95
6.3 Effect of the temperature and density 97
6.3.1 Ignition delay 97
6.3.2 Lift-off length 99
6.4 Effect of oxygen content 100

6.4.1 Ignition delay 100
6.4.2 Lift-off length 101
6.5 Summary 102
7 Conclusion 104
References 108
Appendices 119
A. List of Publications 119
B. List of conferences 120
C. Image processing code 121

List of tables

Table 4.1: Gasoline-biodiesel blended fuel compositions (vol%). 62
Table 4.2: Chemical composition and properties of gasoline. 62
Table 4.3: Chemical composition and properties of biodiesel. 63
Table 4.4: Experimental conditions of the GB fuels for ignition and lift-off length. 64
Table 5.1: Test conditions of the gasoline-biodiesel blended fuels for ignition. 77
Table 5. 2: Composition of the gasoline surrogate. 79
Table 5.3: Composition of the biodiesel surrogate. 79
Table 6.1: Camera specifications. 92

List of figures

Figure 2.1: Advantages of GCI engine technology 13
Figure 2.2: Challenges for GCI engine technology 14
Figure 2.3: Images of the spray combustion evolution sequence. 20
Figure 2.4: The maximum luminosity intensity inside the region of interest during the combustion progress. 21
Figure 2.5: Ignition delay of reference fuels of varying cetane number 23
Figure 2.6: Lift-off length definition from the broadband chemiluminescence imaging. 25
Figure 2.7: The period of time-resolved lift-off length measurements. 26
Figure 2.8: Effect flowchart of the potential parameters on spray combustion with engines fueled with gasoline-biodiesel blends 34
Figure 3.1: Assembled CVCC with different test equipment 36
Figure 3.2: Exploded view of the CVCC with quartz 37
Figure 3.3: Schematic of the CVCC apparatus implemented in the experiments 38
Figure 3.4: Pictorial layout of experimental test bench 38
Figure 3.5: Schematic diagram of supply and exhaust system 40
Figure 3.6: Picture of the RCEM. 41
Figure 3.7: Schematic of control and data acquisition system 42
Figure 3.8: Schematic diagram of control system 43
Figure 3.9: Schematic diagram of data acquisition system 43
Figure 3.10: Pictorial representation of control and data acquisition system 44
Figure 3.11: Control-flow diagram 44
Figure 3.12: Schematic diagram of sequence of filling gases 45
Figure 3.13: Pressure in the combustion chamber when knocking 46
Figure 3.14: The quarts is broken due to the knocking 46
Figure 3.15: Sequence of diagnosis 47
Figure 3.16: Pictorial representation of fuel injection system 49
Figure 3.17: Optical arrangement for the broadband chemiluminescence technique. 51
Figure 3.18: Sequence of image processing 53
Figure 4.1: Scheme of the constant-volume combustion chamber performed in this work. 57
Figure 4.2: The optical set up for the natural light emission visualization. 58
Figure 4.3: Definition of the ignition delay based on pressure trace. 59
Figure 4.4: Images of combustion development sequence. 60

Figure 4.5: Lift-off length measurement from the natural soot emission image. 61
Figure 4.6: Time sequence of flame images for biodiesel, GB40 blend, and gasoline under 750K temperature, 21% oxygen content, and 10 kg/m^3 density.....64
Figure 4.7: Pressure and HRR for GB blends, biodiesel, and gasoline at two ambient temperatures: (a) 750K and (b) 900K. 65
Figure 4.8: Ignition delay under different temperature of 750K, 800K and 900K temperature, 21% oxygen content, and 10 kg/m^3 density.....67
Figure 4.9: Development of flame for GB20 blend under different ambient temperature (750 K, 800 K, and 900 K), oxygen concentrations of 21% condition, and density of 10 kg/m^3....68
Figure 4.10: Lift-off length under different temperature of 750K, 800K and 900K temperature, 21% oxygen content, and 10 kg/m^3 density.....70
Figure 5.1: Schematic diagram of the RCEM.....75
Figure 5.2. Ambient temperature profile in the cylinder during the combustion and expansion stroke.....76
Figure 5.3: Definition of the auto-ignition delay. 78
Figure 5.4: Comparison of the ignition delay time between the gasoline-biodiesel model and LLNL's model or Vanhove's model at 650-1100 K, 20 bar, and stoichiometric ratio.....80
Figure 5.5: Temporal change in pressure with in-cylinder temperature. 81
Figure 5.6: Temporal change in pressure with biodiesel fraction.....82
Figure 5.7: Temporal change in heat release rate with in-cylinder temperature. 83
Figure 5.8: Temporal change in the heat release rate with biodiesel fraction. 84
Figure 5.9: First-stage ignition delay, auto-ignition delay at varying ambient temperature for GB5, GB10, GB15, and GB20.....85
Figure 5.10: Effect of the biodiesel fraction on auto-ignition. 86
Figure 5.11: Effect of the biodiesel fraction on the chemical delay of the blended fuel. 87
Figure 5.12: The path of a fuel parcel in the φ-T plane corresponding to an adiabatic mixing process followed by low-temperature heat release (Ref. [112]). 88
Figure 5.13: Experimental and predicted delay for biodiesel-gasoline blended fuels with an initial temperature of 800 K and mixture equivalence ratio of 1.0 under pressure of 19 bar. .89
Figure 6.1: Optical arrangement for the broadband chemiluminescence technique.....92
Figure 6. 2: Time sequence of flame images for oxygen concentrations of 21 %, 15 %, and 10 % at the ambient temperature of 1000 K, density of 15 kg/m^3, and injection pressure of.....93

Figure 6.3: Relation between ignition delay and fuel injection pressure for GB20 blend under 900 K, 15 kg/m^3, and 15 % O_2. 94
Figure 6.4: Relation between ignition delay and injection duration for GB20 blend under 900 K, 15 kg/m^3, and 15 % O_2. 95
Figure 6.5: Relation between lift-off length and fuel injection pressure for GB20 blend under 900 K, 15 kg/m^3, and 15 % O_2. 95
Figure 6.6: Relation between lift-off length and injection duration for GB20 blend under 900 K, 15 kg/m^3, and 15 % O_2 96
Figure 6.7: Ignition delay of GB20 blend for three different oxygen concentrations under temperature range of 800 K-1200 K in comparison with pure diesel. 98
Figure 6.8: Lift-off length of GB20 blend for three different oxygen under temperature range of 800 K-1200 K, injection duration of 1500 µs, and injection pressure of 50 MPa. 99
Figure 6.9: Ignition delay of GB20 blend for various oxygen concentrations under two different ambient densities of 5kg/m^3 and 15 kg/m^3, injection pressure of 50 MPa, and injection duration of 1500 µs. 100
Figure 6.10: Lift-off length of GB20 blend for various oxygen concentrations under two different ambient densities of 5kg/m^3 and 15 kg/m^3, injection pressure of 50 MPa, and injection duration of 1500 µs. 101
Figure 7.1: Ignition delay of GB20 under different conditions measuring from CVCC and RCEM. 104
Figure 7.2: Relationship between ignition delay and lift off length of GB20 107

Abbreviation and nomenclatures

Ar. Argon

C_2H_2. Acetylene

CDC. Clean diesel combustion

CI. Compression ignition

CN. Cetane number

CO. Carbon monoxide

CVCC. Constant volume combustion chamber

DGC. Dilute gasoline combustion

EGR. Exhaust gas recirculation

GDCI. Gasoline direct-injection compression ignition

HC. Hydrocarbons

HCCI. Homogeneous charge compression ignition

HRR. Heat release rate

ID. Ignition delay

ISFC. Indicated specific fuel consumption

ITE. Indicated thermal efficiency

LTC. Low-temperature combustion

N_2. Nitrogen

NI. National Instruments

NOx. Nitrogen oxide

O_2. Oxygen

PCCI. Premixed charge compression ignition

PFS. Partial fuel stratification

PM. Particulate matter

PRR. Pressure rise rate

RCCI. Reactivity controlled compression ignition

RCEM. Rapid compression expansion machine

SI. Spark ignition

TDC. Top dead center

THC. Total hydrocarbons

UHC. Unburned hydrocarbons

1 Introduction

1.1 Motivation

Since its inception, the compression ignition (CI) engine has been a rugged and reliable motive power with high fuel efficiency [1] [2] [3] [4]. In parallel with the development of control technology, CI engines have overcome the disadvantages of earlier models of higher noise and maintenance costs. It facilitates the CI engines have used commonly as mobile propulsion in automobiles, electrical power generators, and construction equipment. To meet more stringent emission mandates and deal with spiraling demand and diminishing supply of engine fuel, engine researchers must continually find new solutions to make engine emissions cleaner while maintaining performance and power [5] [6]. Under such situations, some after-treatment techniques have applied to remove hazardous gas emissions such as carbon monoxide (CO), nitrogen oxide (NOx), hydrocarbons (HC), and particulate matter (PM) in short-term [7]. However, high costs are an economic barrier against after-treatment devices to apply more widely for IC engines. In the long-term, the search for new combustion concepts and diversifying combustion strategies are the potential approaches to diminish pollutants from engine emission.

New combustion strategies have been developed to improve and optimize internal combustion engines. Low-temperature combustion (LTC), dilute gasoline combustion (DGC), and clean diesel combustion (CDC) are being especially interested as key combustion technologies. LTC involves the staging of the combustion process at a lower temperature and sufficiently lean to stay out of the high soot and NOx formation zones in CI engines. This strategy ameliorates engine efficiency by 20 % compared to conventional diesel engines. The temperature during the combustion process is lower as a result of using large amounts of exhaust gas recirculation (EGR) together with a lean mixture distribution [8] [9]. In DGC, a tiny amount of fuel is supplied to burn in an engine's combustion chamber under either an excess of air or recirculated exhaust gases. This concept can enhance engine fuel consumption by up to 35 % relative to the conventional spark-ignition engines. It may be due to combustion temperature is more moderate and hence reduces heat loss at medium and low loading [10] [11]. In CDC, the sequence of combustion is relatively similar to the standard diesel engines, but more of the air-fuel mixture is prepared mostly before combustion starts. The method allows the air-fuel mixture to burn under cleaner conditions, which leads to less soot formation.

The technical requirements for this method are a high-speed controller, complex injection strategy, high-pressure injection, EGR, and high air flow motion in a cylinder.

At present, dual-fuel combustion is also a potential technology to significantly reduce NOx and soot emissions while retaining high engine efficiency [12] [13] [14] [15] [16]. Many researchers are interested in the dual fuel combustion technology under homogeneous charge compression ignition (HCCI), premixed charge compression ignition (PCCI), and reactivity controlled compression ignition (RCCI) combustion strategies to optimize engine combustion and emission. For example, In the study's Hanson et al. [17], experiments were carried out in a diesel engine under PCCI mode to investigate the ability of governing the combustion phasing by varying the fuel reactivity steered by simulation results from the KIVA-CHEMKIN software. The results showed that dual-fuel PCCI operating conditions with the proper gasoline diesel ratio had significantly lower NOx and soot levels, and the indicated thermal efficiency also achieves high as 53 %. In an experimental study, Yang et al. [18] investigated gasoline blending with diesel fuel under two different combustion modes in an experimental diesel engine and found that the direct injection of blended fuels helps to obtain lower HC emission under low-temperature combustion mode. Early injection timing help to reduce NOx emission under dual-fuel highly premixed charge combustion mode due to the avoidance of high equivalence ratio and high-temperature region in the combustion chamber. An experimental and simulated study also was performed with gasoline diesel dual fuel in a diesel engine by Curran et al. [19]. The authors showed that fuel consumption was simultaneously improved; in particular, NOx and soot emissions experienced an over 90 % reduction in NOx and PM emissions. The brake thermal efficiency reached its highest level of about 34 % by maintaining high cylinder-to-cylinder balancing.

In addition to the discussion above, alternative fuels consisting of biodiesel, dimethyl ether, biogas, and bioethanol also are currently of interest for use in conventional or modified internal combustion engines to reduce pollution emissions. One of these alternative fuels, biodiesel fuel, is a promising candidate that can be used in most diesel engines and emits fewer air pollutants and greenhouse gases. Biodiesel fuel has some advantages, including superior lubrication ability, biodegradability, non-toxic, and mostly free of sulfur and aromatics, making it environmentally friendly. Especially, soot formation, which is a big concern in the diesel engine, can be reduced significantly by using biodiesel fuel combined with high injection pressure as exploded in the study of Wang et al. [20] [21]. Moreover, biodiesel can be

synthesized from plentiful feedstocks, which lead to diverse chemical structures as well as oxygen contents. In the context of fossil fuel depletion, biodiesel fuel is becoming green and sustainable fuel.

In recent studies, gasoline biodiesel blended fuels combined from biodiesel and gasoline presented an excellent potential for GCI engine technology, which is an advanced LTC technique that can address the problems associated with diesel engines. The fuel blend utilizes advantages of biodiesel such as superior lubricity, a renewable source, environmentally friendly fuel, and high ignitability, which improves the ability of cold engine start and avoids the misfiring under low. While, it maintains the benefits of gasoline as high volatility and long ignition delay, which potentially help the mixing process to reduce pollutant emissions. Adams et al. [22] used GB blends at 5 % and 10 % biodiesel content with the partially premixed, split-injection combustion strategy to improve the engine operating range, obtain stable combustion, and reduce the intake temperature requirement. Yanu et al. [23] [24] used GB blends at 5 % and 20 % biodiesel with a change in the injection timings, EGR, and boosting pressure to investigate an optimal area of the GB blends. The authors found some excellent results, i.e., as combustion efficiency increased up to 93 %, total hydrocarbons (THC) and CO emissions were reduced 50 % in comparison with diesel fuel.

GCI engine technology is based on modern CI engines, which operate using mixing-controlled combustion where multiple jets of fuel are directly injected into the combustion chamber of the engine at high pressure close to the top dead center. The fuel jet atomizes, entrains and mixes with the ambient air while penetrating across the chamber. The entrainment of hot ambient gases increases the temperature of the fuel-charge gas mixture, resulting in vaporization and subsequent auto-ignition when the equivalence ratio, temperature, and residence time of the fuel-charge mixture is conducive to rapid chain reactions. The liquid fuel penetration reaches a maximum distance downstream of the injector while the vapor head of the spray continues to penetrate. Following ignition, a quasi-steady, lifted, and the mixing-controlled flame are established. The combustion process ceases once all the fuel has combusted. Injection parameters, fuel chemical properties, and charge gas conditions control the processes of fuel-air mixing, auto-ignition, and mixing-controlled combustion.

Especially related to the ignition delay and lift-off length, two key measurable variables that provide insight into these processes the blend. Because auto-ignition is a driving factor in compression ignition combustion in the CI engine. It influences the delay time due to fuel characteristics from the start of injection until the start of combustion. Ignition delay (ID) affects the combustion phasing in the engine cycle and the degree of fuel vapor/air pre-mixing required to produce the primary mixture prior to combustion. This substantially impacts the shape of the heat release rate (HRR) and pollutant formation, most notably NOx and PM [13]. An improper ID in the CI engine, which causes the combustion phasing to change, can cause negative effects. One common symptom of these negative effects is a decreased power output of the engine. Improper ignition delay also leads to a rise in the phenomenon known as knocking, which can cause combustion instability and significantly decrease the life of the engine [25] [26]. The ID time depends on several parameters, including the type of fuel, engine design, engine operating conditions, and fuel injection strategy. Besides, lift-off length is the location relative to the injector tip that the lifted flame stabilizes following the onset of combustion [27]. The relationship between liquid-length and lift-off length for a given operating condition is linked with the levels of soot formed in the combustion process. Conditions where the lift-off length is less than the liquid length points to insufficient air entrainment before ignition resulting in a fuel rich diffusion flame and increased levels of soot formation and vice-versa [28].

Therefore, a better understanding of how the biodiesel fraction impacts on the ignition delay and lift-off length of its blends with gasoline in the GCI engine is a crucial issue. An optical investigation that is an advantage technology for investigating spray was performed to explode its spray combustion under a wide range of experimental conditions. The research on ignition characteristics using the constant volume combustion chamber (CVCC) and the rapid compression expansion machine (RCEM) is the main topic in the thesis. Besides, the ignition delay is predicted using the self-developed reaction mechanism with 4285 species and 15246 reactions under the CHEMKIN PRO software. Some other essential parameters were analyzed to understand the effects of biodiesel on its combustion well. The authors believe that the experimental study provides experimental data for the mapping of ignition delay; it is vitally important to control the internal combustion engines for obtaining high performance with the GB blended fuel.

1.2 Approach

This thesis investigates the spray combustion in the case of gasoline mixing with biodiesel. Limitation of this work is necessary since spray combustion is, in general, very rich in terms of the physical processes involved. The focus on fully formed dilute spray excludes investigation of the spray formation, liquid break-up, droplet collision and agglomeration, which is an entirely separate field of research. The main focus lies on spray combustion in terms of ignition characteristic and combustion characteristics, the optical investigation of the ignition process in a wide range of engine conditions, and the impact of injection condition and operation condition on them.

First, chemical kinetic modeling can be utilized to measure the ignition delay to investigate how the biodiesel effects on ignition delay behavior and the benefits of gasoline-biodiesel blended fuels. Both gasoline and biodiesel fuel have complex chemical components, so it isn't very easy to develop a detailed chemical kinetic model that can accurately predict the ID for a gasoline-biodiesel blend. In general, a proper model fuel should have a complex component to represent real fuel, but the complex component should depend on the end application. More complex components can better present real fuels but need the number of chemical mechanisms and, thus, have an expensive computational cost. Additionally, HCCI and RCCI combustion are much more sensitive to the chemistry of the fuel and therefore require complex multi-component surrogates to capture fuel reactivity accurately. Ideally, multi-component surrogates are considered to represent both gasoline and biodiesel. Gasoline surrogates range from simple to complex models. They include a simple binary component surrogate, two toluene reference fuels (TRFs), a three-component surrogate, a four-component surrogate, and a five-component surrogate. Biodiesel surrogates include methyl butanoate, methyl decanoate, and a three-component surrogate. The choice of a surrogate composition representing gasoline or biodiesel depends on the application. This study focuses on when combustion occurs in a gasoline compression ignition (GCI) engine. For this application, combustion is very sensitive to fuel chemistry. Therefore, the five-component surrogate and the three-component surrogate were chosen to represent gasoline and biodiesel fuel, respectively.

Second, the GB blended fuels were injected into the rapid compression expansion machine (RCEM) cylinder under 800 bar injection pressure at a 13-degree crank angle before the top dead center (TDC) to clarify how biodiesel additive effects on auto-ignition delay and engine misfire. The compression ratio (CR) of the RCEM was fixed as 11. The RCEM was

installed with all the additional equipment required for its full operation, and control was used to investigate the effect of biodiesel addition on engine misfire. This RCEM was designed to be similar to a type of single-cylinder diesel engine that includes a compression stroke and an expansion stroke and can carry out a wide range of temperatures and pressures. The bore and stroke of the RCEM are 100 mm and 450 mm, respectively. The compression ratio of the RCEM can be changed from 10 to 23.5 by adjusting the clearance volume. The initial temperature ranges from 273 K to 383 K by controlling the heat through a circular band heater on the cylinder jacket and pre-heater on the intake line. A control panel drives an electric motor before the start of the experiments. Once the start signal is generated, the connecting rod starts to move through an electronic clutch, and one compression and expansion cycle occurs. Since there is no previous cycle, the effects of residual gas and lubrication oil can be ignored. Additionally, a rotary encoder (EP50S8-1024) was attached to the crankshaft to measure the piston displacement. The signal pulse and error of the encoder are 0.3515º±15'.

Mainly, the optical investigation is performed to observe the ignition process and combustion characteristics using the CVCC generating high temperature and pressure environment like diesel engine operating conditions. The acetylene (C_2H_2), argon (Ar), oxygen (O_2), and nitrogen (N_2) were filled to form a density of 15.0 kg/m^3 or 5.0 kg/m^3 with a pre-calculated composition. Next, the spark plug was triggered to ignite the premixed charge gas, as reported by Jeffrey et al. [29] and Maximilian et al. [30]. The in-chamber temperature and pressure rise rapidly, then reduce due to heat loss. After the cool-down period, the in-chamber condition reaches the desired state, the injector is controlled to inject the fuel sample into the chamber, and the CMOS camera automatically begins capturing combustion images simultaneously. The GB blended fuels will combust under 800 K-1200 K and 10 % - 21 % O_2 conditions which cover both the conventional and low-temperature combustion regimes. The injection pressure, injection duration, and ambient gas density are also varied to investigate their effects on ignition characteristics and lift-off length. Experiments were performed at least ten times to obtain precise data and the standard deviation at each experimental state.

The emission of light during the combustion process was imaged at high speed to obtain the spray combustion information. The broadband chemiluminescence technique is applied to determine where and when combustion takes place in the combustion chamber. The effectiveness of the method has been presented and demonstrated in many previous studies [31] [32]. One 600 nm optical short-pass filter was used to remove the effects of

later soot incandescence and any species emitting in the high wavelength range while collecting other radicals (e.g., CH*, C2*). A self-written LabVIEW code was made to separate and smoothen the flame from background noise in the image processing. First, the Kittler-Illingworth method is used to calculate the flame threshold for removing background noise. The next method that is required to solve this problem is a morphological structuring element to clears the noise and to fill gaps in the detected flame. Then, a further filter was applied to reject small blobs that were less than 25 pixels. The image processing code was created in the Matlab environment to process uncertain backgrounds in image movies. The Matlab code automatically inputs the video captured by the CMOS camera and then removes the background noise and colors the images following the flame image intensities. Lastly, the flame contour also automatically detected for measuring the ignition information.

1.3 Objective

The present work focuses on the investigation for spray combustion of gasoline biodiesel blended fuel. In detail, the objectives of this thesis are:

- ✓ A gasoline-biodiesel reaction mechanism was developed to predict the chemical ignition delay of the blended fuels. The reaction mechanism with 4285 species and 15246 reactions was validated and implemented using the CHEMKIN PRO software. Aim for the reaction schemes is to provide the thermal file and chemical file that can use in CHEMKIN PRO. Next, the chemical ignition delay was predicted by the simulation, which was further compared to the experimentally measured results.

- ✓ Preparing and assembling the rapid compression expansion machine and the constant volume combustion chamber to simulate high pressure-high temperature conditions. Also, the self-written program is creased in the Labview environment and Arduino IDE to control the RCEM and the CVCC, respectively. For the CVCC, the model of the premixed combustion process will be developed to predict the formation of reactive species at the start of injection (SOI). The validation of the CVCC system and optical setup is performed under some typical conditions with pure diesel fuel before experimenting. The result is analyzed and compared to previous researches to sure the accuracy of the CVCC system and optical arrangement.

- ✓ Gasoline was blended with biodiesel at 5%, 10%, 15%, and 20% by volume, and then tested in a rapid compression expansion machine at a compression ratio of 11 and a

temperature range of 720-850 K to observe the auto-ignition delay phenomenon under low-temperature conditions. The experimental conditions are focused on improving the auto-ignition characteristic of gasoline direct-injection compression ignition (GDCI) combustion strategies under low load and cold start.

- ✓ The optical investigation for the gasoline biodiesel blended fuels were performed to explode its spray combustion under a wide range of experimental conditions in terms of the ignition delay and lift-off length using the CVCC. The ambient temperature varied in the range of 800 K to 1200 K; the oxygen concentration varied in the field of 10 % to 21 % to represent the EGR rate. Other parameters that are essential factors influencing spray combustion, such as ambient gas density, injection pressure, and injection duration, are also investigated. The ignition delay and ignition distance were methodically analyzed by the broadband chemiluminescence technique and the image processing.
- ✓ A piezoelectric pressure transducer was used to measure the pressure inside the chamber and to calculate ignition delay and heat release rate.

1.4 Thesis outline

Chapter 1 presents the scope of the thesis and gives a brief explanation to the topic of the research and to put it in context with preceding studies done on the same issue. The improvements are briefly described with the research aims and objectives.

Chapter 2 aims to provide a review of the literature relevant to the GCI engine and the effect of ignition delay and lift-off length on its combustion characteristics and emission characteristics. In the first section, a review of the GCI engine is given, which a powerful method to reduce soot and NOx in the CI engine, also increase the efficiency of usage of gasoline fuel. Second, the ignition delay and lift-off length are discussed, which is a complicated process and impacts firmly on engine efficiency and engine emission. Third, the theory of ignition delay and measurement is provided. Finally, a review of the demand for transport energy and the role of alternative fuel in terms of climate change and harmful gas emission is given.

Chapter 3 describes the setup of the constant volume chamber experiment system and the rapid compression expansion machine. The gas feeding system and fuel delivery system

are described as well. The optical diagnostic methods are briefly presented. The experimental test and analysis procedures are introduced. It also shows the way of image segmentation to process the combustion image.

Chapter 4 aims to explain the effects of biodiesel fraction on the ignition of its blends with gasoline under low-temperature range using an optically accessible CVCC. Natural soot luminous images from the combustible flame were captured by a CMOS camera to determine the ignition delay and the flame lift-off length. The ignition delay was also obtained by analyzing pressure traces from a high-frequency piezoelectric pressure transducer. Based on experimental data, the moderate biodiesel addition (less than 20%) was found to improve the ability of cold engine starting. The blend ratio also improves engine misfire under low-load-condition operation due to its flammability while maintaining the advantages of gasoline with great volatility and high ignition delay, which significantly enhances the mixture formation process.

Chapter 5 aims to perform the experimental study that is focused on improving the auto-ignition characteristic GDCI combustion strategies under low load and cold start. The heat release rate of the blended fuels was calculated from the pressure trace and displacement history of the piston to identify first-stage ignition and second stage (auto-ignition) ignition delay. Second, a gasoline-biodiesel reaction mechanism was developed to predict the chemical ignition delay of the blended fuels. The reaction mechanism with 4285 species and 15246 reactions was validated and implemented using the CHEMKIN PRO software.

Chapter 6 employs the same approach as Chapter 4 and applies to perform a comprehensive study focused on the lift-off length and ignition delay of the GB20 combined from 20 % biodiesel and 80 % gasoline showed the excellent potential for engine fuel application due to utilizing superior lubrication ability, renewables, environmental friendliness, high ignitability from the biodiesel and high volatility from the gasoline in a constant volume chamber under a wide range of experimental conditions simulating engine operating conditions. The GB20 was injected into the combustion chamber under different conditions: gas density (5 kg/m^3 and 15 kg/m^3), ambient temperature (800 K-1200 K), and oxygen content (10 % - 21 %). The single-hole injector with a 0.2 mm diameter is used to inject the fuel sample at various injection pressures (30 MPa - 130 MPa) and injection durations (400 μs – 3500 μs). This experimental study provides experimental data for the mapping of ignition delay; it is

vitally important to control the internal combustion engines for obtaining high performance with GB20 blended fuel.

Chapter 7 contains the summary and conclusions of this thesis and summarizes the experimental studies and combines the understanding from different diagnostics to gain an insight into the spray combustion. Significant findings are presented.

2 Literature review

The purpose of this part is to provide an outline of the background information relevant to the current research. In the first section, the GCI engine technology is given. Also, the opportunities and challenges of this kind of engine are presented. The second section of the chapter discusses past studies relevant to the ignition delay and lift-off length, which is a complicated process and impacts firmly on engine efficiency and engine emission. Besides, a summary of past work on the influences of injection conditions and operation conditions on ignition processes and fuel spray flame lift-off is given. Finally, the review of the demand for transport energy and the role of alternative fuel in terms of climate change and harmful gas emission are presented.

2.1 GCI engine technology

The CI engine is an internal combustion engine fueled by diesel-like high cetane fuels in which ignition of the fuel is caused by the elevated temperature of the air in the cylinder due to the mechanical compression. The CI engine has the highest thermal efficiency of any practical internal or external combustion engine due to its very high expansion ratio. However, real CI engines almost are diesel engines that use diesel fuel auto-ignited very quickly, causes emitting high soot and NOx that are the big concern in this type of engine. The diesel engines required to control PM and NOx cause the diesel engine quite challenging and expensive. Besides, the upper compression ratio is limited by the occurrence of ignition knock, thus limiting the spark ignition (SI) engine efficiency. In the future, gasoline with a higher octane is essential to prevent knocking and increase the SI engine efficiency. On the opposite side, gasoline with low octane will become available in the foreseeable future. In this situation, the GCI engine technology has interested. It is a potential engine technology that utilizes the advantage of gasoline with high volatility under the high compression ratio. This can address the problems associated with diesel engines such as soot and NOx emissions while maintaining high efficiency like the diesel engines. The GCI engines can efficiently operate on optimum gasoline with the RON between 70 and 80. The GCI technology merges the benefits of a higher compression ratio of the CI engine and the positive features of the gasoline.

2.1.1 GCI technology

The GCI is the advanced combustion with high thermal efficiency and low emissions without many modifications of standard diesel engines. GCI can be achieved with any

combustion mode from fully premixed homogenous combustion mode to totally diffusion-controlled combustion mode. Based on the proper mixing between the fuel and the in-cylinder gas, partially premixed combustion is hybrid combustion of HCCI mode and diesel combustion mode, which has a great potential in reducing the fuel consumption. In the partially premixed combustion mode, the fuel-air mixture is auto ignited under the combination of diffusion and premixed mechanism. At load conditions, the homogeneous mixture can be obtained by early-injection strategy at the start of combustion or intake stroke. Whereas, at high load conditions, the fuel is directly sprayed into a cylinder near the top dead center (TDC) to achieve diffusion-controlled combustion mode. In the GCI engine, level of fuel stratification is required to manage under high engine load conditions, since the ignition delay lengthens with the increase in load. So, a small amount of combustible mixture takes place by auto-ignition, and the remaining majority of fuel mixture governed by the diffusion process.

Work by Kalghatgi et al. [33] sparked a recent interest in using higher octane fuels with increased volatility. A single late fuel injection pulse with fixed width was utilized to keep fueling constant while comparing the performance of diesel fuel with CN=56 with an 84 RON and 95 RON gasoline. His experiment showed that at the low speed and load condition, the gasoline-like fuels resulted in longer ignition delay, which successfully reduced NOx emissions from the light-duty engine. However, a problem was found that the start of ignition is too advanced, leading to combustion instability. It is due to lean of the local in-cylinder mixtures. This demonstrated that an optimal distribution of fuel inhomogeneity or stratification is needed to obtain combustion stability and emissions performance. Another problem is excessive pressure rise rate (PRR) and NOx formation at high loads due to more premixed type combustion as fuel mass per injection. However, the use of EGR can suppress excessive PRR and NOx formation at high loads. Dec et al. [34] [35] [36] investigated the effects of partial fuel stratification (PFS) on the equivalence ratio distribution, PRR, and the extension of the high-load operating limit. The PFS allowed for the advancement of combustion phasing leading to an increase in the thermal efficiency of about 1%. IMEPg was below 2.4%; combustion efficiency was between 96.8 and 97.8% and indicated gross thermal efficiency was between 44.1 and 45.3% while maintaining low NOx and soot emissions. Also, the effects of intake boost on the gasoline HCCI high load limit is investigated. Fuel was provided via a fully premixed system utilizing a GDCI injector and fuel vaporizer located upstream of the intake plenum. The author found that the maximum load attainable increased with increasing intake

boost pressure from 5 bar to 16.34 bar of IMEPg. The authors believed the key enable to achieving these results was their ability to retard combustion phasing while maintaining good combustion stability with intake boost.

Adams et al. [37] studied the effect of biodiesel–gasoline blends on GCI combustion by examining 5 and 10% biodiesel using a partially premixed, split-injection strategy, finding that these additions of biodiesel significantly reduced the intake temperature requirement. They also concluded that higher NOx and lower CO and unburned hydrocarbons (UHC) were emitted, due to gasoline's higher averaged spatial bulk temperature. Yanuandri [23] compared GB20 (gasoline 80%, biodiesel 20%) and diesel fuel modes in a single-cylinder diesel engine to investigate the peak of PRR, combustion phasing, ignition delay, and NOx and hydrocarbon (HC) emissions. They observed a shorter ignition delay and less HC emission using GB20. This finding indicates that biodiesel has a strong potential to solve several problems in GCI engine applications, such as low lubricity when blended with gasoline. Yanuandri [23] also studied a 5% biodiesel blend with gasoline under pilot and main injection strategies and observed that GB05 offered better combustion stability. Because the use of blended fuels of biodiesel and gasoline is becoming increasingly common, it is important to understand the spray development process under different biodiesel fractions.

2.1.2 Opportunities and challenges associated with GCI

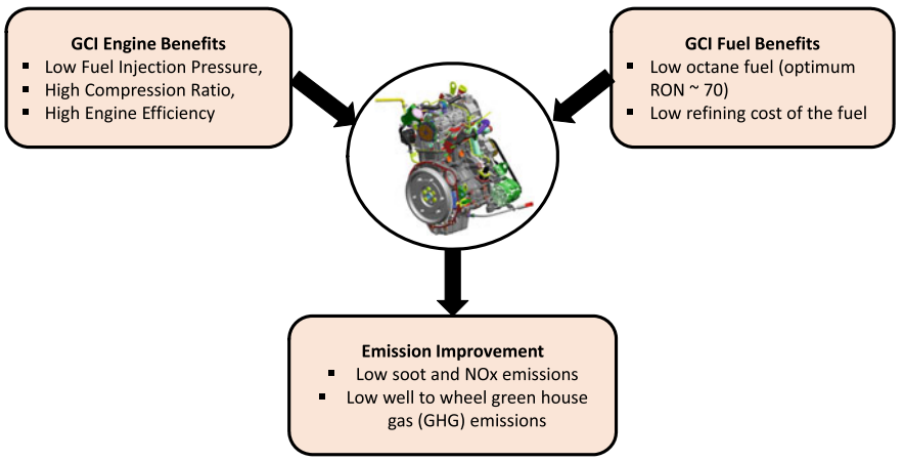

Figure 2.1: Advantages of GCI engine technology

Due to the selected strategy of gas exchange in a part load area of the operation map, low-pressure fuel pump, high volatility, long ignition delay period, wide-open throttle condition, and high compression ratio, the newly developed GCI combustion process allows

low fuel consumption approximately a diesel engine and low exhaust emissions. Also, extremely low NOx emissions can achieve under the LTC mode in the GCI engine. The CO emission also decreased significantly because of an over stoichiometric relative air-fuel ratio and a proper mixture preparation in comparison to the spark-ignited mode. Additionally, successful commercial development of GCI vehicles could open the way for more efficient cars in markets where diesel fuel is not widely available for passenger car applications. Figure 2.1 shown some main advantages of GCI technology.

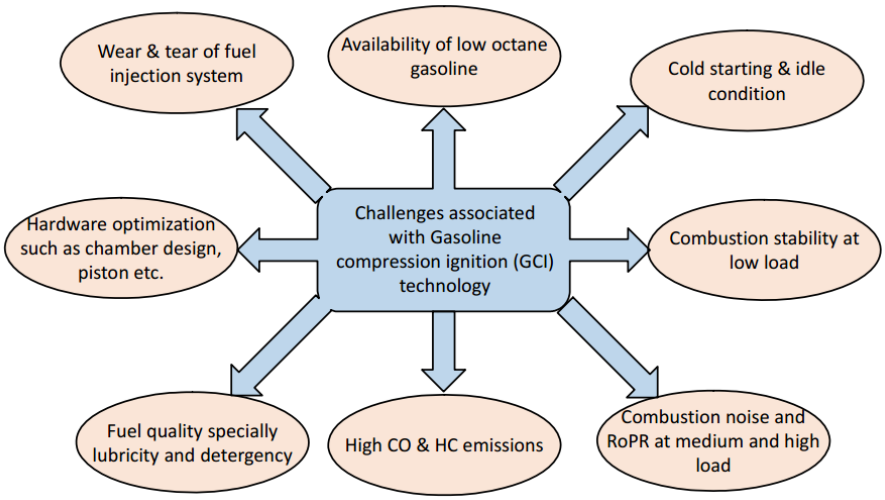

Figure 2.2: Challenges for GCI engine technology

The cetane number (CN) of gasoline in the market usually to be less than about CN15, which makes the gasoline hard to auto-ignite at low-load and cold starting conditions in the GCI engine. A very low CN lengthens significantly the ignition delay so the gasoline must be injected earlier in the compression stroke compared with typical diesel injection. At that conditions, the temperature and pressure is low, makes achieving ignition even more difficult. Therefore, further studies are required to address the issues associated with GCI engine technology before its adaptation in commercial vehicles. Main challenges associated with GCI technology are captured in Figure 2.2 [38]. However, almost problems can be resolved by optimizing the combustion and much simpler than diesel engines. Because of that, the implementation of GCI technology could be beneficial to both the automotive industry, and the oil companies and balance demand for light and heavy fuel oils in future fuel.

2.2 Effect of various control strategies on GCI engine

2.2.1 Injection strategy

Fuel injection strategies strongly effect on engine combustion, performance, exhaust emissions, and treat the maximum PRR, which was higher for gasoline. However, the HRR could be alleviated by retarding the injection timing, which resulted in retarded heat release, or by utilizing multiple injection strategies [33]. An arbitrarily chosen multiple injection strategy, three injections during the compression stroke can reduce the maximum HRR of gasoline-like fuels at higher loads. The triple injection strategy results in a longer combustion duration lead to a lower peak HRR. This result highlights the importance of fuel and stratification on GCI combustion strategies. Goyal et al. [39] investigated the particular role of the first injection and fuel ignition quality in controlling the homogeneous mixture and second injection in controlling combustion phasing. The author found that the first injection proportion leads to an increase in the mixture homogeneity, as evidenced by the rise in the initial burning rate, leading to the increased peak of the HRR and higher indicated engine efficiency but increased noise and NOx emissions. Lu et al. [40] studied single fuel injection and multiple-pulse fuel injection in extending engine load, improve emissions, and thermal efficiency tradeoff. The author used the multi-injection strategy; it can extend the engine load and decreased the ignition delay because of the increase in the collision of fuel molecular and oxygen molecular. Besides, both leanness and homogeneity of the mixture can be improved by the earlier injection. The CO, UHC, and soot emissions are significantly reduced, and the indicated thermal efficiency is also increased with no large expense of NOx emissions. Kalghatgi et [41] found that an arbitrarily chosen multiple injection strategy, using three injections during the compression stroke that were not optimized, demonstrated the ability of multiple injections to alter the shape of the heat release, thus, reduce the maximum HRR of gasoline-like fuels at higher loads.

2.2.2 Fuel ignition quality

The gasoline is injected earlier in the compression stroke due to longer ignition delay compared to diesel fuel. Usage of EGR in the GCI engine, the ignition delay is further retarded [42]. Ignition delay measurement showed that gasoline (less than 15 CN) has ignition delay longer two times in comparison with baseline diesel. Aydek Erman et al. [43] found that the effect of the physical and chemical properties of the fuel on NOx and soot are more sensitive at higher load conditions. In general, the differences in the physical fuel properties and molecular structure influenced on combustion and emissions. Yang et al. [44] showed that kinematic viscosity, lower heating value, closed-cup flash point, density, and cetane number strongly effected on HC, CO, and soot, NOx emissions, and fuel consumption. The gap and

near the wall are the place where most HC and CO emissions are formed. Cho et al. [45] carried out experiments with different gasoline (RON 92 and RON 80) using Delphi's 2nd generation GCI engine combined with a high amount of EGR. The author found that high reactivity RON 80 gasoline has the ability to enhance combustion behavior and to reduce fuel consumption at light-to-medium load conditions in comparison with the RON 92.

2.2.3 EGR strategy

In the CI engine, the EGR is a useful method to reduce and control the NOx emission. The EGR goes back to the combustion chamber, leading to reduce oxygen concentration and flame temperature of the working fluid. Ra et al. [46] investigated the GDCI combustion using a conventional light duty diesel engine through simulation and experiment. The author found that the usage of EGR paralleled with the reduction of combustion temperature, both soot and NOx emissions significantly reduced to levels of about 0.1 g/kg-f while maintaining high indicated specific fuel consumption (ISFC) at about 180 g/kw-hr. The operation maps were found to be very sensitive to the EGR ratio, initial gas temperature, and boost pressure, especially for operations at high split ratios. The increase in the EGR ratio can help to retard injection timing for optimum GCI combustion. Similarly, Kolodziej et al. [47] demonstrated that uncooled EGR might successfully raise intake temperature and the simultaneous reduction to in-cylinder trapped mass. The slight decrease in oxygen concentration has a more significant effect on lessening the mixture reactivity. Yao et al. [48] showed that the lower octane gasoline combined with a high level of EGR could improve the NOx-PM trade-off. The author obtained high indicated thermal efficiency (ITE) up to 51.57% with lower maximum PRR and regulated emissions by using a multi-injection strategy with 50% EGR.

2.3 Ignition delay and lift-off length

The GCI is an advanced combustion technology, using low-octane gasoline as an alternative for diesel in CI engines and can be adopted in modern CI engines with small modifications. Fuel spray characteristics are vital since they play a critical role in the mixing between fuel and air in the engine cylinder. The GCI engine works under the homogenous combustion mode at low load, partially premixed combustion mode at medium load, and diffusion-controlled combustion mode at high load condition. Based on the level of mixture homogeneity, partially premixed combustion lies in-between the HCCI and CI combustion modes. In the PPC model, the fuel-air mixture is burned in combination with both diffusion

and pre-mixed mechanisms with bulk auto-ignition. The processes controlling fuel-air mixing, auto-ignition, and combustion are the fuel vaporization rate, the entrainment rate of charge gases, and the reactivity of the fuel. Past studies have defined five key measurable variables that provide insight into these processes. Two of these are ignition delay and lift-off length, which result in exhaust emission, engine efficiency, and engine noise.

2.3.1 Ignition delay

Ignition delay is defined as the time delay between start of liquid fuel injection and ignition. A common expression for ignition delay is the Arrhenius type of equation 2.1. For a combustion spray, this includes the time for liquid breakup and vaporization and for the radical pool to build to a critical value to initiate the rapid chain branching required for ignition. Therefore, ID depends not only on physical properties of the fuel and charge gas but also the chemical reactivity of the fuel. ID controls the proportions of heat released in premixed burn phase relative to the mixing-controlled combustion phase and has a direct effect on combustion phasing and pressure rise rates in an engine [49]. Further, ID also has a direct effect on engine emissions and performance [50]. For an engine operating conditions, fuels with short ID lead to more PM emissions due to insufficient mixing whereas fuels with long ignition delays lead to increases in NOx and noise levels. In addition, IDs longer than those the engine has been designed for can lead to excessive fuel impingement. ID has been found to decrease with increase in injection pressure, ambient density, ambient temperature, ambient oxygen concentration, and increases with increase in nozzle diameter.

$$\tau_{id} = a\Phi^{-k^*}P^{-n^*}\exp\left(\frac{E_a}{R_u T_{cyl}}\right) \tag{2.1}$$

Where, τ_{id} = Ignition delay time

Φ = Equivalence ratio

E_a = Activation energy

T_{cyl} = Gas temperature in cylinder

R_u = Gas constant value

$a, k^{*} and\ n^{*}$ = Empirical constants

Asanas et al. [51], the pressure and temperature are measured to predict ignition delay time. The pressure and temperature at injection timing are calculated as following equations.

$$T_{cyl} = T_m . \varepsilon_{eff}^{c-1} \tag{2.2}$$

$$P_{cyl} = P_m . \varepsilon_{eff}^{c} \tag{2.3}$$

Where, $\varepsilon_{eff} = \frac{V_{disp}}{V_{soi}}$ Effective compression ratio (2.4)

c = Polytropic constant

P_{cyl} = Cylinder charge pressure

P_m = Manifold pressure

T_{cyl} = Gas temperature in cylinder

T_m = Manifold temperature

V_{disp} = Cylinder displacement

V_{soi} = Cylinder volume at injection timing

Polytropic exponent is calculated by expression of Hardenberg and Hase [52] as below.

$$c = k^{+} - \frac{k^{+} - 1}{f . u_p + 1} \tag{2.5}$$

Where, K^{+} = Specific heat ratio of a gas, $c_p / c_v = 1.4$

f = Constant 1.1

u_p = Average speed of the piston

In the above correlation of ignition delay, oxygenated fuel is not accounted for Lahiri et al. [53] introduced fuel to oxygen ratio in place of equivalence ratio. This makes ignition

delay a function of the oxygen content in the fuel. The Cetane number truly represents the compression ignition quality of fuel. Here, the correlation developed by Hardenberg and Hase [54] can be employed.

$$E_A = \frac{B}{CN + 25} \tag{2.6}$$

Where, B = a constant

CN = Cetane number

Cetane number, viscosity of fuel, nozzle hole-size, injected quantity and injection pressure also contribute to the delay time. However, for diesel fuels, ignition delay time can be achieved by Wolfer [55].

$$ID = 3.45 \exp(2100 / T_m) p_m^{-1.02} \tag{2.7}$$

2.3.2 Measurement of ignition delay

There are two different approaches to the definition of ignition delay. One method to measure ignition delay is by tracking the pressure inside the combustion chamber. A pressure transducer with a high frequency response must be used to ensure adequate time resolution. Prior to ignition, fuel spray vaporization occurs, which decreases the bulk ambient gas temperature slightly and in turn causes a slight dip in pressure. Heat release from autoignition causes the temperature and pressure to increase again, and the start of ignition is defined as the point where pressure recovers to the initial ambient pressure or to a slightly higher threshold. Another method is by measuring combustion luminosity. The approach is to measure OH luminescence, which was found to not correlate very well with pressure-based ignition delay. Soot luminescence, which is considered to indicate the beginning of a diffusion flame, can also be used and has been found to have a better correlation amongst different fuel types. Luminosity can either be measured using a CCD camera, photodiode, or a photo transistor.

The ignition delay is the time interval between the fuel injection and the fuel ignition. The fuel injection refers to the time at which the fuel emerged in the combustion chamber, by means of an injector. Every injector has a delay (called injection delay) due to the inertia of the nozzle tip. The injection delay was measured in time by macroscopic spray images [56]. The

fuel injection was determined from the electrical opening signal, which was sent to trigger the injector, subtracts the injection delay.

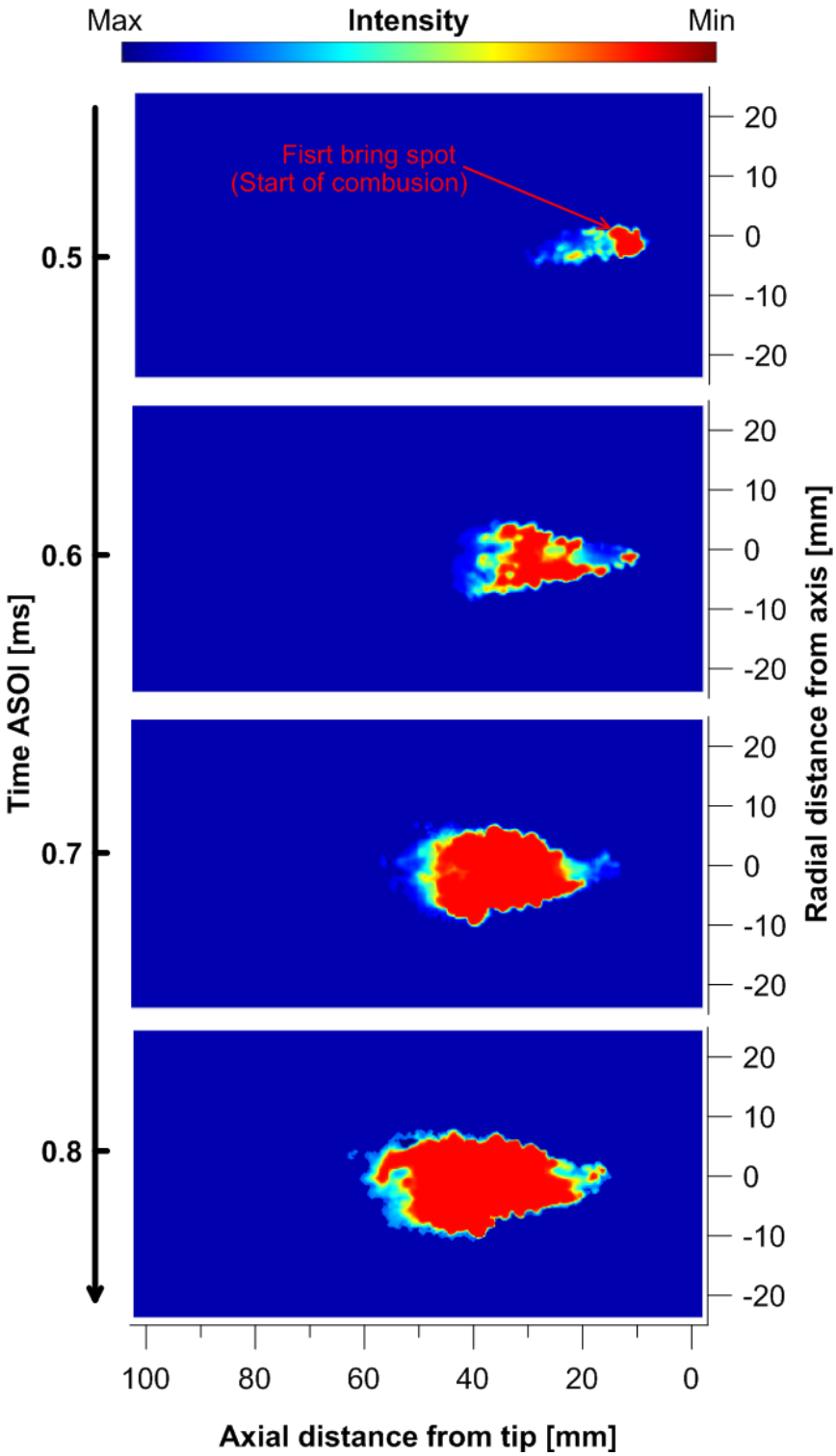

Figure 2.3: Images of the spray combustion evolution sequence.

In this work, the fuel ignition is judged on the luminosity of flame from the combustion process. The series of visualized images for each tested condition are captured using a high-speed camera and then analyzed to detect the ignition timing. The photos undergo the image processing to detect bright spots from the background. The bright spot, which is considered to be the fuel ignition, must grow to become the flame kernel. In the example, the first spot that appears on the combustion images at 0.50 ms is defined to be the start of combustion due to satisfying two rules. First, the bright spot develops into the combustion frame. Second, the density of the bright spot goes above a certain threshold (ignition threshold). This method has proved to correspond with the results of the OH-chemiluminescence images [31] [32] [57], as shown in Figure 2.3.

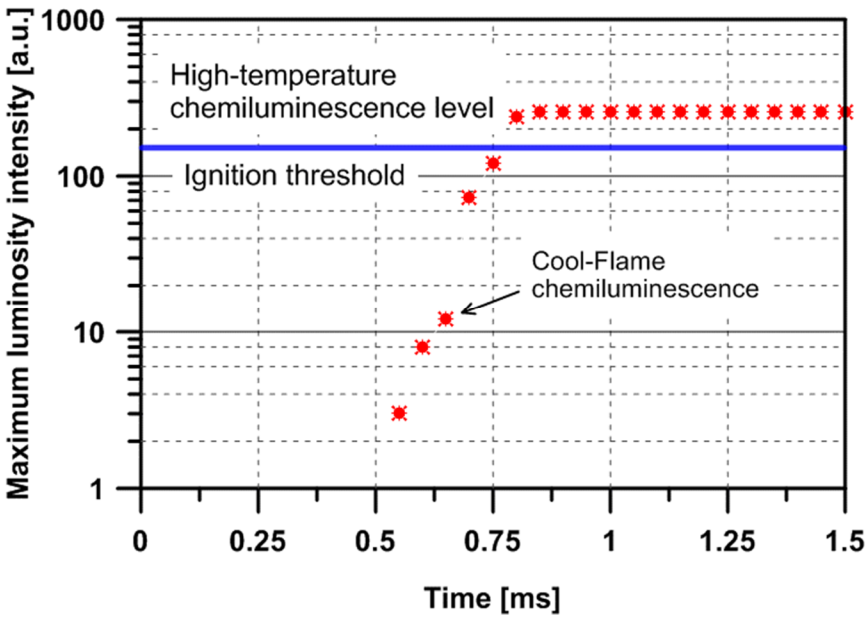

Figure 2.4: The maximum luminosity intensity inside the region of interest during the combustion progress.

The ignition threshold for determining the fuel ignition bases on analyzing luminosity from three different sources as background noise, cool-flame, and high-temperature flame. In theory, soon after fuel penetrates, the air-fuel mixture starts generating weak chemiluminescence due to cool-flame and then turned to the high chemiluminescence speedily with a high heat release due to the high-temperature flame. The flame reaches a stable status with a certain chemiluminescence level called the high-temperature luminosity. The 50 % magnitude of the high-temperature luminosity is selected to be the ignition threshold, which sufficiently above radiance from background noise and cool-flame and below the high-

temperature flame. This value agrees with previous studies and following the ECN standard methodology [58] [59]. Figure 2.4 illustrates the development of the maximum luminosity intensity during the combustion process and the ignition threshold for ignition determination. The maximum luminosity intensity calculated by the LabVIEW code grows from weak to high chemiluminescence. When its value is above the ignition threshold, the high-temperature combustion starts.

2.3.3 Factors affecting ignition delay

2.3.3.1 Ambient Conditions

Ambient temperature is the most important variable that strongly affects and drives ignition delay. Higher temperature not only increases the speed of the physical process influents to the physical delay but also raise the rate coefficients related to the chemical delay. The 50% reduction of ignition delay is resulted in the increase of ambient temperatures from 950 K to 1038 K in Fuller's study et al. [60]. Further decrease of ignition delay as 80% causes from the rise of temperature from 950 K to 1125 K. The same tendency was found in the other studies. Kobori et al. [61] investigated that ignition delay of diesel fuel decreases approximately 90% due to the decrease of temperature from 625 K to 1000 K. Ramesh et at [62] showed that 100 PPM of NO was sufficient to change the ignition characteristics of the tested fuels, even at very low concentrations. The magnitude and direction depended on the temperature regime and the nature of the fuel. Example, an increase of NO from 0 ppm to 50 ppm reduces the ignition delay about 35% but, an increase of 50 ppm to 100 ppm only decreases 10% ignition delay. Other components such as CO_2, CO, and H_2O also influents ignition delay, however, it is little bit effects on delay. The ignition delay had an exponent function of ambient pressure due to effects of gas density. The rise of pressure from 60 bar to 80 bar decreases the ignition delay about 20-30% for diesel fuel in Hoogterp's study et at. [26]. The reason for the decrease is due to higher density increases collision between the air entrainment and molar concentration of oxygen in the spray zone.

2.3.3.2 Fuel Injection

Air entrainment entering to spray zone is a key factor driving ignition delay of fuel sprays. In general, parameters of fuel injection influents ignition delay by way how fast the air enters into the spray zone. Any change effects on droplet sizes, injection velocity of fuel spay

will increase/decrease ignition delay. Example, increase orifice diameter of the injector from 0.1 to 0.2 mm causes the increase ignition delay increase of 30% due to the increase of droplet sizes, decrease of injection velocity and air entrainment, thus increase in physical delay in total ignition delay [61]. The increase from 0.176 to 0.212 of orifice diameter of the injector increases a 25% ignition delay in Schihl and Hoogterp [26]. However, there were minimal effects from increasing the diameter to 0.025 and 0.05 mm. It effected on the physical delay to increase to a point where chemical delay plays dominantly on the ignition process. Nguyen et al. [63] found that the orifice diameter had a moderately little impact on ignition delay. An increase in injection pressure also could increase ignition delay slightly. Increasing injection pressures and decreasing injector hole diameter causes to the increase in injection velocity, which make smaller sizes of fuel droplet, speeding up vaporization rates, and air entrainment. However, these effects are getting to smaller when injection pressure from 60 Mpa to 100 Mpa, the ignition delay is almost constant.

2.3.3.3 Fuel Properties

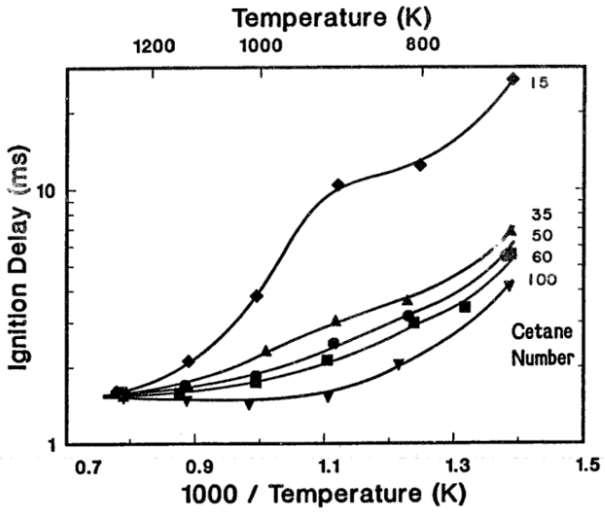

Figure 2.5: Ignition delay of reference fuels of varying cetane number

In all properties of the fuel, the cetane number is the governing factor driving ignition delay. The cetane number is studied in Lee and Bae [64], the authors found that ignition delay is dependent strongly than any others parameters such density, volatility, and viscosity. And also, the authors measured and compared two different cetane numbers of 39 and 46, the result showed that ignition delay decreases to 5 to 13% (0.1 to 0.2 ms) when cetane number increases from 39 to 46. It is agreement with the study of Pickett and Hoogterp, who investigated that jet

propellant evaporates quicker than diesel fuel, yet has a longer ignition delay due to a lower cetane number [65]. The authors concluded that physical properties, such as evaporation, viscosity, and density, that influence fuel injection, can have minor impacts on ignition delay, but they are still a driving factor by cetane number. It is further confirmed by Siebers obtained the ignition delay of reference fuels with different cetane numbers in the CVCC, and results presented in Figure 2.5.

2.3.4 Lift-off length

Lift-off length is an indicator of local mixture formation and the location relative to the injector tip, is the driving parameter for identifying the combustion rate and pollutant formation that the lifted flame stabilizes following the onset of combustion. The flame stabilization process is controlled by a complex set of interactions between turbulent fluid mechanics and flame chemistry processes [66]. The flame remains lifted during the diffusion-burn phase of heat release, allowing fuel and ambient gases to premix upstream of the reaction zone and strongly affecting combustion and soot formation processes downstream [67]. The oxygen in the entrained air is believed to react with fuel in a rich reaction zone in the central region of the spray just downstream of the lift-off length [68]. The relationship between liquid-length and lift-off length for a given operating condition is linked with the levels of soot formed in the combustion process. Conditions where the lift-off length is less than the liquid length points to insufficient air entrainment before ignition resulting in a fuel rich diffusion flame and increased levels of soot formation and vice-versa [69]. The products of such a rich reaction zone are ideal for forming soot, suggesting a strong link between soot formation and the amount of air entrainment, or fuel–air mixing, that occurs upstream of the location of flame lift-off. More air-entrainment upstream of the lift-off length is likely to lead to less soot formation. The parameters that have been shown to influence lift-off length are nozzle orifice diameter, injection pressure, ambient density, ambient temperature and oxygen concentration. The lift-off length decreases with an increase in the latter three parameters and increases with nozzle diameter and injection pressure.

Right after the fuel reaches a limitation temperature to auto-ignite, the high-temperature flame becomes relatively stable in the downstream zone. The distance between the injector tip and the relatively stable position of the high-temperature flame is defined as the lift-off length as presented in Figure 2.6. The lift-off length depends on the engine operating conditions, fuel

properties, and injector characteristics. It is an important parameter that impacts on the mixture formation process and pollutant emissions during the combustion process [70] [71]. The lift-off length represents the spray area where the relatively cool fuel breaks into droplets. The droplets continue to disperse, evaporate, and mix in a turbulent jet to form an initial air-fuel mixture. Then, the air-fuel mixture comes into the initial combustion zone where the mixture reacts as a fuel-rich premixed flame and soot precursors are formed. The lift-off length was measured by analyzing the OH-chemiluminescence images, which obtained by an ICCD camera with a 310 ± 5 nm interferometric filter [72].

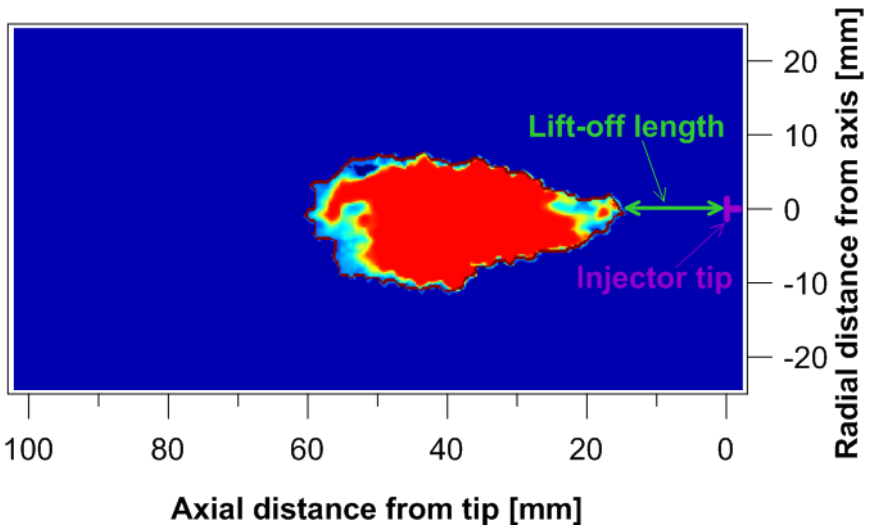

Figure 2.6: Lift-off length definition from the broadband chemiluminescence imaging.

In this technique, the optical bandpass filter was used to remove the natural light emission out of the 310 nm range and gain OH chemiluminescence from high-temperature combustion chemistry. The intensity threshold for image segmentation is 125 on a digital scale corresponding to 50 % of the image intensity range. As with ignition delay, we measure the lift-off length through broadband chemiluminescence of the flame. The fundamental premise of the method is to remove the low radiation, the light reflection of the liquid and fuel vapor, and background noise. However, the bright spot is predominant by luminous soot emission from the combustion process. It appears in a region downstream of a combusting diesel fuel jet. Therefore, the threshold level was normally determined to be relatively low from 3.5 % – 10 % maximum density to minimize the difference between this technique and the OH chemiluminescence technique [73] [74] [75]. In this study, the threshold for lift-off length determination is calculated using the Kittler-Illingworth method [76] [77]. When processing those low-intensity images, the Kittler-Illingworth method calculates the threshold, which

removes the whole background noise as well as the image of the liquid jet. The average lift-off length is shown by averaging values after the start of ignition 0.5 ms and lasting 1 ms, which corresponded to the quasi-steady spray combustion period under the different conditions, as illustrated in Figure 2.7.

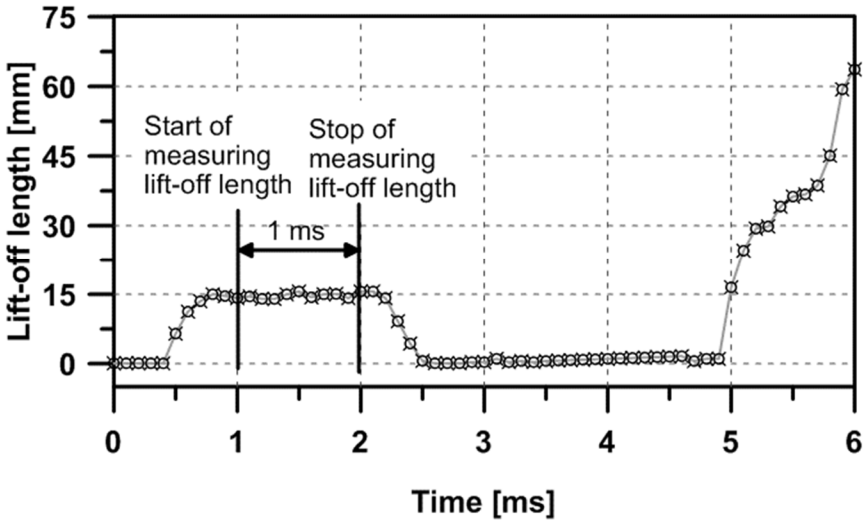

Figure 2.7: The period of time-resolved lift-off length measurements.

2.3.5 ID and LOL effect on compression ignition combustion

The ignition delay period consists of physical delay, wherein atomization, vaporization and mixing of air fuel occur and of chemical delay attributed to pre-combustion reactions. Physical and chemical delays occur simultaneously. This is different from the combustion performance of the fuel, which influences the efficiency of the engine. The ignition delay of a combustion spray is important from the viewpoint of preparing the fuel before injecting into the engine as well as selecting optimum injection timing. So, the ignition delay strongly influences on combustion characteristics and the exhaust emissions of CO, NOx, PM and exhaust particle number (PN) was investigated [45]. The ceiling on NOx is dipping to such a low level that accurate prediction of ignition delay has become important even if it is small. A strong positive correlation was found between ignition delay duration and CO emissions. For both sets of fuels, CO emissions increased with increased ignition delay, at both timings and both loads. Wolfer et al. [15] showed that Ignition delay of spray combustion is a strong function of ambient temperature and pressure as in Arrhenius's study [42] experimentally shown the strong influence of the injection parameters like the hole size, injection pressure and types of fuel and hence quality of fuel on the measured delay. However, the physical delay has

not been modelled satisfactorily in the literature. The phenomenological calculations of the cooling of spray surface have shown that the physical parameters and fuel type influence the temperature of the mixture of air and the vapor produced by the first parcel of the injected fuel throughout its life up to ignition. This is either a constant or variable according to the characteristics of the injector and has a form of Wolfer's correlation. Andrea [44] emphasized the importance of basic research to investigate the physical and chemical complexities involved in igniting and burning hydrocarbon fuels. Detailed consideration of droplet formation, evaporation fuel and pre-flame reaction has enabled prediction of delay period and location of the ignition accurately within the experimental errors and errors in the input to the calculations.

The delay affects the pressure and temperature of combustion, which both affect the formation of especially NOx. It also affects the engine efficiency and therefore the amount of all pollutants if not the concentration of NOx formed. Delay period is one of factor in starting of combustion and hence time available for complete combustion of fuel. As delay period increases, the time for combustion decreases hence will increase chance for incomplete combustion. Which will result in formation more carbon particle. There is a difference between delay of combustion and delay of ignition. Delay of combustion leads to reduced NOx when reduced peak temperature simultaneously, reduced CO because of increased time for CO2 conversion, increased particulate matter because of increased time for particles building, low effect on HC, but can lead to a certain increase of HC. Delay of ignition leads to high pressure increase and thus high temperatures: high NOx and CO emissions, low particulates, eventually lower HC. Cetane number is closely linked to the ignition delay of a fuel, which is one of the most critical factors controlling the combustion characteristics in compression ignition engines. Improper ignition delay in an engine can cause changes in combustion phasing, which can have detrimental effects. The most common symptom of improper ignition delay is decreased power output. Excessive ignition delay can also lead to extreme pressure rise rates and combustion stability issues, which can drastically decrease the life of an engine.

The control systems of modern diesel engines are equipped with a map-controlled servo control of the ignition angle. In order to increase the efficiency for all operating points of the diesel engine it is important to control the ignition timing and the ignition angle, respectively. One criterion for the evaluation of the optimum ignition angle is the location of the center of combustion mass. The center of combustion mass is the point where the half of the fresh injected diesel fuel is combusted. Of all variables, ID is influenced by the widest set of

parameters and can be measured Therefore, ID is often the primary metric for development, calibration, and validation of CFD models. Common methods of ID measurement rely on experiments conducted in either a shock tube or a rapid compression machine to characterize only the gas-phase chemical kinetic delay. These measurements have been extensively used to develop and validate traditional engine CFD models that primarily rely on accurately modeling the impact on chemical kinetics, typically using a single-component fuel, while simplifying the physical effects of fuels on combustion [78]. While these models have helped greatly to improve diesel engine efficiency and pollutant emissions over the past two decades, these improvements represent the low-hanging fruit. The sustained advancement of diesel engines requires the inclusion of realistic multi-component compositions and the physical properties of fuels in order to accurately simulate combustion [79]. Since simulations can only be as good as the physical measurements used to validate them, using ID as a metric for model development requires accurate measurements. These measurements should include the effects of physical processes such as liquid breakup, atomization and vaporization at engine relevant conditions, for them to be useful in developing advanced diesel engine simulation tools. The fuel delivery system used in these measurements must be representative of conventional diesel engines to accurately reproduce the effect of transient rate-of-injection on jet breakup, entrainment and mixing. The boundary conditions must include effects of all primary parameters, such as temperature and density, as well as influence of variations between experimental operations.

Lift-off length is the location relative to the injector tip that the lifted flame stabilizes following the onset of combustion. The relationship between liquid-length and lift-off length for a given operating condition is linked with the levels of soot formed in the combustion process. Conditions where the lift-off length is less than the liquid length points to insufficient air entrainment before ignition resulting in a fuel rich diffusion flame and increased levels of soot formation and vice-versa. The parameters that have been shown to influence lift-off length are nozzle orifice diameter, injection pressure, ambient density, ambient temperature and oxygen concentration. The lift-off length decreases with an increase in the latter three parameters and increases with nozzle diameter and injection pressure.

Many of the details of the flame stabilization process are not yet agreed upon, there is growing evidence to suggest that flame lift-off length plays a significant role in DI diesel combustion and emissions formation processes, making lift-off length of significant practical

importance to diesel engines. The lift-off length is a critical parameter for soot formation in compression ignition engines. The effect of lift-off length on diesel combustion occurs as a result of premixing of injected field and entrained air upstream of the lift-off length. Additionally, measurements of lift-off length established well after ignition will also be made and compared to the ignition location. This will test the validity of using models of lift-off length and spray penetration to estimate the ignition location and thereby modeling the pressure wave delay. The discussion above implies that lift-off length, which defines the amount of air entrainment and fuel air premixing that occurs upstream of any combustion in a DI diesel spray, plays a pivotal role in diesel combustion and emission formation processes, especially soot formation processes. However, our understanding of how various parameters affect flame liftoff under diesel conditions is limited. The only information available on diesel spray flame lift-off must largely be inferred from images of visible luminosity in literature, which do not accurately reflect the farthest upstream location of combustion. Moreover, Model of diesel combustion has soot formation beginning in the product gas of the central reaction zone, with soot growth occurring as the gas is transported downstream in the penetrating, reacting fuel jet. This soot formation concept is supported by a recent modeling effort, coupling a phenomenological spray model with detailed chemical kinetic modeling [36] [80].

2.4 Fuel

2.4.1 Current transport fuels

Liquid fuels have high energy density per volume, is easy to store and use upon demand in comparison with electricity, can transport easily and handle in comparison with solid fuels, and need the small tanks comparison with gaseous fuels. Therefore, the liquid fuel has become the undisputed option for the mean of transport for the last century, and a pervasive global infrastructure has contentiously constructed for the production and distribution of liquid fuels worth trillions of dollars. Besides, gaseous fuels must compress and liquefy to decrease their specific volume before they are employed to power the means of transportation. It needs additional energy and infrastructure, and this may hinder the application of gaseous fuels in the field of transportation. Transportation sector energy consumption mostly comes from crude oil, and this is still maintained even though the change in transportation appears as a process of substitution in a specific sector. In the first years of the 2000 decade, around 95% of transport energy was derived from petroleum, and by 2040, this share is expected to be still approximately 90% [81].

Liquid fuels for transportation are fundamentally produced in oil factories, beginning with raw oil and then combining the products of some other processes. The raw oil comprises diverse chemical compounds with different boiling points. Firstly, the raw oil is distilled to divide into the separate boiling range fractions. Approximately 2% of the raw oil can be decayed to gases, which are made at a higher ambient temperature and create liquid petroleum gas (LPG) with a component of around 75% propane. The light portion from the refined process boils approximately in the gasoline range from 20 to 200 atom of carbon is called ‘‘straight run gasoline’’ (SRG). The generic term ‘‘naphtha’’ is named for products, which come into possession of different processes in the refinery in this boiling range. Naphtha regularly is further processed to reach high resistance to auto-ignition to create the blended constituents for gasoline and primary feedstock for petrochemicals.

The requirement for transportation fuel cannot be reached if there are no processes to remove heavier and low-value fractions into lighter fractions to use for fuel components. The complex refinery processing is pointed out to increase the anti-knock quality of the different component streams. The anti-knock quality of fuel in a given engine operating condition and depends on the molecular structure of the fuel. Detailed chemical reaction mechanisms controlling ignition properties typically include hundreds of species and thousands of elementary reactions, especially in the low-temperature regime. Petroleum refining processes are the chemical engineering processes and other facilities used in petroleum refineries to convert crude oil into useful products such as the LPG, gasoline or petrol, kerosene, jet fuel, diesel oil, and fuel oils. A description of refinery and other processes used for making fuel components.

2.4.2 Alternatives to conventional fuels

The potential issues surrounding the use of fossil fuels is climate change due to CO2 emissions. The problem has become a hot-button topic over the last few decades. Today, there is a general shift towards environmental awareness, and the sources of our energy are coming under closer scrutiny. This has led to the rise of many alternative energy sources. While the viability of each can be argued, they all contribute something positive when compared to fossil fuels. Lower emissions, lower fuel prices, and the reduction of pollution are all advantages that the use of alternative fuels can often provide. Currently, of the total global transport energy, biofuels supply about 4% and the rest, which includes compressed natural gas (CNG), LPG,

and liquefied natural gas (LNG) about 1%. The contribution of electricity is negligible, and hydrogen is nonexistent.

Most governments provide an array of subsidies to increase the consumption of biofuels such as tax breaks, grants, loans, and loan guarantees to reduce oil imports and to some extent, support agriculture and rural employment. However, biofuels more costly than fossil fuels. The generation of biofuels might increase competition for land between the food production and energy industry, resulting in increased prices and rising water and energy demand due to the increased need for crop irrigation and energy for transportation. Moreover, the environmental benefits of biofuels are unclear and indistinct in some sides. Any increase in biofuel yields strongly affects the restructuring of agricultural land. Example, the International Energy Agency (IEA) predicts that to make a 27% share of transportation energy for biofuels by 2050 will need 100 million ha corresponding to from 12 to 165 million ha [82]. The huge added requirement of land in a world parallel with an increase of population and demand for food makes it extremely difficult to manage.

Hydroelectric energy carries with it several benefits. Not only is it a clean source of energy, which means it doesn't create pollution and the myriad issues that arise from it, but it is also a renewable energy source. The most common form is the hybrid electric vehicle (HEV). For example, Toyota Prius is a full hybrid electric automobile developed by Toyota and manufactured by the company since 1997. The model uses a battery and an electric motor to manage the flow of energy between the IC engine intended to achieve either better fuel economy than a conventional vehicle or better performance. Such technology is expected to be very widely deployed in the future, but the combined power of both is often less than that of a gas-powered engine. It is therefore suited for city driving and not for speed and acceleration, so its benefits are most marked when the vehicle operates at low loads with frequent stops and starts. Modern HEVs make use of efficiency-improving technologies such as regenerative brakes, which convert the vehicle's kinetic energy to electric energy, which is stored in a battery or supercapacitor. Battery electric vehicles (BEV) is a type of electric vehicle (EV) that uses chemical energy stored in rechargeable battery packs. Plug-in hybrid electric vehicle (PHEV) is a hybrid electric vehicle whose battery can be recharged by plugging it into an external source of electrical power. Its on-board engine and generator can drive the car over a limited range (currently around 50 miles), which can extend the range. However, now, BEVs and PHEVs are small cars because of limitations on the size and weight of the battery.

Natural gas sources have been in use for decades, but it is through the progression of compression techniques that it is becoming a more viable alternative energy source. In particular, it is being used in cars to reduce carbon emissions. It is in the form of CNG or the GTL. CNG is used in traditional gasoline/internal combustion engine automobiles that have been modified or in vehicles manufactured explicitly for CNG use, either alone, with a segregated gasoline system to extend the range or in conjunction with another fuel such as Diesel. The technology for CNG road vehicles is well-developed, but the lack of distribution infrastructure constrains its use. In contrast, GTL produces liquid fuels, which can use the existing infrastructure but is very expensive. Due to lower maintenance costs than other hydrocarbon-fuel-powered vehicles and safer than gasoline-powered cars, Natural gas vehicles is increasing rapidly in the transport sector in recent years. EIA predicts the global reserves of shale gas at 207 trillion m3 more massive than the current conventional gas reserves of 187 trillion m3. ExxonMobil estimates that by 2040, natural gas will provide about 5% of global transportation energy as related to about 1% currently. The low the cost and availability of natural gas has the potential to increase to be wide regional variations, however, depending on many factors.

2.4.3 Biodiesel fuel

As a clean, biodegradable and renewable fuel, biodiesel is attracting great interest in engine community. Biodiesel is beneficial to PM reduction of diesel engines since the oxygen in biodiesel provides an effective way to enhance the combustion process and inhibit soot formation in diesel engines. Biodiesel is an alternative fuel similar to conventional or ‘fossil’ diesel. Biodiesel can be produced from straight vegetable oil, animal oil/fats, tallow, and waste cooking oil. The process used to convert these oils to biodiesel is called transesterification. Most Biodiesel produced at present is produced from palm oil, soybean oil, rapeseed oil, and used cooking oil [83] [84]. At present, oil straight from the agricultural industry represents the greatest potential source, but it is not being used for commercial production of biodiesel simply because the raw oil is too expensive. However, biodiesel, which is most often used as a blend with petroleum diesel fuel, can be used in many diesel vehicles without any engine modification. The most common biodiesel blend is B20, which ranges from 6% to 20% biodiesel blended with petroleum diesel. The brief explanation of the biodiesel standards around the world is presented in table 2.1 [85] [86].

Table 2.1: Biodiesel standards around the world.

Properties (units)	Malaysia	Korea	Thailand	USA	EU	Brazil
Flash point (°C)	182 ↑	120 ↑	120 ↑	130 ↑	120 ↑	100 ↑
Viscosity at 40°C (cSt)	4.415	1.9-5.0	3.5- 5	1.9- 6	3.5- 5	-
Sulphated Ash (% mass)	0.01 ↓	0.01 ↓	0.02 ↓	0.02 ↓	0.02 ↓	0.02 ↓
Sulphur (% mass)	0.001 ↓	0.001	0.001 ↓	0.001↓.	0.001 ↓	-
Cloud point (°C)	15.2	-	-	-	-	-
Cu corrosion (3hr, 50°C)	Class 1	Class 1	Class 1	Class 3	Class 1	Class 1
Cetane number	-	-	51 min.	47 min.	51 min.	-
Water & Sediment (vol.%)	0.05 ↓	0.05 ↓	-	0.05 ↓	-	0.05 ↓
Carbon residue (wt%)	-	0.1 ↓	0.3 ↓	0.05 ↓	-	0.1 ↓
Acidity (mg, KOH/gm)	-	0.5 ↓	-	0.05	0.05	0.08
Free glycerin (% mass)	0.01 ↓	0.02 ↓	0.02 ↓	0.02 ↓	0.02 ↓	0.02 ↓
Total glycerin (% mass)	0.01 ↓	0.16 ↓	0.25 ↓	0.24 ↓	0.25 ↓	0.38 ↓
Phosphorus (% mass)	-	0.001 ↓	0.001 ↓	0.001 ↓	0.001 ↓	-
Distillation temperature	-	-	-	<360°C	-	<360°C
Oxidation stability, hrs	-	6 ↑	6 ↑	3 ↑	6 ↑	6 ↑

2.5 Summary

This literature review has revealed the study on CI engine fueled with gasoline and/or blended with the others fuels especially running on GCI mode or its similar method. Study about GCI with different kinds of fuel is provided such as gasoline and biodiesel blends. Besides, the methods aim to extend range of engine operation such as using boost pressure, controlling intake temperature, controlling local air-fuel stratification by injection strategy and modifying fuel property. However, the GCI engine technology still exists some challenges, further studies about the kind of this engine have required due to the complexity of CI engine, which is operated in GCI combustion mode.

In GCI engine, controlling last injection is the most important issue to govern combustion phasing. This effects on local air-fuel stratification driving combustion characteristics and emission characteristics. Ignition delay has been demonstrated that a method for quickly and quantitatively determining the local air-fuel stratification is of supreme importance in GCI combustion as it dictates stable ignition as well as the level of PRR and engine-out emissions. Air-fuel stratification can be altered by changes in injection pressure, injection timing, fuel mass split while utilizing split injection strategies, in-cylinder turbulence and swirl. Therefore, it is important to understand the role that these parameters play on the manipulation of the local equivalence ratio distribution.

Especially, ignition delay and lift-off length play an important role in the combustion process. Some simulated and experimental results on them demonstrated it is sensitive parameter governing combustion phasing, heat release rate, fuel efficiency, soot formation, and etc. However, there have not any investigation in detail on these parameters on combustion of GCI engine. For GCI engine with gasoline-biodiesel blends as an alternative is very rare if cannot be mentioned as "never conducted". Further investigation of ignition delay and lift-off length analysis under GCI with gasoline-biodiesel blend on simulated and experimental work would greatly give a better understanding on the effect to control combustion phasing, thus optimizing combustion and emission.

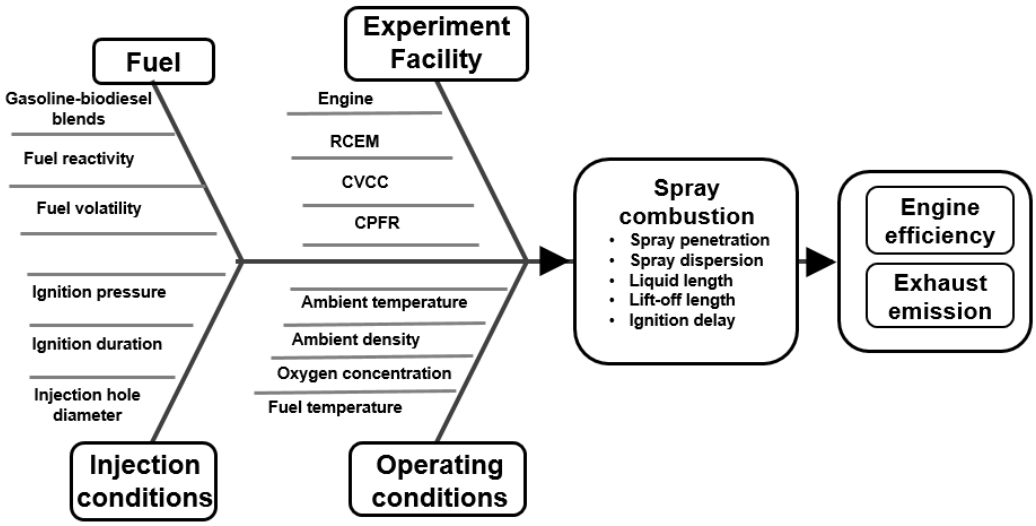

Figure 2.8: Effect flowchart of the potential parameters on spray combustion with engines fueled with gasoline-biodiesel blends

To explode understanding about the processes controlling fuel-air mixing, auto-ignition and combustion are the fuel vaporization rate, the entrainment rate of charge gases and the reactivity of the fuel. Past studies have defined five key measurable variables that provide insight into these processes: spray penetration, spray dispersion, liquid length, flame lift-off length, and ignition delay. Some sequential experimental works will be conducted to identify the important parameters and phenomena related to spray combustion of CI engine fueled with gasoline-biodiesel blends. The brief explanation on how to obtain the targets can be summarized in the effect flowchart as seen in the Figure 2.8.

3 Experiment setup and methodology

This chapter provides the information on laboratory test benches for investigation of ignition delay and other parameters that were used as investigation tools for this study. First, RCEM designed to be similar to a type of single-cylinder diesel engine was used to measure ignition delay under low-temperature condition presented low-load engine and cold engine start. Second, the measurements were performed using a customized premixed burn type constant volume combustion chamber. The CVCC can achieve a range of chemical and thermodynamic conditions representative of modern diesel engine operation with varying levels of EGR. The CVCC is paired with a high-speed, high-resolution data acquisition system for chamber pressure measurements, a high-pressure common-rail fuel injection system, an exhaust gas sampling system, and an optical system designed to resolve the spray combustion characteristics during fuel injection.

3.1 CVCC System

3.1.1 Constant Volume Combustion Chamber

The CVCC is a basic investigation tool and commonly used to investigate a variety of combustion and spray phenomena at elevated temperatures and pressures like the diesel engine conditions. Oren et al. [87] firstly presented the concept of a CVCC in their 1984 paper. The CVCCs are hollow chambers made of high strength material with access ports for chamber operation and instrumentation. The pressure and temperature conditions in the chamber are obtained with a chemical heating process. The use of a CVCC in combustion research provides the possibility to isolate the injection and combustion processes from all other influences in engines. The optical access makes it possible to see inside of the combustion chamber, and this facilitates the use of a high-speed camera and the implementation of the image analyzing tools to achieve a better understanding of the injection and the combustion processes.

The chamber is first evacuated and then filled with a gaseous combination of fuel, oxidizer, and inert gas collectively called the premixed charge, the composition of which is tailored to create the desired ambient conditions. Homogeneity of the premixed charge is achieved either using a mixing fan or by means of turbulent mixing created by directional gas intake ports. The premixed charge is ignited with one or more spark plugs, and the resulting heat release causes a rapid increase in chamber temperature and pressure. The products of the premixed charge slowly cool due to heat transfer to the cooler chamber walls, and the chamber

pressure falls accordingly. In this manner, a wide range of ambient densities and temperatures can be achieved. For the purposes of ignition delay measurements, liquid fuel can be injected as the desired conditions are slowly traversed. Because the autoignition of fuel sprays occur much quicker than the cooling of the premixed charge products, autoignition is assumed to take place at constant ambient conditions. Many CVCCs have both spherical or cylindrical interiors, with common volumes ranging from 0.13 to 2.3 liters for cylinders and 1.8 to 4.2 liters for spheres.

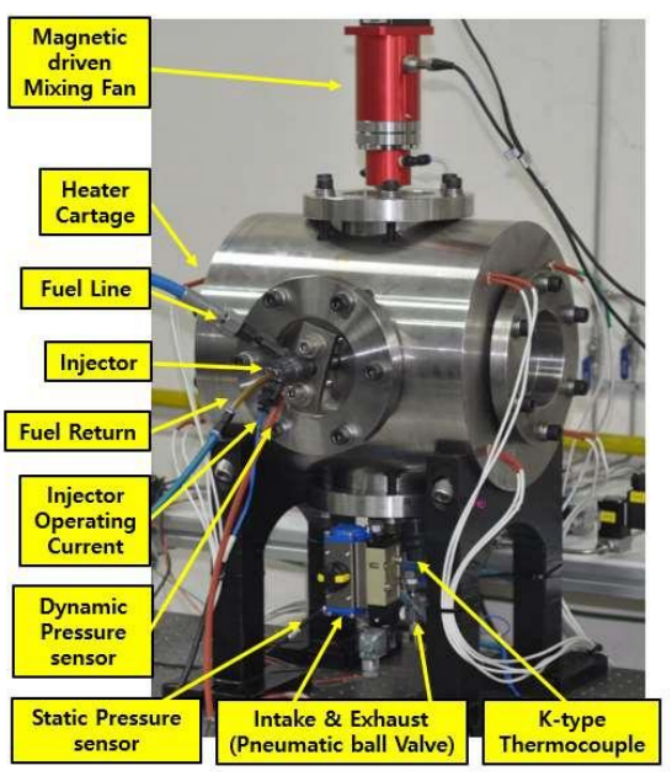

Figure 3.1: Assembled CVCC with different test equipment

The Smart Powertrain Lab's CVCC is cubically shaped with an internal volume of 1.3 L (with all side solid) and 1.5L (two side quartz and others side solid), respectively. Optical access is obtained by quartz windows of 120 mm diameter and 50 mm thickness. At this moment, the combustion vessel is optically accessible from two sides. To protect the glass and for safety purposes, a relief valve has been placed in the chamber. This limits the chamber maximum pressure up to 120 bar. No higher pressures can be obtained over 100 bars due to safety purposes. Inside the combustion chamber, equipment is placed to collect data from an experiment. The equipment is mounted in the vertical and horizontal sections from the different sides of the vessel, as shown in Figure 3.1. The magnetically driven mixing fan is employed to

achieve a homogeneous mixture during the filling of the different gasses and uniform temperature distribution during the pre-combustion. The spark plug is used to ignite the gas mixture, thus initiating the pre-combustion. A fuel injector is placed in the combustion chamber in such a way that the injected fuel will propagate along the vertical axis of the chamber. This allows the fuel to travel the longest possible way before impinging to the opposite chamber wall.

In a real engine, successive combustion cycles will heat the cylinder walls, affecting the internal processes. For this reason, all the chamber walls can be heated up to 100°C by using the heater cartridge directly mounted in the chamber walls. Heating the chamber walls is also employed to avoid the condensation of the quartz windows after pre-combustion. Smart Powertrain Lab's CVCC has been modified to ensure the full control of different types of equipment at the same time domain. In the current modification, intake and exhaust valves can automatically and directly control from the LabVIEW program. A control box ensures the homogeneous mixing of the combustible gas by using a magnetically driven stirrer. The spark plug can now initiate the spark ignition automatically after a given time duration in milliseconds, and the spark duration can be able to adjust by the user in the microseconds scale. After the desired thermodynamic condition, fuel is injected for a short time frame, and the NI DAQ assistant records the value from the beginning of the pre-combustion until a specific time after completing the spray combustion.

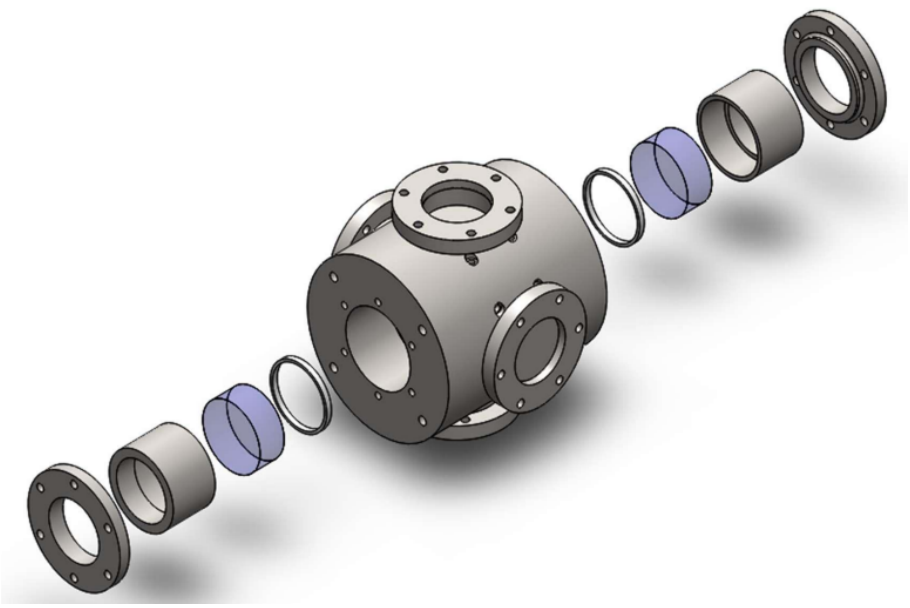

Figure 3.2: Exploded view of the CVCC with quartz

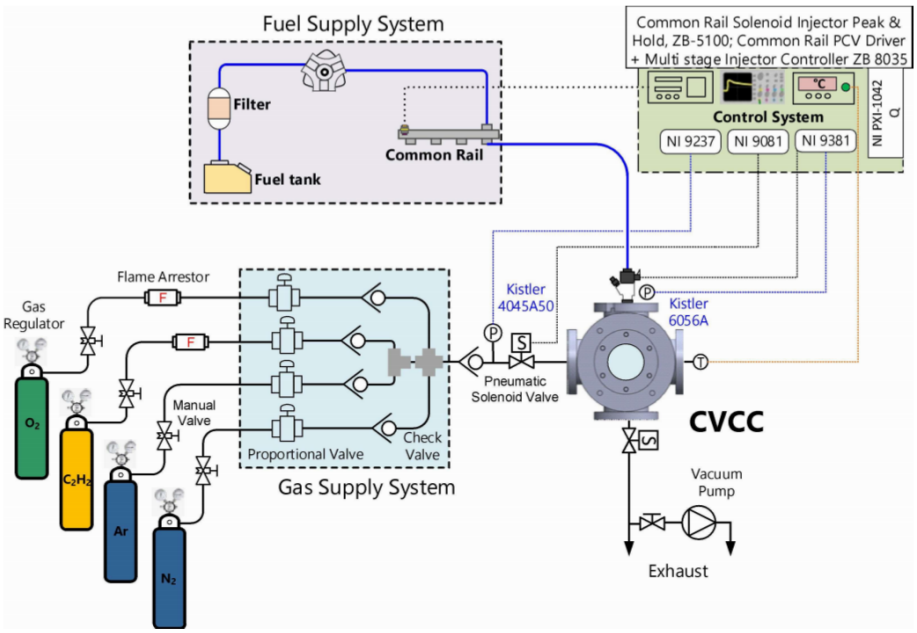

Figure 3.3: Schematic of the CVCC apparatus implemented in the experiments

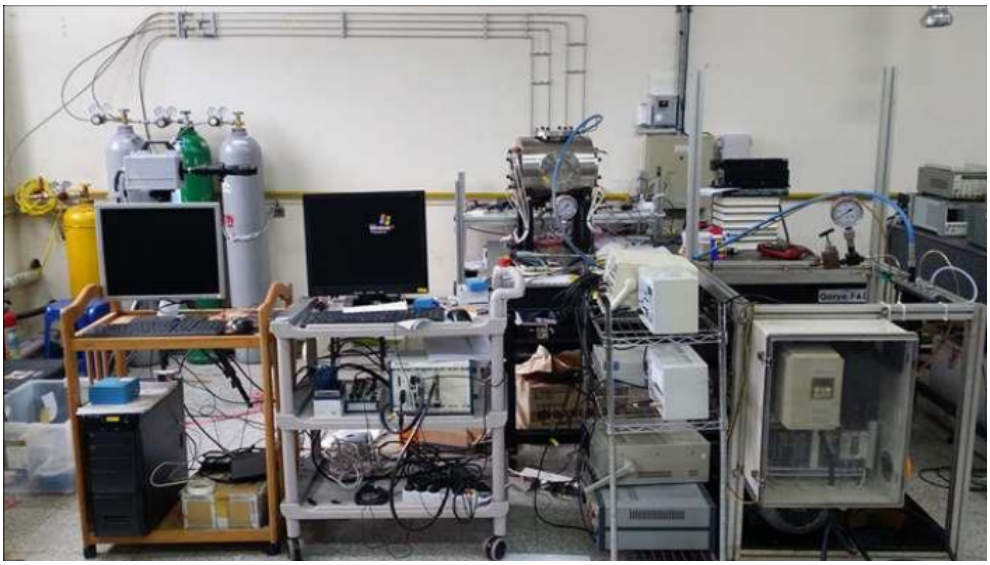

Figure 3.4: Pictorial layout of experimental test bench

A schematic drawing and a picture of the experimental test facility are shown in Figures 3.2 to 3.4. As it can be seen from the cut-through schematic, the CVCC is a cube-shaped vessel which has a large optically accessible combustion chamber of 110 mm from different sides, allowing extensive visualization of the fuel spray before wall impingement. For example, the top window can be used for mixing fan and turbulence generation by using a rotating fan. Besides that, there are inlet and exhaust valves to deliver and vent gas in and out of the chamber,

respectively. A dynamic pressure transducer (Kisler 6001) was placed in the bottom corner of the combustion vessel with a pressure range of 0 to 250 bar. The combustion vessel is truly one of a kind experimental apparatus to understand the physics of combustion (spark-ignition or spray combustion) inside the vessel. Main chamber dimensions, sensors and acquisition apparatus are collected in Table 3.1.

Table 3.1: An overall information of the test system and additional equipment

Basic Parameter		Unit
Shape of the internal chamber	115 × 115 × 115	mm
Window aperture	110	mm
Injector mounting	Side Window	
Number of spark plugs	1	
Spark plug position	Bottom Window	
Combustible gas fill	Sequential	
Mixing fan location	Top window	

Measurement Condition			
	Minimum	Maximum	Unit
Ambient denstiy	5	20	bar
Ambient temperature	298	1000	K
Oxygen concentration	0	0.21	vol fraction
Wall temperature	293	443	K
Fuel temperature	Ambient	NA	K
Common rail pressure	300	1350	bar
Injection duration	800	2000	μs

Auxiliary system		
Proportional valve	Burkert 2875(only N_2), Burkert 2873	0-25, 0-16 bar
Intake Valve	Pneumatic ball Valve	0- 10 bar
Exhaust Valve	Pneumatic ball Valve	0- 10 bar
Vacuum pump	Spaemax Rocker 400	.5mbar Hg
Ignition coils driver	Mobiq Ignition Coil Driver	
Sprak Plug	Denso IRIDIUM(SK16PR-A11)	
Mixing Fan	Propeller type magnetic driven fan	

Sensor & Data Acquisition		
DAQ & control software	NI PXI 1042Q & LabVIEW	
Static gas pressure sensor	Peizo resistive Kristler 4045A50	0 - 50 bar
High Pressure calibrator	Sensys PSHHC020BCPG	0- 20 bar
Low pressure calibrator	Sensys PSHHC002BCPG	0- 2 bar
Dynamic gas pressure sensor	Peizo resistive Kristler 6056A	0 -250 bar
Vessel temperature sensor	Thermocouple K type **mm	
Module for Pressure measuement	NI 9237	
Module for Proportional Valve	NI 9238	

3.1.2 Supply and Exhaust System

The schematic diagram of supply and exhaust system is described in Figure 3.5. The premixed charge is selected as acetylene, argon, oxygen, and nitrogen. Each gas is filled into the CVCC step by step by promotional valves (Burkert 8605) to reach desired partial pressure targets. The Labview program controls the filling procedure by the PID method as a filling program. A pressure transducer (4045A50) is used to measure in-chamber pressure as feedback to the filling program during the filling process. The filling procedure is automatic during the experiment and probably produces stable test conditions.

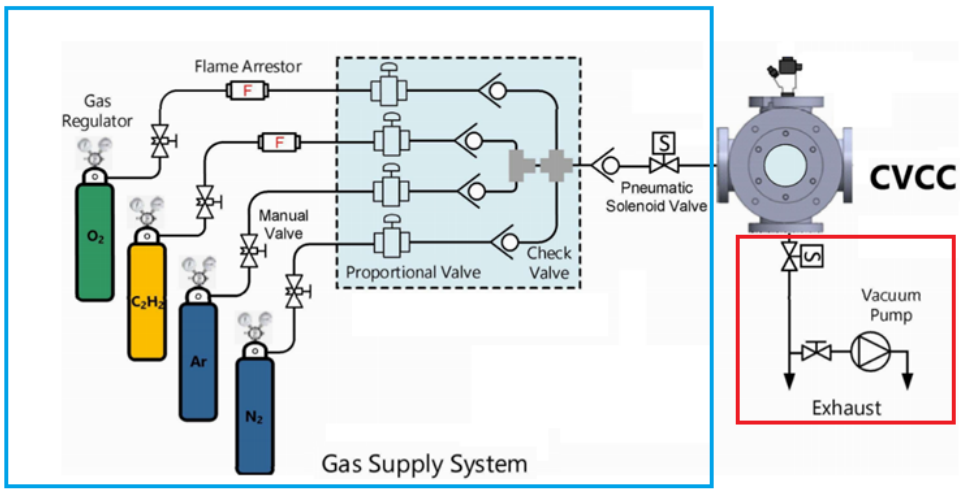

Figure 3.5: Schematic diagram of supply and exhaust system

3.2 RCEM System

The RCEM was installed with all the additional equipment required for its full operation and control, as shown in Figure 3.6. This RCEM was designed to be similar to a type of single-cylinder diesel engine that includes a compression stroke and an expansion stroke and can carry out a wide range of temperatures and pressures. The bore and stroke of the RCEM are 100 mm and 450 mm, respectively. The compression ratio of the RCEM can be changed from 10 to 23.5 by adjusting the clearance volume. The initial temperature ranges from 273 K to 383 K by controlling the heat through a circular band heater on the cylinder jacket and pre-heater on the intake line. A control panel drives an electric motor before the start of the experiments. Once the start signal is generated, the connecting rod starts to move through an electronic clutch, and one compression and expansion cycle occurs. Since there is no previous cycle, the effects of residual gas and lubrication oil can be ignored. A piezoelectric pressure sensor (Kistler

6053C60), which was coupled to a charge amplifier (Kistler 5018), was used to measure the dynamic pressure in the combustion chamber. LabVIEW software was installed on a National Instruments computer (NI PXI-8106) with a multifunction DAQ (model NI PXI-6251) and a reconfigurable I/O (model NI PXI-7813R). The multifunction DAQ was used to collect pressure data in the combustion chamber. The reconfigurable I/O was used to control an injector and spray the test fuel. This measurement system can measure an extensive range of dynamic pressures during compression, combustion, and expansion. The system also allows for registration of higher frequencies (up to 100 kHz). Additionally, a rotary encoder (EP50S8-1024) was attached to the crankshaft to measure the piston displacement. The signal pulse and error of the encoder are 0.3515º±15'. The fuel injection system of the RCEM was equipped with common-rail flexible injection hardware (Zenobalti ZB-1100) to control the fuel pressure in the fuel supply system up to 1600 bar. A common-rail solenoid injector peak and a hold driver Zenobalti ZB-5000 (controlled by the NI computer mentioned above) were used to drive the injector to spray the test fuel into the combustion chamber.

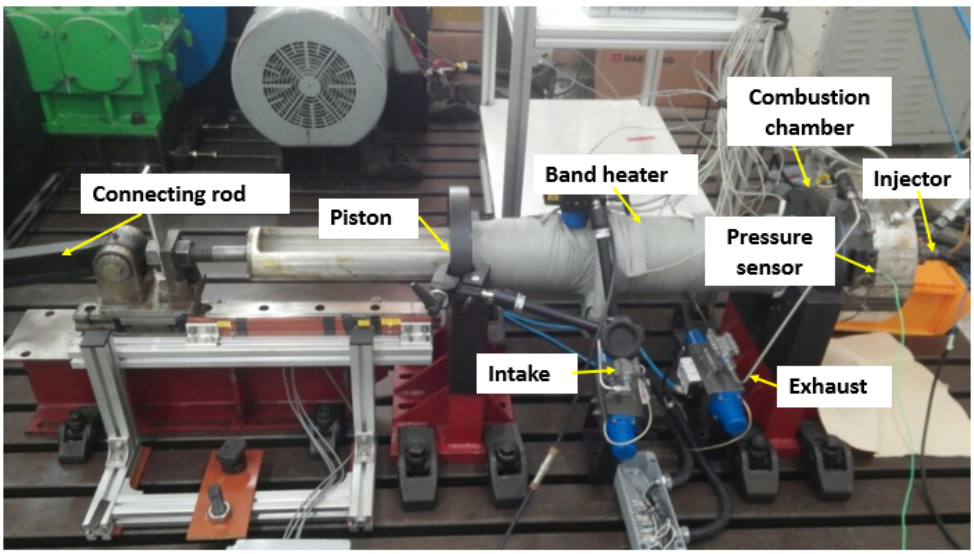

Figure 3.6: Picture of the RCEM.

3.3 Data acquisition and control system

The schematic of the control and data acquisition system is presented in Figure 3.7. All control and data collection activities are automatically controlled by the IN computer, which is used to run an in-house designed LabView interface for controlling the filling of gas, the flushing of exhaust, and the initiation of the combustion sequence. This interface also allows for adjusting all the relevant operating parameters. A second computer is used to control the

high–speed camera and to change all the camera settings. The ignition signal from LabView is used to trigger the recording of the high-speed camera.

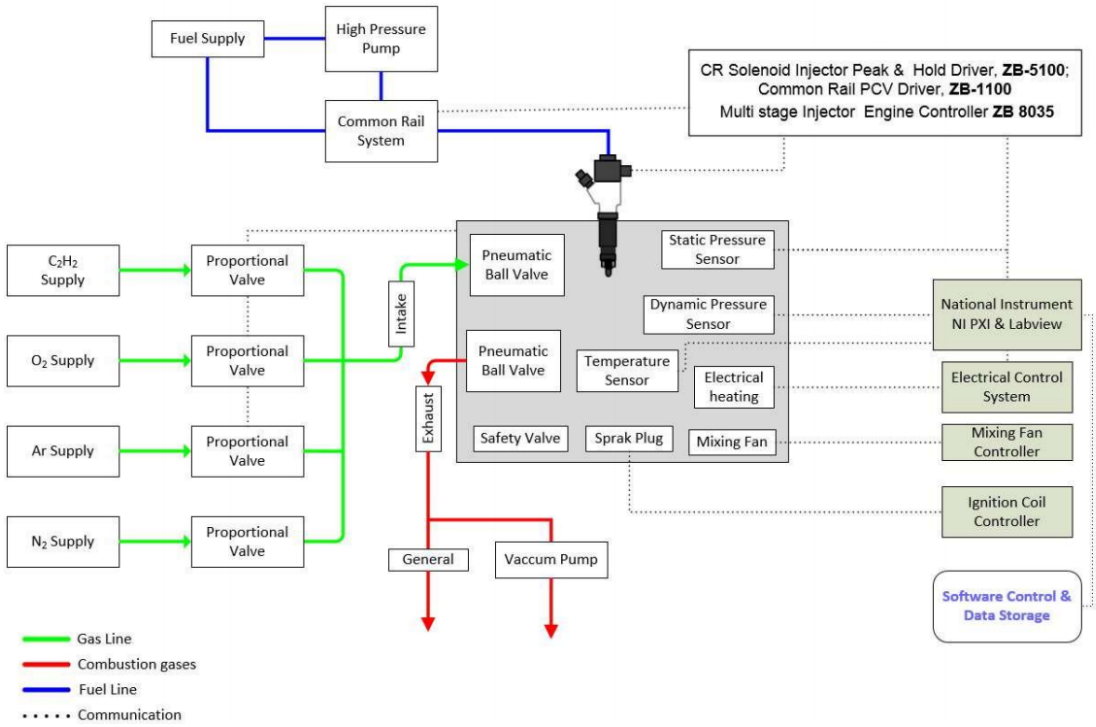

Figure 3.7: Schematic of control and data acquisition system

3.3.1 Control system

Figure 3.8 shows a schematic of the control system used in the current study. The tasks were divided into four main categories: high-speed, high resolution, mid-speed, low speed, and digital tasks. The experiments were controlled using a National Instruments (NI) PXI-7813R connected to NI 9472, NI 9237, NI 9381, and NI 4910 through cRIO 9515 expansion chassis. NI 9472 connects and controls the intake valve, exhaust valve, sensor valve, bump valve, total valve, mixing fan, and vacuum pump. IN 9237 connects to two pressure sensors to measure the pressure in the combustion chamber during the filling process. NI 9381 links and manages four promotional valves to fill up the charged gases. NI 9410 is tasked to trigger the spark plug and injector. All high-speed analog data (vessel pressure, injection command, spark command, and injection pressure) were monitored using a 24-bit, 50 kHz. Oxidizer inlet pressure, acetylene inlet pressure, and mixing fan speeds were monitored using a 16-bit, 50 Hz NI 9237 module. Hydraulic cylinders were used to actuate the intake valve and exhaust valve.

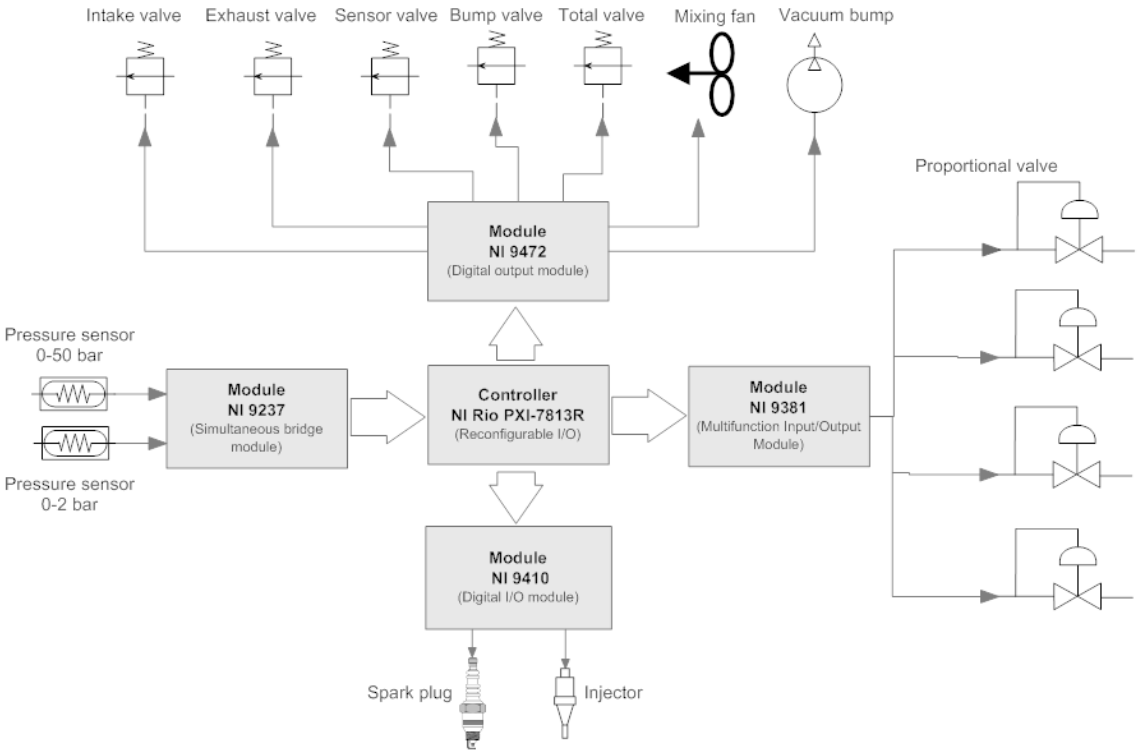

Figure 3.8: Schematic diagram of control system

3.3.2 Data acquisition system

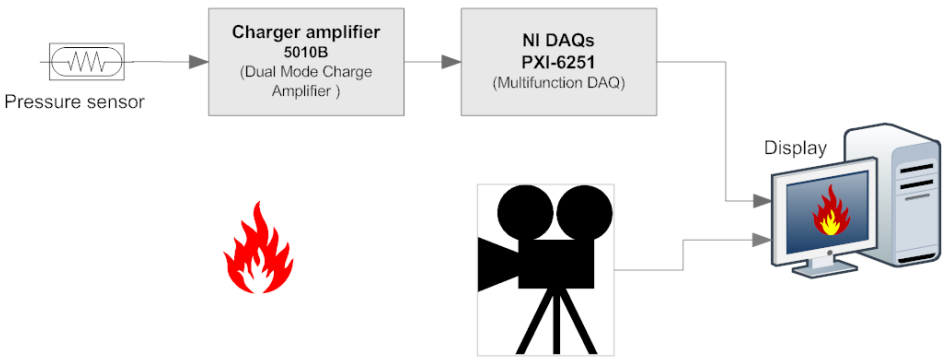

Figure 3.9: Schematic diagram of data acquisition system

Figures 3.9 and 3.10 show a schematic and picture of the data acquisition system used in the current study, respectively. The data acquisition system has collected the data using the NI PXI 6251 multifunction DAQ, coupled with the BNC-2120 module. The tasks were divided into two main categories: pressure history in the combustion chamber and the imaging of the combustion flame of the fuel sample. The high-speed camera with PFV software is used to obtain a series of images of the combustion process. The high dynamic pressure transducer is

also unitized to record the pressure trace generated the heat release from fuel burning. The charge amplifier 5010B and IN PXI 6251 amplifies and convert the signal from the pressure sensor to proper digital signal and automatically saved to excel file.

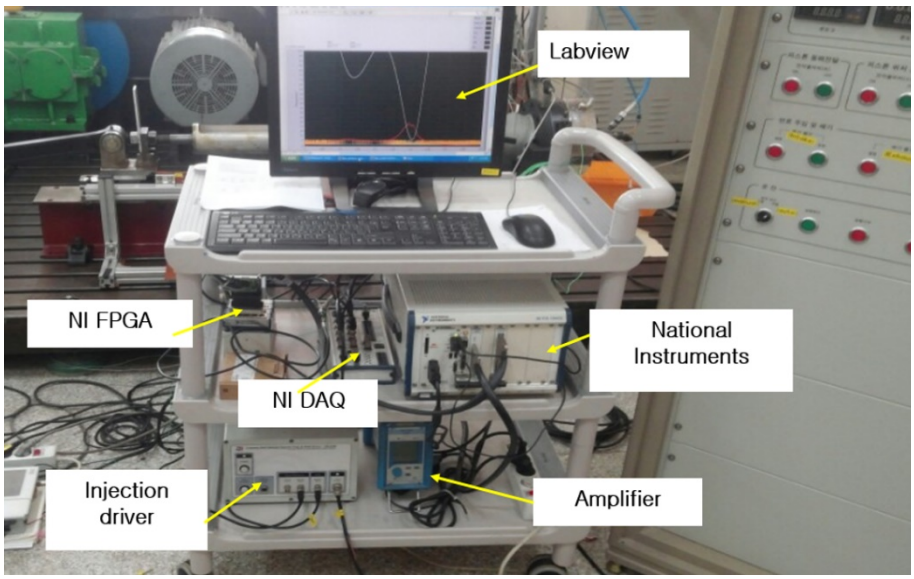

Figure 3.10: Pictorial representation of control and data acquisition system

3.3.3 Control program

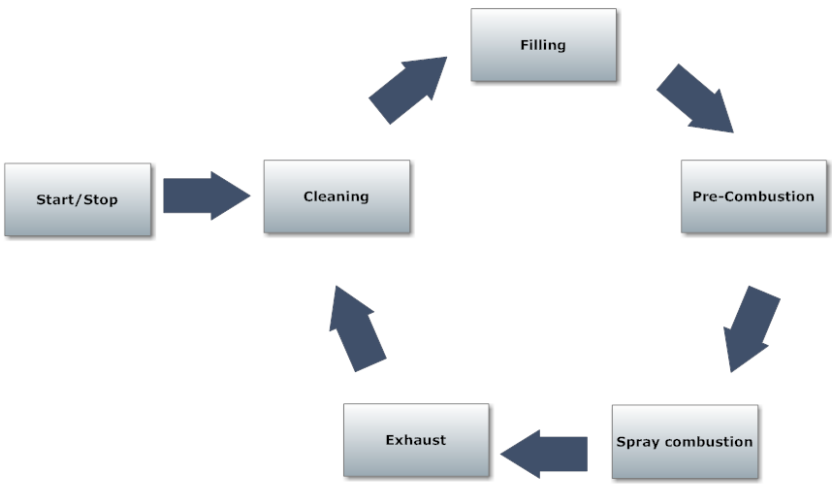

Figure 3.11: Control-flow diagram

The operation of the CVCC is formed in a logical order or sequence, as illustrated in Figure 3.11. The start/stop button is used to turn on or turn off the CVCC operation. Soon after the start/stop button is turned on, the cleaning process begins to throughout all gases inside the chamber; then the filling process starts, etc. the last one is exhaust process.

3.3.3.1 Filling process

The filling process is an important step because this process effects the precise of experimental results. The sequence of the process is illustrated in Figure 3.12. First, Argon (Ar) is filled by the PID control method to reach the desired target. Then, the gas is filled as Acetylene (C_2H_2). Next, oxygen (O_2) is filled. The last one is Nitrogen (N_2). During the filling process, there are two different pressure sensors used to monitor the in-chamber pressure. One is high-precise sensor uses for monitoring the acetylene and argon; the another is typical pressure sensor used for measuring nitrogen and oxygen.

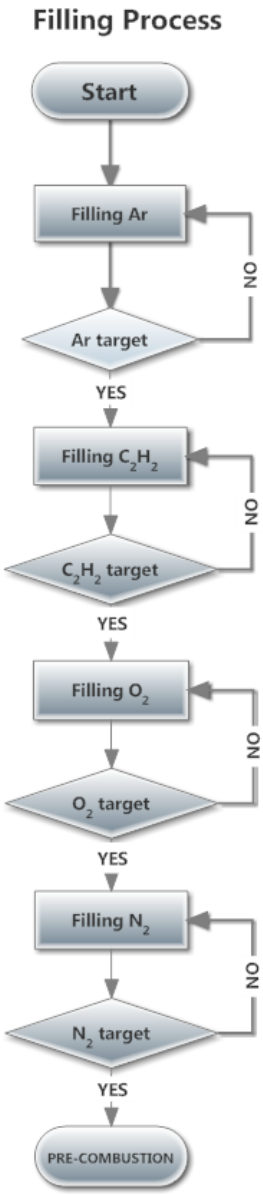

Figure 3.12: Schematic diagram of sequence of filling gases

This process is essential and effects the error of the test results, also the stability of the system of the result. In particular, it can cause detonation called knocking is an extremely dangerous situation. The knocking occurs when the amount of C_2H_2 is somehow too rich in the combustion chamber. The spark plug is triggered, the mixture will be burned in the very fast way, consequently in-chamber pressure suddenly abnormally rises and makes a sound like a bomb. Figure 3.13 presents the increase of in-chamber pressure when the knocking occurs. It may cause an explosion in the pipe, chamber and harm the human's life.

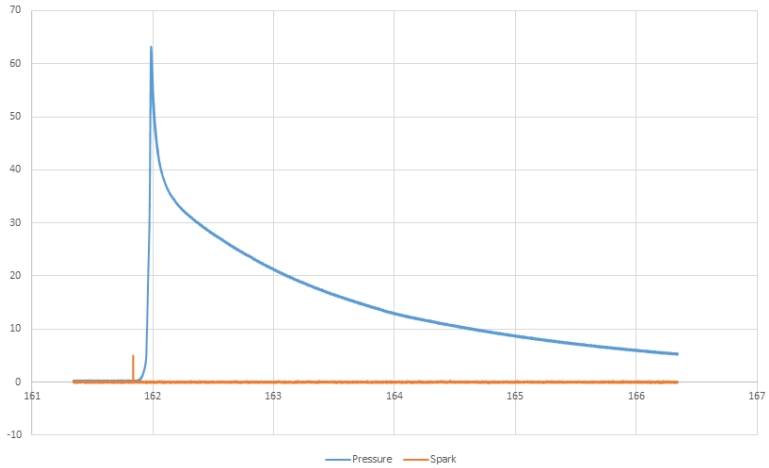

Figure 3.13: Pressure in the combustion chamber when knocking

Figure 3.14: The quarts is broken due to the knocking

The knocking causes the breaking up of the devices such as the glass window, as shown in Figure 3.14. Therefore, to reduce the severe problem, the diagnostic program is designed for this problem. The diagnostic application is functioning as diagnose the problem that occurred

in the process and gives the warning and turn off the program to prevent the knocking until the problem is fixed.

3.3.3.2 Diagnostic function

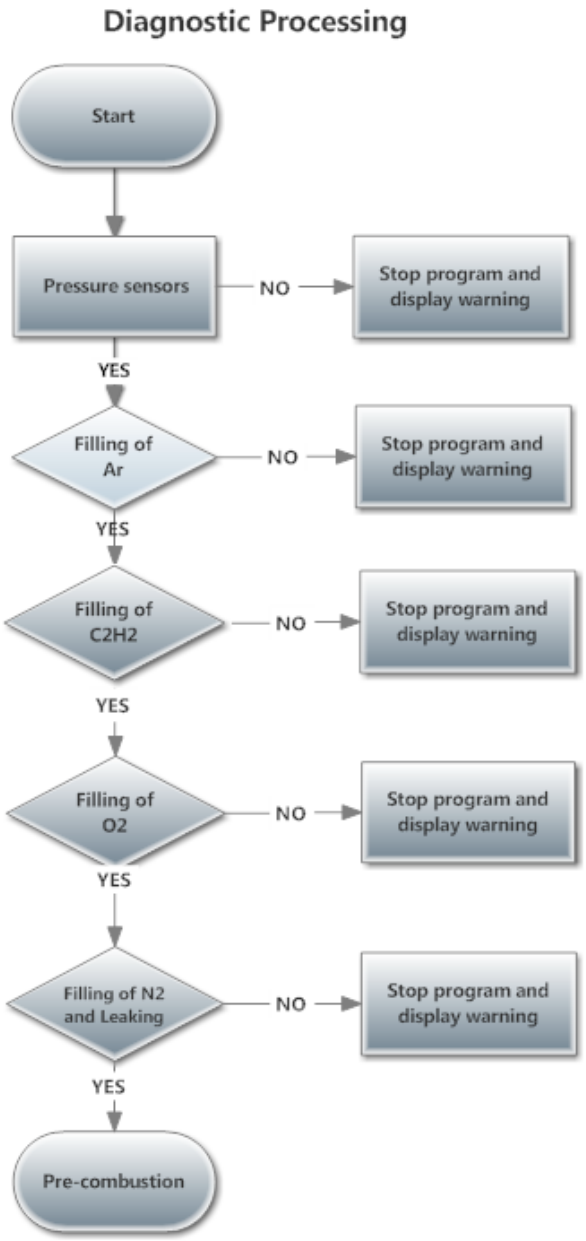

Figure 3.15: Sequence of diagnosis

The operation of CVCC is fully automatic and highly reliable. However, the unexpected events that happened in that process are inevitable. For example, the pressure sensor after a long period of operation may be inaccurate or disconnect, do not transmit the data to the controller, which causes the signal to be sent to the controlled unit to no longer be accurate.

This can lead to a dangerous situation, for example, because of misunderstanding the pressure in the combustion chamber may cause the filling too much fuel of C_2H_2, thus the knocking phenomena damaging the glass window as shown in Figure 3.14. So, the diagnostic program to prevent knocking is very necessary. The diagnostic application is designed as Figure 3.15 and devised into five steps as below.

Step 1: the program checks the connection of the sensor and the sensor properties at the atmospheric condition. The rule is that there is not any connection problem; the value from both pressure sensors will be approximately zero. Because during this time, the combustion chamber connects with the atmosphere, so the in-chamber pressure must reflex the pressure of air as around 0. The received value of both sensors is approximately zero; the sensor and the connection are considered good. Otherwise, there is a problem with the connection or the sensor; then, a warning message is displayed.

Step 2: The program is to check the filling of argon. Soon after the argon filling process ends, the diagnostic process is activated; the sensor receives the combustion chamber pressure value and compares it with the target value. If the error between the sensor and the target is less than 0.001 bar, the filling of argon is considered to be good, and the consequence go to the next step is the filling of acetylene. On the contrary, the error exceeds the target value, the warning message is given, and the program will be stopped.

Step 3: the program checks the filling process of acetylene, similar to argon.

Step 4: the program checks the filling process of oxygen is like the argon, but only the sensor with lower accuracy is used as a feedback signal, and the diagnostic threshold value is 0.01 bar. In this case, the pressure in the combustion chamber is higher than the range of the high-precision sensor, so the sensor valve is closed to isolate the sensor and chamber to protect the sensor.

Step 5: the program checks the nitrogen is also like the last step. However, this step is also used to check chamber leakage. After the combustion chambers are isolated by closing all valves for 10 minutes, the pressure in the chamber is measured and compared with the target pressure. If the difference exceeds 0.02 bar, the warning message is given. Because the reason may be a wrong filling process, this pressure doesn't reach the desired value. Another reason may be due to the combustion chamber is leaked, so after a few minutes, the large amount of

gas goes out. Whereas the value is lower than the threshold, the filling process is complete, and the next process is getting to start as the pre-combustion process.

3.3.3.3 Exhaust and cleaning process

When the program starts, firstly, the exhaust and cleaning process performs. The exhaust valve is open to exhaust gas products to the venting. The bump valve is opened to connect the vacuum pump to the combustion chamber. The sub-exhaust valve is closed to prevent the combustion chamber connecting outside. The vacuum pump runs to suck gas products for 60 seconds. The intake valve is opened to fill Nitrogen gas (N_2), and the fan runs to mix for 30 seconds, and the sub-exhaust gas is opened to exhaust the gases to the venting, the vacuum bum is rerun to suck gas in the combustion chamber for 60 seconds. Next, Nitrogen gas is filled to the chamber (1bar), then sub-exhaust and exhaust valves are opened to exhaust gas to the venting until gas pressure in the chamber is environmental pressure (1atm). The exhaust valve is closed. The exhaust and cleaning process finishes.

3.4 Fuel supply system

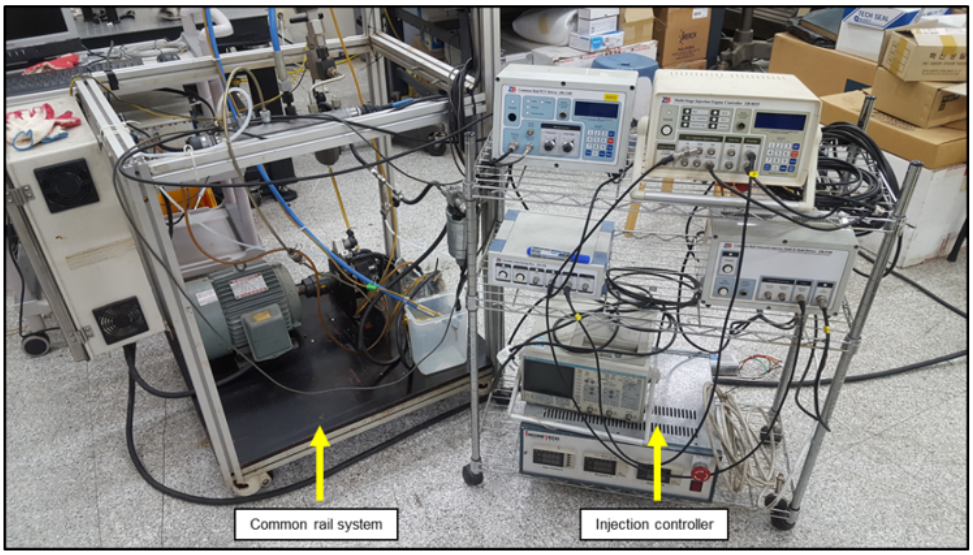

Figure 3.16: Pictorial representation of fuel injection system

The fuel system is a common-rail direct fuel injection system that features a peak and hold injector driver (ZB-5100), a common-rail injection pressure controller (ZB-1100), pressure control valve, rail pressure sensor, high-pressure pump, low-pressure pump, and a single-hold. The pressure controller is used to manage the fuel pressure through the pressure control valve up to 1800 bar. Additionally, a LabVIEW program installed on the NI computer

is used to control the injection timing and injection duration by using feedback from the pressure sensor installed in the chamber.

3.5 Pressure trace

Table 3.2: Technical data of pressure sensor

Change Input		
Connector Type	BNC neg. or TRIAX neg.	
Measuring range FS	pC	±2 … 2 200 000
Measurement uncertainty		
Ranges FS <10 pC	%	<±2
Ranges FS <100 pC	%	<±0,6
Ranges FS ≥100 pC	%	<±0,3
Drift, measuring mode DC (Long)		
at 25 °C, max. relative Humidity RH of 60 % (non-condensing)	pC/s	<±0,03
at 50 °C, max. relative Humidity RH of 50 % (non-condensing)	pC/s	<±0,3
Max. common mode voltage between input and output ground	V	<±25
Overload	%FS	≈±110

Table 3.3: Technical data of pressure sensor

Range	bar	0 ... 250
Calibrated partial ranges	bar	0 ... 50
	bar	0 ... 2,5
Overload	bar	300
Sensitivity	pC/bar	≈–25
Natural frequency	kHz	≈90
Linearity, all ranges	% FSO	≤±0,5
Acceleration sensitivity		
axial (with cooling)	bar/g	<0,01
radial (with cooling)	bar/g	<0,001
Operating temperature range	°C	<50 ... 350
Cooling water flow	l/min.	0,3 ... 0,5
Sensitivity shift		
50 ±35 °C	%	≤±0,5
50 ... 350 °C	%/°C	≤0,01
Thermo shock		
bei 1 500 1/min, 9 bar p_{mi}		
Δp	bar	<±0,2
Δp_{mi}	%	<±1
Insulation resistance at 20 °C	TΩ	≥10
Shock resistance	g	2 000
Tightening torque	N·m	10
Cooling water pressure	bar	≤6
Capacitance, with cable	pF	110
Weight	g	18
Plug, ceramic insulator	Type	M4x0,35

The quartz pressure sensor in the current study, referred to as the thermo-dynamic quartz pressure sensor (6061B), is the use of polystable quartz elements and well suited for thermo-dynamic measurements in small combustion engines. The sensor was paired to the single-channel laboratory charge amplifier (Kistler 5018A) and sampled at 200 kHz with 12-bit A/D resolution. However, the care amplifier is flexible by adjusting the setting panel to adapt each sensor and test condition as described below.

3.6 Optical diagnostic system

The emission of light during the combustion process was imaged at high speed to obtain the spray combustion information. The broadband chemiluminescence technique is applied to determine where and when combustion takes place in the combustion chamber. The effectiveness of the method has been presented and demonstrated in many previous studies [21] [32]. Figure 3.17 illustrated the optical arrangement, and Table 3.4 listed the camera settings for the broadband chemiluminescence method in this work. One 600 nm optical short-pass filter was used to remove the effects of later soot incandescence and any species emitting in the high wavelength range while collecting other radicals (e.g., CH*, C2*).

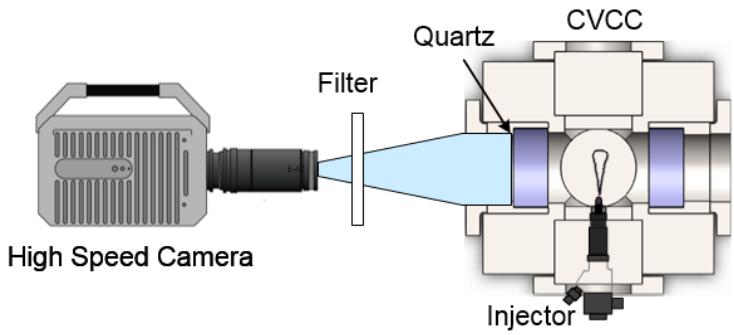

Figure 3.17: Optical arrangement for the broadband chemiluminescence technique.

Table 3.4: Camera specifications.

Camera	Photron SA1.1
Lens	AF Micro-Nikkor 60mm f/2.8D
Frame rate	20000 fps
Optical filter	600 nm Shortpass
Exposure time	50 μs
Resolution	512x256
Scale	0.196 mm/pixel

3.7 Image processing

Image processing is an important step for detecting the bright spot in the combustion images in this study. The computer algorithms used to separate the frame and the background are based on the criteria of thresholding, image segmentation, and morphological filtering. In general terms, the background slightly changed during the combustion process due to the brightness of the flame. Therefore, the Gaussian method was applied to detect frames on the image background. The background detector required a certain number of video frames to initialize the Gaussian mixture model. This analysis uses the first 30 frames to initialize the Gaussian modes in the mixture model. However, the Gaussian method to split the image into the foreground and background often contains noise. The morphological structuring element was adopted as the filtering technique to reject the noise blobs and to fill gaps in the detected objects. A further noise removal technique was added to clear small spots that have a size of lesser than 25 Pixels. The image was then converted to the intensity picture with the minimum and maximum intensity values. The image processing was coded by Matlab software to automatically obtain a combustion flame in the natural soot luminous image video captured by the CMOS camera. The area of the high-temperature flame is highlighted and zoned by the red line using the ignition threshold as the previous discussion. In addition, the flame contour automatically determined to measure the flame lift-off length. The natural light emission visualization setup and image processing scheme were unchanged to ensure repeatability and accuracy. The sequence of the image processing, which undergoes five steps, is presented as the Figure 3.18 below.

Step 1: Image processing with Kittler-Illingworth method in which the flame is segmented from the background.

Step 2: The background after using filters (morphological structuring element + removing small blobs)

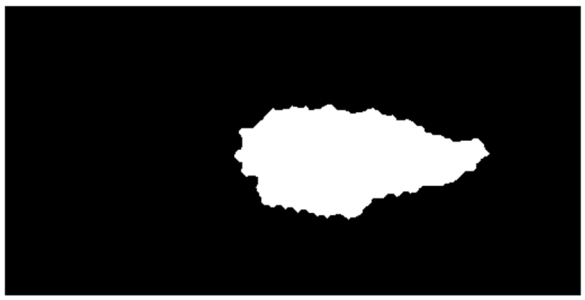

Step 3: Flame image after removing background noise

Step 4: Flame images with the pixel intensities plotted in color contour mode

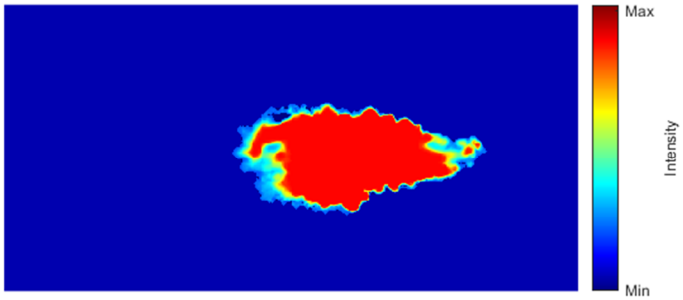

Step 5: Flame images with the flame boundary zoned by the brown line for measuring the lift-off length.

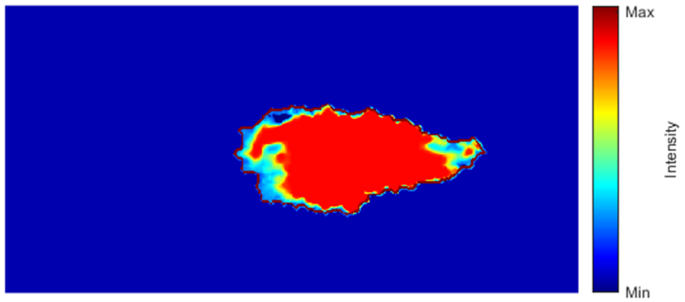

Figure 3.18: Sequence of image processing

4 Effect of biodiesel addition on auto ignition delay and lift of length under low-temperature condition

A detailed experimental study on gasoline biodiesel fuel blends was conducted to investigate its ignition and combustion characteristics under low-temperature range using an optically accessible constant volume combustion chamber. The fuel samples were four GB blends including GB20, GB40, GB60 and GB80 corresponding to 20 %, 40 %, 60 %, and 80 % volumetric biodiesel respectively, neat gasoline, and neat biodiesel. Fuel samples were injected into the CVCC to com-bust using a single-hole research-grade injector. Natural soot luminous images from the combustible flame were captured by a CMOS camera to determine the ignition delay and the flame lift-off length. The ignition delay was also obtained by analyzing pressure traces from a high-frequency piezoelectric pressure transducer. The results regarding the ignition process for the pressure-based and luminosity-based ignition delays showed that both approaches presented similar tendencies. However, the pressure-based ignition delay is always a little longer than the luminosity-based ignition delay. The difference between the two definitions of ignition delay tends to decrease with the longer ignition delay or the enhanced mixing, and vice versa. As lower 60% biodiesel fractions, the increase of biodiesel significantly reduced ignition delay and produced a lower maximum peak of heat release rate. The combustion characteristic of blend with a higher 60% biodiesel is almost similar to pure biodiesel. In general, lift-off length lengthens with an increase in biodiesel because of its high viscosity and high surface tension. However, for the 750 K case, the lift-off length decreases due to a rapidly reduced ignition delay with the increase in biodiesel fraction (less than 60 % biodiesel). Based on experimental data, the moderate biodiesel addition (less than 20%) can improve the ability of cold-engine starting, also solve engine misfire under low-load-condition operation due to its flammability while maintaining advantages of gasoline with great volatility and high ignition delay which significantly enhance the mixture formation process.

4.1 Introduction

Over their hundred-year development, compression ignition engines have evolved into one of the world's most capable and reliable forms of motive power for transportation due to high fuel efficiency and high-power output. To meet stringent emission standards and satisfy the demand for decreasing fuel consumption, the CI engines need to continue to adapt the fuel consumption and improve to reduce emissions while retaining engine performance and power

output. Emissions of nitrogen oxides, total hydrocarbons, carbon monoxide, particulate matter, and greenhouse gases have been a severe problem that needs to be solved for CI engines. Hence, near-term solutions, including diesel oxidation catalysts, diesel particulate filters, selective catalytic reduction, and lean NOx trap regeneration, have been used to remove the emissions. High cost is a big barrier to the after-treatment techniques to apply commonly in IC engines. Additionally, diversifying combustion methods and using alternative fuel are long-term solutions to reduce pollutant emissions.

One of the long-term solutions, gasoline fuel has been used for CI engines to increase engine efficiency and significantly reduce hazardous emissions such as NOx and soot emission. The prospective combustion method is referred to as the gasoline compression ignition since it relies on gasoline fuel to reach its auto-ignition limitation in CI engines. The GCI utilizes the advantage of low-temperature combustion to stay out of the high soot and NOx formation zones while increasing thermal efficiency such that it approaches that of a diesel engine [88] [89] [90]. However, the future challenge of GCI engines is somewhat questionable due to its limitation in the low load operating range. Gasoline is highly volatile and shows poor self-ignition. Therefore, it helps to extend the air-fuel mixing time to reach a homogeneous charge compression ignition mode. But the problem is that it is hard to combust/ignite at low-temperature conditions such as cold-start, low-load engine conditions. To solve these problems, the fuel must be highly chemically reactive, and so diesel or biodiesel [91] is added and mixed with the gasoline to improve its ignition characteristics.

For example, Hanson et al. [92] used reactivity controlled compression ignition approach for gasoline-diesel dual fuel to reduce NOx and PM emissions, while maintaining high efficiency using the KIVA 3V software combining with experiment. The authors found that brake thermal efficiency was improved from 37% to 40%, increasing combustion efficiency to 96%, and low NOx and PM emissions. Yang et al. [18] carried out numerical simulation and experiments for gasoline-diesel fuel under two different combustion strategies: highly premixed charge combustion and low-temperature combustion. The authors found that low-temperature combustion mode leads to a fast heat release rate and a high maximum pressure rise rate because of the coupling combustion reaction of gasoline and diesel taking place in regions with higher fuel concentration. The early-highly premixed charge combustion reduces NOx and soot emissions due to the avoidance of high equivalence ratio and high-temperature region in the combustion chamber. Curran et al. [19] experimented the fuel

blending of gasoline with diesel controlled the combustion phasing to improve efficiency and emission. The authors found that the controllability of cylinder-to-cylinder balancing is the most important determinant for obtaining stable combustion and high thermal efficiency. The study also showed an increase in thermal efficiency, and an approximate 90% reduction in NOx and PM and brake thermal efficiency of 33.5 %. Adams et al. [22] used gasoline blending with biodiesel content at 5% and 10% levels to extend to the low load conditions, enhance the combustion stability, and reduce the intake temperature requirement. Yanu et al. [23] [24] studied the change of injection timing, exhaust gas recirculation, and different intake air temperatures to gain an optimum region for GB blended fuels with 5%, 10%, 15%, and 20% biodiesel. The research showed that the thermal efficiency archives approximately 92 %; also, THC and CO emissions diminished 50% compared to diesel. Use of biodiesel fuel blending with gasoline is a possible way to extend GCI combustion to low load condition due to its high ignitability. Moreover, biodiesel fuel is an alternative fuel that can be used in regular diesel engines without making any changes to the engines and is currently of great interest and an important research subject for reducing soot formation, harmful gas emissions, and greenhouse gas. It is a clean and renewable energy source with superior lubricity, free of sulfur, and free of aromatics. Biodiesel can synthesize from abundant feedstocks, which drive to various chemical structures and contain oxygen in biodiesel molecules resulting in the ability to complete combustion [93] [94]. In such situation of fossil fuels resources depletion, biodiesel fuel has attracted more and more attention.

Although many optical investigations have conducted for diesel fuel, there are no experimental measurements for GB blended fuels. Therefore, the CVCC with an optically accessible ability was used to investigate GB blends on the aspect of ignition delay and lift-off length in this work. Natural luminous soot emission images and pressure profiles were used to determine the ignition behavior and lift-off length for GB blends under low-temperature range representing cold-start and low-load engine conditions where pure gasoline is difficult to burn because of extremely high ignition delay, causing the misfiring. Both parameters play an essential role in combustion spray, which governs the engine operating range as well as engine efficiency and soot emission. The ignition delay affects the degree of fuel atomization and the amount of air entrainment into fuel spray to create an initial mixture for spray combustion [13]. Besides, the lift-off region is a critical zone where is bounded by the injector tip and the high frame region wherein the air entrainment into the jet takes place [58] [95]. We have confidence

that these experimental results will help promote the application of GB blends in low-temperature range and spray combustion modeling in the future.

4.2 Experimental methods

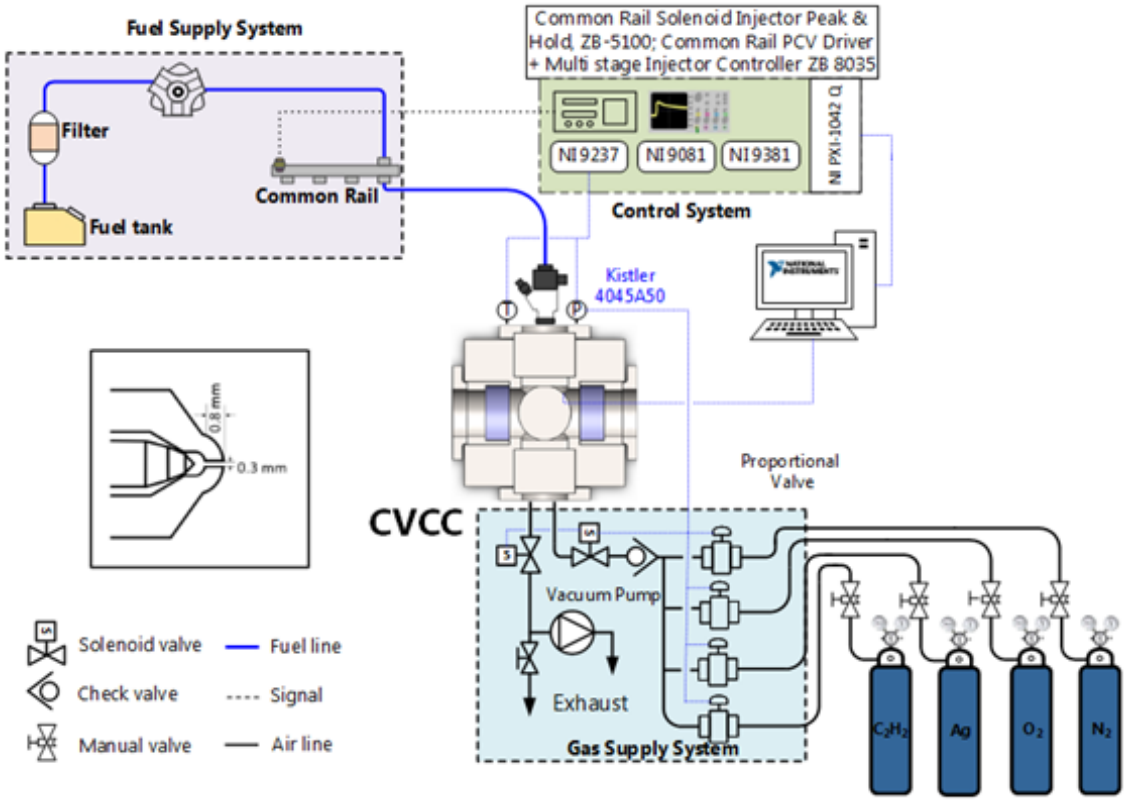

Figure 4.1: Scheme of the constant-volume combustion chamber performed in this work.

Figure 4.1 presents the CVCC including a gas supply system, a chamber body, the intake and exhaust lines, a fuel system, a fan, and a National Instruments (NI) computer. The chamber was added quartz windows to allow the optical investigation of ignition delay and lift-off length via natural luminous soot emission. The premixed charge was composed of acetylene (C_2H_2), argon (Ar), oxygen (O_2), and nitrogen (N_2) filled sequentially to reach the desired partial pressure targets. A self-written Matlab program controls proportional control valves to fill the premixed charge and a fan to mix the premixed charge homogeneously before the spark plug ignites them. The fuel system is a common-rail direct fuel injection system and can feature a high-pressure of up to 1600 bar. Eight heater elements with a PID temperature controller maintain wall temperature (353 K) to ensure complete combustion of the premixed charge gases. A high-frequency pressure sensor coupled with a charge amplifier measures dynamic pressure. The high-pressure solenoid valves were used to exhaust the hot gaseous product. On

the other hand, the chamber was quickly and automatically evacuated using a vacuum pump to remove any remaining gas to ensure the chamber is empty for the next experiment.

4.3 Optical arrangement and ignition calculation

4.3.1 Optical arrangement

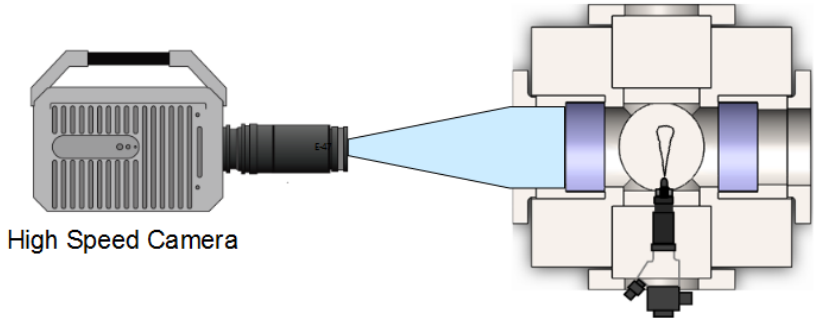

Figure 4.2: The optical set up for the natural light emission visualization.

Figure 4.2 presents the setup for observation of the natural light emission from spray combustion of gasoline-biodiesel blended fuels. A high-speed CMOS camera (Photron SA3) with a Nikkor lens was used to obtain the natural soot luminosity imaging at 512×128 pixels and rate of 20,000 frames/s, which corresponds to a 40 μs increment for each image. The injected signal from the injector triggers the camera to start recording the set of combustion images.

4.3.2 Definition of ignition delay

The time interval from the start of injection to the start of combustion was defined as the ignition delay. The start of injection is the time at which the fuel appeared at the injector tip, and the injection began. The start of injection was determined from the injected current signal, which was given to trigger the injector. All injectors have a delay due to the inertia of the needle valve and spring assembly. The injection delay was determined through macroscopic spray images in Shubra's research [56]. The start of combustion was determined via two different techniques, i.e., pressure-based ignition delay and the luminosity-based ignition delay.

The pressure ignition delay was determined by tracking the combustion pressure. The starting point of combustion was designated to be the point where the pressure starts to depart from a slight initial drop because of heat release from the combustion process. Before this point, adiabatic mixing between fuel and ambient gas takes place. In this process, the fuel is atomized,

vaporized, mixed in the chamber and slightly decreases the bulk ambient gas temperature. This definition produces the smallest difference between luminous and pressure ignition delay [73] as illustrated in Figure 4.3.

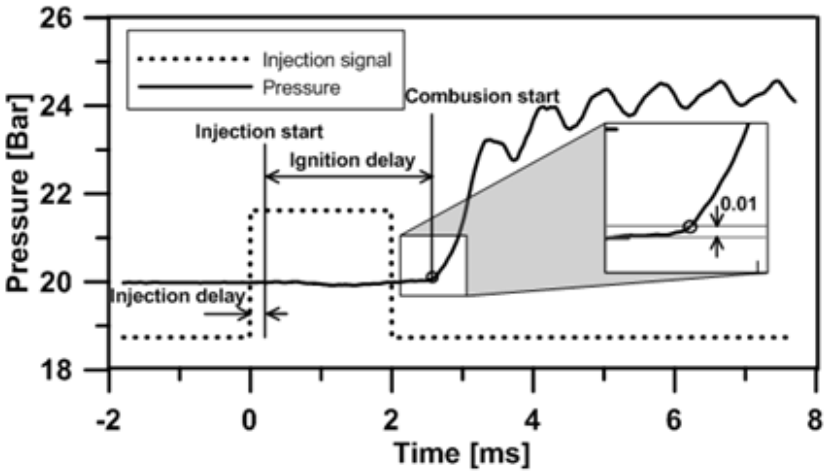

Figure 4.3: Definition of the ignition delay based on pressure trace.

The luminous ignition delay is the elapsed time from the start of injection to the time of high-temperature flame, which based on the light of the flame from the combustion of fuel. Set of combustion images captured by the CMSO camera is processed to determine the start of combustion. The image undergoes the image processing in order to extract ignition information from it. The start of combustion is timing when the high-temperature flame is getting started with high chemiluminescence and heat release. The high-temperature flame generates an intense and stable radiation called the high-temperature luminosity. The 50% digital level (125) of this value was chosen as the thresholding of high-temperature flame segmentation. This is recommended by Engine Combustion Network (ECN) guidelines and adopted in previous studies [31] [71] [59]. The threshold is significantly higher than luminosity emission from low/intermediate temperature chemistries of gasoline which generated before the main ignition stage. In this stage, the temperature can increase during the autoignition, and hence, a tiny fraction of soot could be generated. The threshold has to ensure removing it in the image processing. The threshold is also significantly lower than high high-temperature flame. The appearance of the first high-temperature flame is at 0.85 ms reflects the start of combustion. The approach has demonstrated to correspond with results from broadband chemiluminescence images, and the high-temperature flame is bounded in the red line, as shown in Figure 4.4.

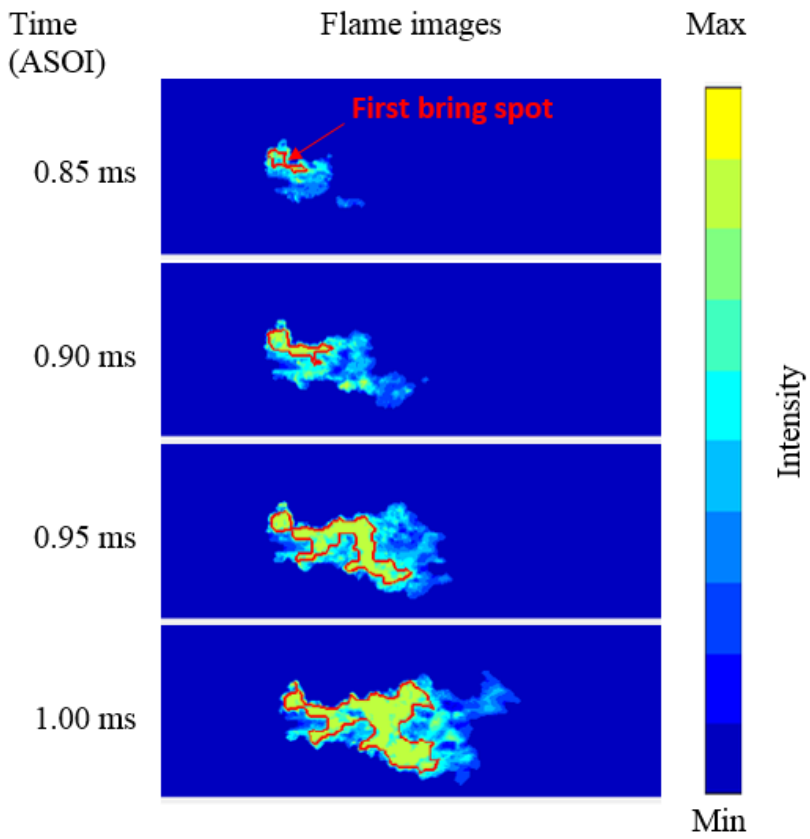

Figure 4.4: Images of combustion development sequence.

4.3.3 Evaluation of the flame lift-off length

Immediately after the fuel ignites, spray flame will locate in a relatively stabilized position slightly away from an injector orifice. The distance is called flame lift-off length, which was measured through natural light emission by soot emission, as presented in Figure 4.5. There are many factors affecting lift-off length, such as engine operating conditions, fuel properties, and injection characteristics. The lift-off length is an important factor of the spray combustion process that affects the chemical reaction directly, thus governing pollutant emission. It is the driving parameter to identify the combustion rate and soot formation and determine the amount of fuel-air premixing before combustion [74] [96]. A high-speed ICCD camera combined with optical bandpass filters was utilized to obtain the emission of light from OH radicals to determine the lift-off length [97]. However, the test equipment for this measurement requires a complicated optical setup. In some cases, there can be confusion due to the release of OH radicals from other sources. In this work, the lift-off length is measured through natural light emission by soot emission. It is much easier and simpler to perform than using OH radicals. The fundamental premise of the technique is to clear the low intensity

emission/reflection of the liquid/vapor core, and background noise. The Gaussian method is utilized to process the flame images and presented in detail in next section.

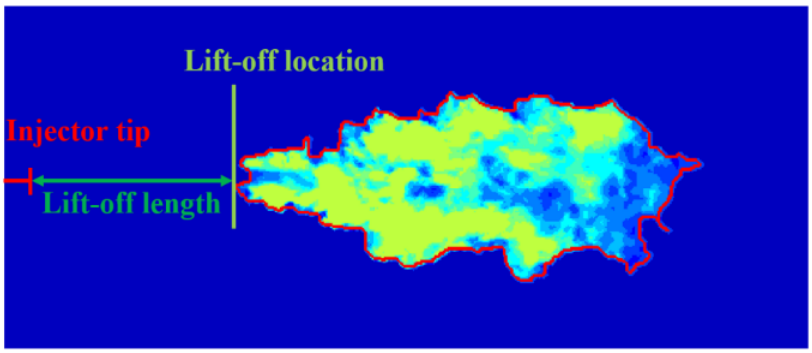

Figure 4.5: Lift-off length measurement from the natural soot emission image.

4.4 Image processing

Image processing is an important step for detecting the bright spot in the combustion images in this study. The computer algorithms used to separate frame and background are based on the criteria of thresholding, image segmentation, and morphological filtering. In general terms, the background slightly changed during the combustion process due to the brightness of the flame. Therefore, the Gaussian method was applied to detect frames on the image background. The background detector required a certain number of video frames to initialize the Gaussian mixture model [98]. This analysis uses the first 30 frames to initialize the Gaussian modes in the mixture model. However, the Gaussian method to split the image into the foreground and background often contains noise. The morphological structuring element was adopted as the filtering technique to reject the noise blobs and to fill gaps in the detected objects [99]. A further noise removal technique was added to clear small spots that have a size of lesser than 25 Pixels. The image was then converted to the intensity picture with the minimum and maximum intensity values. The image processing was coded by Matlab software to automatically obtain combustion flame in the natural soot luminous image video captured by the CMOS camera [100]. The area of the high-temperature flame is highlighted and zoned by the red line using the ignition threshold as the previous discussion. Addition, the flame contour automatically determined to measure the flame lift-off length. The natural light emission visualization setup and image processing scheme were unchanged to ensure repeatability and accuracy.

4.5 Fuel and test condition

This work aims to investigate the effects of difference gasoline-biodiesel blending ratio on its combustion spray. Therefore, a wide blending range of fuel samples, including GB20, GB40, GB60, and GB80 (biodiesel fractions of 20%, 40%, 60% and 80% by volume respectively as listed in Table 4.1) was created, then burn in the CVCC, and compare with the combustion of pure gasoline and pure biodiesel. The biodiesel was derived from soybeans, and the gasoline comes from the S-oil network, South Korea. All fuels were stored in a controlled temperature and humidity device. The homogeneous GB fuels were prepared by a rotary mixing/shaking process for 10 min to avoid phase separation and crystalline colloids. The chemical composition and properties of gasoline and biodiesel following the Korean standard had very different properties as exhibited in Table 4.2 and 4.3.

Table 4.1: Gasoline-biodiesel blended fuel compositions (vol%).

Fuel	**Component (vol%)**
G	Gasoline 100%
GB20	Gasoline 80% + Biodiesel 20%
GB40	Gasoline 60% + Biodiesel 40%
GB60	Gasoline 40% + Biodiesel 60%
GB80	Gasoline 20% + Biodiesel 80%
B	Biodiesel 100%

Table 4.2: Chemical composition and properties of gasoline.

Specification Name	**Value**	**Test Method**
RON	94	KS M 2039
Sulphur, max (ppm)	10	KS M 2027
Lead, max (g/l)	0.013	KS M 2402
Benzene, max (vol. %)	0.7	ASTM D6296
Aromatics, max (vol. %)	24	ASTM D1319
Olefins, max (vol. %)	18	ASTM D1319
RVP @ 37.8 C, max (kPa)	60c	KS M ISO 3007
Oxygen, min (wt. %)	0.5(s) / 1(w)	KS M 2408 ASTM D4815
Oxygen, max (wt. %)	2.3	
Methanol, max (vol. %)	0.1	
Distillation		
T_{10}, max (C)	70	KS M ISO 3405
T_{50}, max (C)	125	
T_{90}, max (C)	170	
FBP, max (C)	225	

Table 4.3: Chemical composition and properties of biodiesel.

Specification Name	**Value**	**Test Method**
Ester content, mass%	97.8	KS M 2413
Flash point, °C	190	KS M 2010
Viscosity at 40 °C, mm^2/s	4.4	KS M 2014
Carbon residue, wt%	0.01	KS M ISO 10375
Sulfur content, mg/kg	1	KS M 2027
Ash, wt%	0.001	KS M ISO 6245
Copper strip corrosion (3h at 50°C)	1A	KS M 2411
Density at 15 °C, kg/m^3	878	KS M 2411
Water content, %	0.04	KS M ISO 12937
Total contaminant, mg/kg	7	EN 12662
Acid value, mg KOH/g	0.2	KS M ISO 6245
Total glycerol, mass%	0.16	KS M 2412
Monoglyceride, mass%	0.47	KS M 2412
Diglycereol, mass%	0.17	KS M 2412
Triglycereol, mass%	0	KS M 2412
Free glycerol, mass%	0.0132	KS M 2412
Oxidation stability, 100 °C, h	15	EN 14112
Methanol content, mass%	0.01	EN 14110
Metal (mg/kg) Na + K Ca + Mg	LT1 LT1	EN 14108, 14, 109 Pr EN 14538
Phosphorous content, mg/kg	LT1	EN 14107
Color (ASTM)	1	ASTM D1500
Pour point, °C	0	KS M 2016
CFPP, °C	−2	KS M 2411
Appearance	Clear	Naked eyes

The CVCC is an optical efficiency investigation tool for spray combustion by generating the target experimental conditions from the chemical heating process. The pre-filled diluted combustible mixture, including C_2H_2, Ar, N_2, and O_2, is ignited to generate the high pressure and temperature under 10 kg/m3 density and then lets these cool down for a relatively long period to meet the desired conditions covering the range of 750 K - 900 K where the gasoline has a long ignition delay, leading to the misfiring. Fuel samples are injected to determine the ignition delay and the flame lift-off length at 400 bar injection. The oxygen concentration is selected to be 21%, which is an air simulated oxidizer for the primary combustion in internal combustion engines. Table 4.4 lists the experimental conditions and all other relevant parameters. Every experiment was implemented at least ten times for each operating condition to obtain good average results. The standard deviation formulas were used to calculate the error at each tested condition for every fuel samples. Pressure data was recorded

for 1s at 100000 samples per second and automatically smoothed via the Savitzky-Golay method using a ten-point average.

Table 4.4: Experimental conditions of the GB fuels for ignition and lift-off length measurement.

Parameters	Value
Fuel type	G, GB20, GB40, GB60, GB80, B
Injection pressure (bar)	400
Ambient gas density (kg/m3)	10
Orifice diameter (mm)	0.30
Injector type	Bosch CRIN 2
Injection duration (μs)	5000
Chamber body temperature (K)	353
Injector nozzle type	Single hole SAC
Fuel temperature	318
Frame rate (frame/sec)	20000 frames/second
Image resolution	512x128 pixels
Premixed gas reactants (%)	21O2, 7.6CO2, 3.8H2O, 65.3N2, 2Ar
Ambient temperature (K)	750-900

4.6 Ignition Delay Results

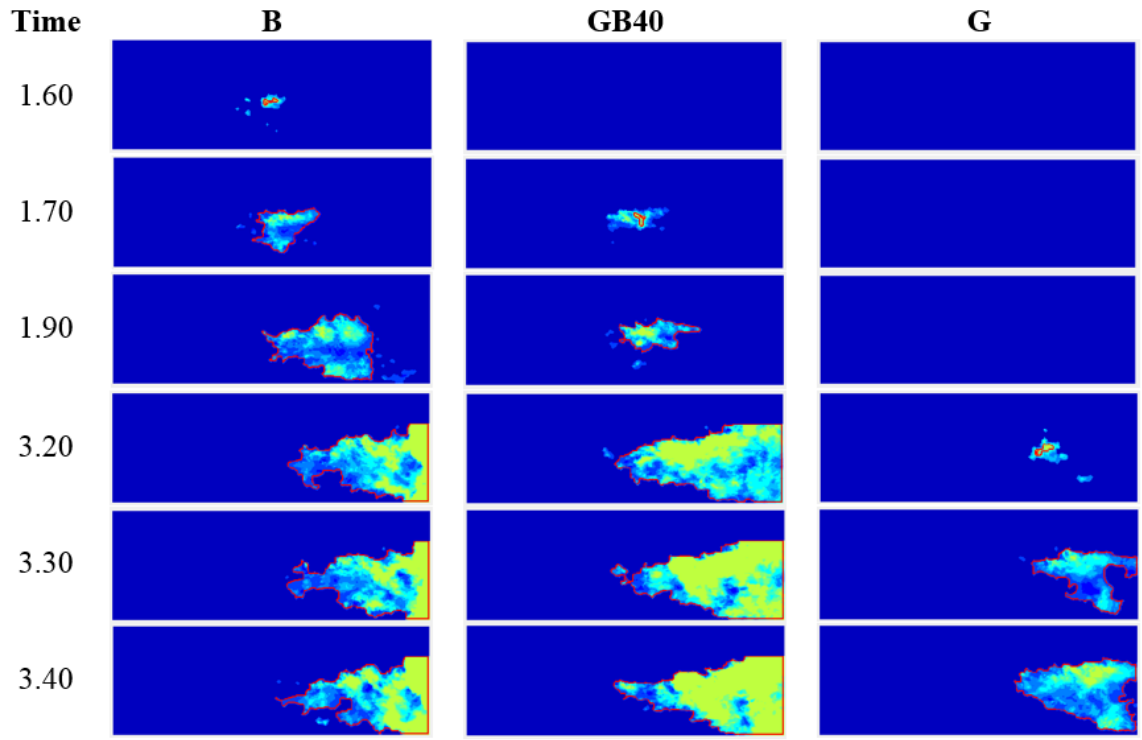

Figure 4.6: Time sequence of flame images for biodiesel, GB40 blend, and gasoline under 750K temperature, 21% oxygen content, and 10 kg/m^3 density.

The focus of this section is to measure the ignition delay of the GB blends via two different methods referred to as pressure-based and luminous-based ignition delay. As discussed earlier, the natural soot luminous emission images were employed to achieve the high-temperature ignition for different gasoline biodiesel blended fuels under low-temperature conditions [30] [32]. Figure 4.6 manifests the typical sequences of combustion images for three fuel samples at an ambient gas temperature of 750 K, an oxygen concentration of 21 %, and a density of 10 kg/m^3. The displayed sequence begins at the start of combustion of biodiesel and ends slightly after the start of combustion of gasoline. The time-resolved image sequences help to easily visualize the ignition process and receive the ignition information. The area bounded in the red line is to emphasize the high-temperature reactivity zone. The difference in the GB blend ratio has a notable influence on ignition in particular conditions. The first bright spots appeared at 1.6, 1.7 and 3.2 ms for biodiesel, GB40 and, gasoline respectively. The occurrence of the first bright spot signalizes the start of the combustion, and it advanced with an increase of biodiesel concentration.

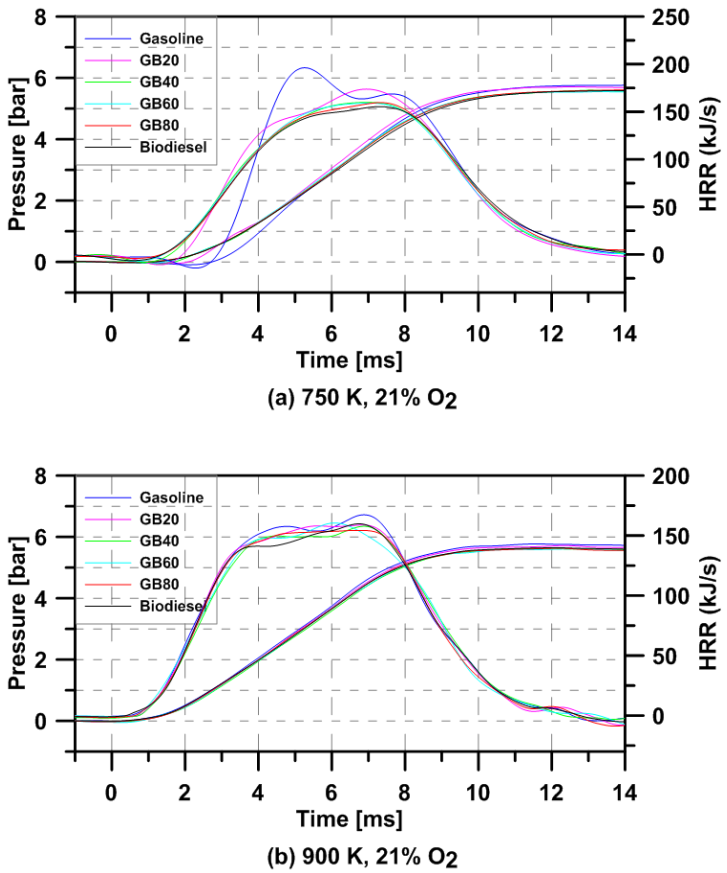

Figure 4.7: Pressure and HRR for GB blends, biodiesel, and gasoline at two ambient temperatures: (a) 750K and (b) 900K.

Figure 4.7 demonstrates the development of global pressure and heat release rate (HRR) of different GB ratios for two typical conditions. The global gas pressure is calculated by subtracting the pressure at the injection timing from the pressure measured by the pressure sensor. Shortly after fuel injection, the in-chamber pressure has a slight dip due to heat loss by cold fuel in the area of the non-reacting spray. The phenomenon can be demonstrated evidently through the appearance of a negative heat release rate after the fuel injection timing. The pressure showed a downtrend while the biodiesel concentration increases because of lower heating value for blended fuel with a higher biodiesel ratio. The decrease of input energy results in a reduction of total heat release, thus reducing the maximum global pressure. The difference in combustion phasing can be observed more clearly while biodiesel content is lower than 60% due to the notable decrease of chemical delay. The advance in combustion phasing has a cause from the biodiesel component, which has a higher value of the cetane number compared to pure gasoline. The GB blend with a higher biodiesel content reduced the chemical delay, leading to the advanced combustion phasing. Pure gasoline has a RON and MON that cause the most prolonged ignition delay; hence, it retarded the combustion phasing. For the 750 K case, biodiesel addition remarkably advanced the combustion phasing; it proved its potential to assist the cold-engine starting and solve misfiring under low-engine load. However, over 60% biodiesel ratio the combustion phasing is not different so much. The increase of biodiesel content even retards combustion phasing in 900 K case. Moreover, the gasoline exhibited a maximum peak of HER because of the extension of the mixing process that leads to a larger mass of air and fuel prepared prior to the start of combustion. The opposite side, biodiesel showed the minimum peak of HRR, and the heat release rate curve is relatively flat and smooth. The GB60 and GB80 have similar behavior like biodiesel in both pressure profile and HRR curve.

The results showed that the fuel blend having a lower biodiesel fraction burns with a shorter duration of combustion in all tested conditions in comparison to pure biodiesel. It implies that its combustion characteristic gets more resembling the Otto cycle, thus guarding higher-engine efficiency following engine combustion network guidelines. Besides, the longer ignition delay obtained from fuel blend with lower biodiesel will enhance the fuel evaporation to make leaner air-fuel combustion, therefore diminishes soot formation. For these reasons, gasoline mixing with moderate biodiesel owns the great potential to obtain high efficiency and low emission because of maintaining advantages of gasoline. The GB blend with small

biodiesel (less than 20%) will meaningfully extend the engine operating range to low-load conditions while retaining the high thermal efficiency and low emission.

Figure 4.8 presents average ignition delays and error values versus biodiesel fraction under three ambient gas temperatures (750 K, 800 K, and 900 K) for both the pressure and luminous methods. The error values which were calculated using standard deviation formulas point out total absolute uncertainty. The experimental results showed similar trends in ignition delay for both techniques. However, the pressure-based ignition delay is always a little longer relative to the luminous ignition delay. This difference between the two definitions of ignition delay is almost identical to other studies in CI engines. The reason for the difference is that a small amount of fuel first reaches the limitation reaction conditions and then produces a first little bright spot, which generates a small amount of energy. This energy is not enough to increase the pressure. A small amount of time is required for the heat to compensate for a slight pressure drop due to the adiabatic mixing process, and then reach the pressure sensor.

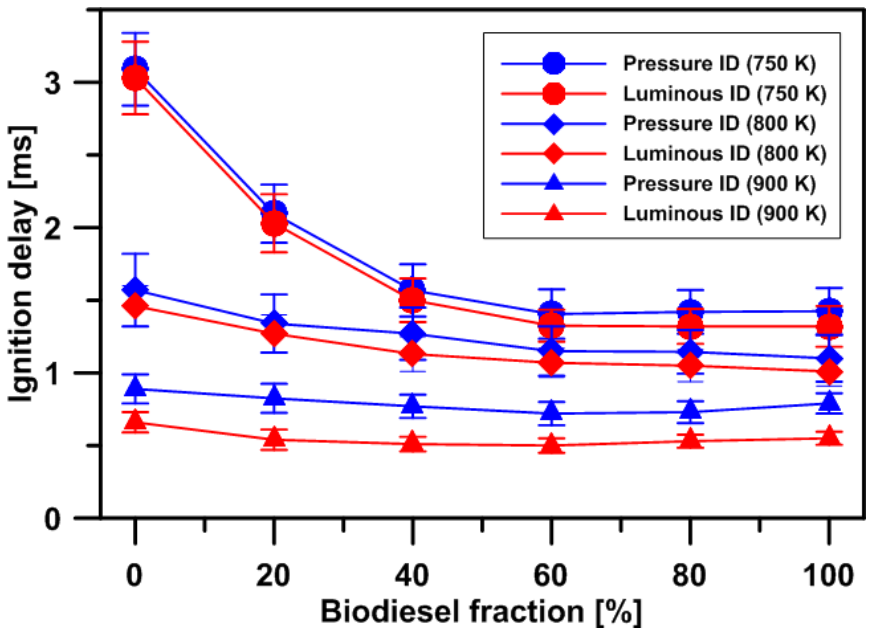

Figure 4.8: Ignition delay under different temperature of 750K, 800K and 900K temperature, 21% oxygen content, and 10 kg/m^3 density.

The difference between the two definitions becomes more severe as the ambient temperature increases. As the ambient temperature increases from 750 K to 900 K, the average value of difference increases from 0.08 to 0.23 ms. The reason for the bigger difference is the shorter time for atomization, vaporization, and mixing with air. Therefore, the amount of air-

fuel mixture that reaches a self-ignition temperature is smaller. The smaller amount of air-fuel mixture before the start of combustion causes a decrease in the rate of expansion of the flame. In contrast, the longer ignition delay causes a higher concentration of oxygen at the fuel-rich combustion zone, which accelerates oxidation reactions and speeds up the flame speed. The time required for generating enough energy to reach the pressure sensor is shorter. Conversely, the luminous ignition delay considered from the bright flame is independent the flame speed. For all these reasons above, the difference be-tween the two definitions can increase or decrease de-pending on the mixing process and the period of ignition delay.

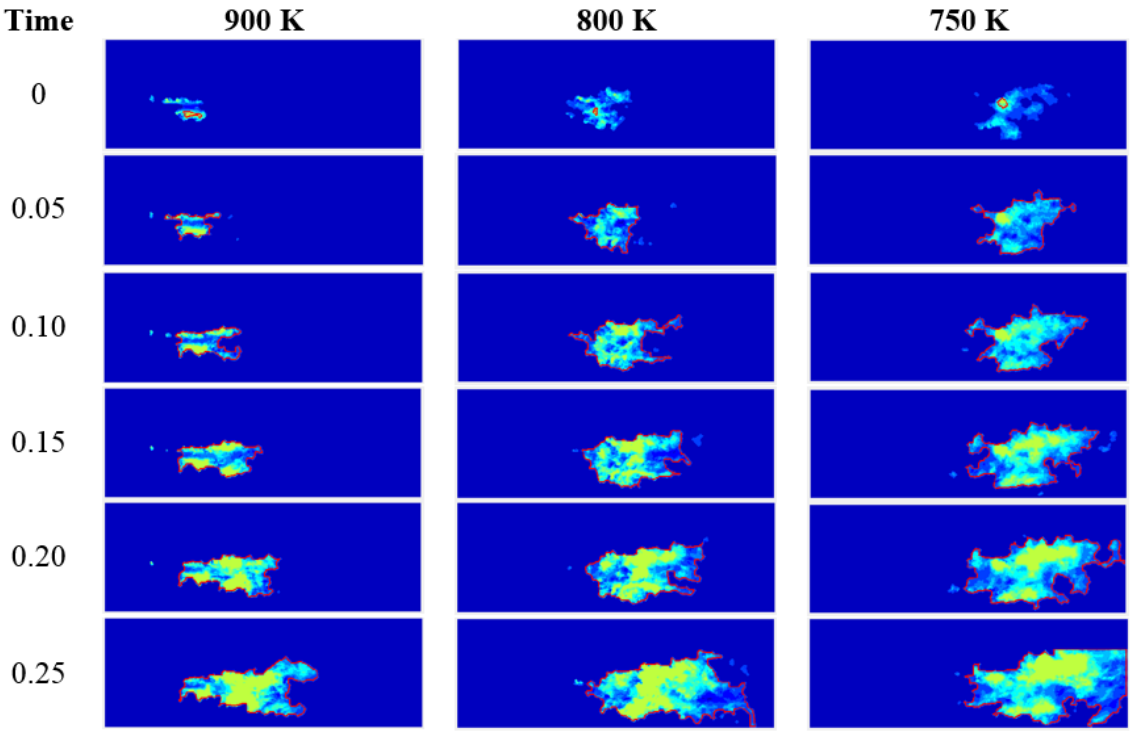

Figure 4.9: Development of flame for GB20 blend under different ambient temperature (750 K, 800 K, and 900 K), oxygen concentrations of 21% condition, and density of 10 kg/m^3.

The ambient gas temperature effect on the difference of two definitions are also clearly demonstrated through time-sequenced flame footages as shown in Figure 4.9 for the spray combustion of GB20 under different temperatures (750 K, 800 K, and 900 K). For the better collation of different ambient temperatures, the ignition delay was ignored to make all sequences begin at the same time (the start of the combustion). The time scale of each spray combustion image inscribes at the left column, which signifies the different evolutions of spray combustion at that specific time after the start of ignition. For 750 K the development of contour plots of flame (rate of expansion of the flame in a combustion reaction) is faster than

the others during the spray combustion process, thus reducing the time requirement to reach the pressure sensor. In this case, the difference between the two definitions is smaller than 800 K and 900 K cases.

Generally, the ignition delay decreases with increase biodiesel content due to increasing of cetane number. But for an ambient temperature of 900 K, first, the in-crease in biodiesel decreases the ignition delay due to its higher cetane number. However, the content of biodiesel is higher than 60 %; the ignition delay becomes slightly longer with the increases of biodiesel. The increase in physical delay could explain this. The ignition delay is the sum of the physical delay and the chemical delay. The increase in biodiesel content increases viscosity, thus reducing the atomization of droplets and volatility of GB blends. The bigger droplets decrease spray break-up, evaporation, and mixing; therefore, the physical delay increases. In contrast, the chemical delay decreases due to the highly flammable characteristic of biodiesel. The cumulative effect of the two factors increases the ignition delay after the biodiesel content continues to grow by over 60% due to the dominance of physical delay. Besides, the ignition delay sharply decreases when the ambient temperature rises. It agrees with previous studies, which were carried out using diesel fuels and other alternative fuels.

4.7 Lift-off length results

Here will discuss the lift-off length parameter for the different blended fuel samples. Properties of liquid fuel, including viscosity, volatility, density, etc. play a crucial role in the lift-off length result. The natural soot luminous imaging technique was used to observe the effect of variations in GB blends on the lift-off length. Figure 4.10 plots the measured lift-off length of the GB blends for different ambient temperatures (750 K, 800 K and, 900 K), 21% oxygen content, and 10 kg/m^3 density. In general, the lift-off length significantly increased with increasing biodiesel concentration under gas temperature conditions as 800 K and 900 K. As the discussion above, although the gasoline fuel has the most extended ignition delay, it has the shortest lift-off of length. One reason for its shortest lift-off length is very low viscosity and surface tension. It can easily cause cavitation in the nozzle flow, resulting in a drop in the discharge coefficient of the nozzle and reduced flow characteristics. Another probable reason for the shorter lift-off length is the gasoline radial dispersion characteristics. The gasoline has high instability on the spray surface due to its low viscosity and surface tension characteristics, so spray development in the direction of the spray axis is slow, thus the shortest lift-off length. The increase in biodiesel ratio caused the rise of lift-off length. Because the higher biodiesel

ration increases the viscosity and surface tension of the blended fuel, leading to an increase of the size of fuel droplets and momentum in the fuel spray. Therefore, the combustion flame moves further downstream, and the lift-off length increases.

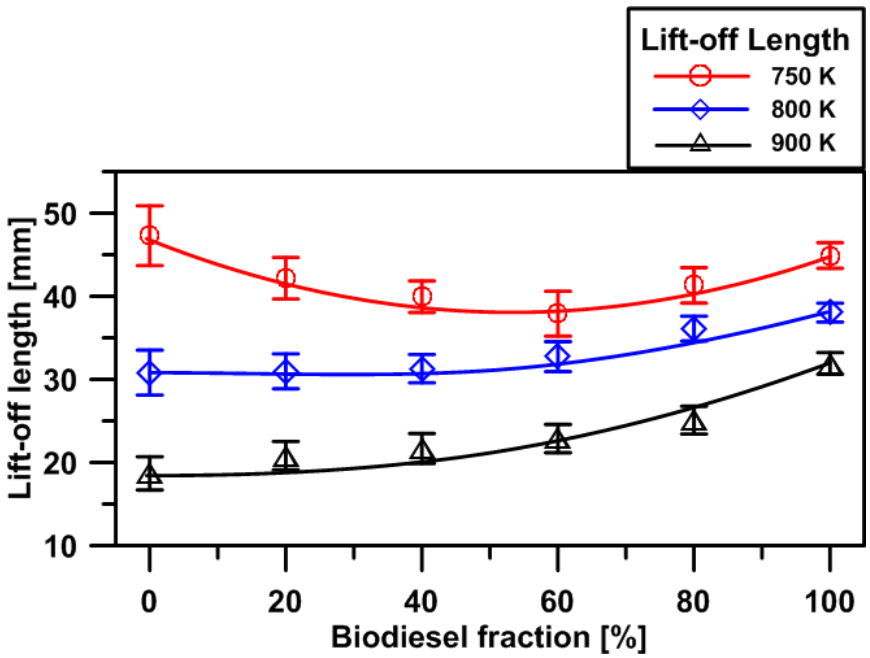

Figure 4.10: Lift-off length under different temperature of 750K, 800K and 900K temperature, 21% oxygen content, and 10 kg/m^3 density.

Differently, the lift-off length tends to decrease with increasing biodiesel concentration (less than 60 % biodiesel) at 750 K, 21% oxygen content, and 10 kg/m^3 density. The differences observed between this and the cases mentioned above can be explained by the effect of biodiesel addition on the ignition delay. The significant decrease in ignition delay leads to reducing the time for movement of combustion flame at the downstream area, thus decreasing lift-off length. It is dominant in comparison to the increase lift-off length due to the increase in viscosity and surface tension. In this ratio range, the increase in biodiesel significantly reduces the chemical delay, which has the most powerful impact on the decrease of lift-off length. However, above 60% biodiesel content, lift-off length trended to rise again like previous cases with the increase of biodiesel content. In this range, the increase of the ignition delay is a little bit with the rise of biodiesel content, so it is not a substantial impact on lift-off length. We note that increase in viscosity and surface tension are dominant in this case. The biodiesel fuel has high viscosity and high surface tension properties, so spray of the fuel blend with higher biodiesel content develops faster in the direction of the vertical axis. Also, high viscosity and

surface tension, the fuel droplets become bigger size with higher momentum flux, hence the spray penetration of fuel blend with higher biodiesel content is accelerated in the direction of the vertical axis, resulting in the increase in lift-off length.

4.8 Summary

This chapter analyzed the effects of the different gasoline-biodiesel ratios on its ignition delay and lift-off length under low-temperature range using the constant volume combustion chamber. The ignition delay is obtained using two different methods: pressure-based ignition delay and luminosity-based ignition delay. The natural soot luminous emission from combustion images was utilized to measure the lift-off length. Based on the experimental results, several main conclusions can be drawn as follows:

1. The experimental results showed that the ignition delay presented similar trends for both pressure and luminous approaches. However, the pressure ignition delay is always a little longer than the luminous ignition delay. This difference can increase or decrease depending on the mixing process and the period of ignition delay. These results also agree with the previous researches and elucidated the effect of gasoline-biodiesel blend ratios on ignition delay, lift-off length, combustion phasing, and heat release rate.

2. For below 60% biodiesel, the GB blend with a higher biodiesel content reduced the chemical delay, leading to the advanced combustion phasing. The gasoline shows the maximum peak of HRR because of the extension of the mixing process that results in a more substantial mass of air-fuel mixture before the start of combustion. The 750 K case, biodiesel addition significantly advanced the combustion phasing; it confirmed its capacity to help the cold start and prevent the misfiring at low-engine load. However, over 60% biodiesel ratio, the combustion phasing is not different so much.

3. Generally, the ignition delay decreases with an increase in biodiesel content due to the higher cetane number. But for an ambient temperature of 900 K, the content of biodiesel is more top than 60 %; the ignition delay becomes slightly longer with the increases of biodiesel due to the significant rise in physical delay in total ignition delay.

4. The lift-off length increased with an increase in biodiesel fraction under gas temperature conditions as 800 K and 900 K because of very high viscosity and surface tension of biodiesel. Differently, the lift-off length tends to decrease with the rise in

biodiesel concentration (less than 60 % biodiesel) at 750 K case. Because the sharp reduction of ignition delay leads to reducing the time for movement of combustion flame at the downstream area, thus decreasing lift-off length.

5. The evolution of the combustion frame for pure gasoline, GB20, GB40, GB60, GB80, and pure biodiesel were not similar during the combustion process. This phenomenon can be explained by the difference in cetane number, which reduces the chemical delay time while the different fuel properties change the size of fuel droplets, thus enhancing or hindering the air-fuel mixing process.

5 Effect of small amount of biodiesel on auto ignition and combustion characteristics under engine-like conditions

The purpose of this chapter is to demonstrate the effects of biodiesel fraction on auto-ignition for gasoline-biodiesel blended fuel, which combines two fuels with widely different auto-ignition characteristics. First, gasoline was blended with biodiesel at 5%, 10%, 15%, and 20% by volume, and then tested in a rapid compression expansion machine at a compression ratio of 11 and a temperature range of 720-850 K to observe the auto-ignition delay phenomenon under engine-like conditions. The experimental conditions are focused on improving the auto-ignition characteristic of GDCI combustion strategies under low load and cold start. The heat release rate of the blended fuels was calculated from the pressure trace and displacement history of the piston in order to identify first-stage ignition and second stage (auto-ignition) ignition delay. Second, a gasoline-biodiesel reaction mechanism was developed to predict the chemical ignition delay of the blended fuels. The reaction mechanism with 4285 species and 15246 reactions was validated and implemented using the CHEMKIN PRO software. Finally, the chemical ignition delay was predicted by the simulation which was further compared to the experimental measured results. These results revealed that a higher biodiesel fraction helps to obtain shorter ignition delay, which reduces the requirement of intake temperature. The blended fuel with 20% biodiesel showed the lowest ambient temperature at the injection timing requirement and was 80 K lower than gasoline. Each blended fuel exhibited two-stage ignitions in the measured temperature range. The combustion duration and pressure peak of every blended fuel were similar to each other after increasing the biodiesel fraction.

5.1 Introduction

In the last few decades, gasoline has been used as a compression ignition (CI) engine fuel to achieve better thermal efficiency than gasoline spark-ignited combustion or diesel compression-ignited combustion [6] [14], as well as lower emissions of hazardous air pollutants such as nitrous oxide (NOx) and particulate matter (PM) [6] [14] [101]. However, homogeneous charge compression ignition (HCCI) technology with gasoline in the CI engine presents a major drawback related to the excessive rate of pressure rise (ERoPR) due to short HCCI combustion. Recently, a new concept for a gasoline-fueled compression ignition (GCI) engine that intends to prevent the ERoPR by using GDCI combustion has been developed [102].

Unlike HCCI, in the GDCI engine, gasoline is injected at initially to obtain the same combustion phasing as with diesel fuel. The mixing process of fuel and air is improved due to extra time, so combustion occurs with much greater mixing compared to diesel fuel. In this framework, the fuel must not be injected too early to obtain a homogeneous mixture, similar to the HCCI condition [103]. The partially pre-mixed combustion has demonstrated a great deal of potential for reducing the ERoPR, but low load operation is a challenge because of the high octane number of gasoline and its resistance to auto-ignition at low mixture temperatures, thus requiring a high intake air temperature [104] [37] [105]. A small amount of biodiesel added into gasoline improves the auto-ignition of gasoline and reduces the intake temperature requirement while maintaining a high thermal efficiency and lower NOx and soot emissions [37] [105] [24]. Additionally, biodiesel is a renewable fuel, so utilizing it to prepare this blend is a potential way to reduce emissions of greenhouse gases and other pollutants, as well as to address the shrinking reserves of fossil oil [93] [106] [94] [107]. However, there are few studies concerning gasoline-biodiesel blended fuels, especially related to the ignition characteristics of the blend. Therefore, one of the most important factors investigated in this study is the ignition delay characteristics of the blended fuel.

Auto-ignition is a significant factor in compression ignition combustion in the CI engine. It influences the delay due to fuel characteristics from the start of injection until the start of combustion. Ignition delay (ID) affects the combustion phasing in the engine cycle and the degree of fuel vapor/air pre-mixing required to produce the primary mixture prior to combustion. This substantially impacts the shape of the heat release rate (HRR) and pollutant formation, most notably NOx and PM [13]. An improper ID in the CI engine, which causes the combustion phasing to change, can cause negative effects. One common symptom of these negative effects is a decreased power output of the engine. Improper ignition delay also leads to a rise in the phenomenon known as knocking, which can cause combustion instability and significantly decrease the life of the engine [1] [25]. The ID time depends on several parameters, including the type of fuel, engine design, engine operating conditions, and fuel injection strategy. Therefore, a better understanding of how the biodiesel fraction impacts on the auto-ignition in the CI engine is a key matter investigated in this study.

In this study, the gasoline-biodiesel blended fuels were chosen with 5%, 10%, 15%, and 20% biodiesel by volume to investigate the auto-ignition delay and compare it to pure gasoline fuel. Experiments were conducted under different conditions in a rapid compression

expansion machine (RCEM) to measure the auto-ignition delay for the experimental fuels to provide a fundamental understanding of the blended fuel in relation to the auto-ignition delay parameter. The influence of ambient temperature and different biodiesel fractions on the auto-ignition and combustion behavior were investigated in the RCEM with ambient temperatures at injection timing ranging from 720 K to 850 K and a compression ratio of 11. Additionally, the measured auto-ignition delay was compared to a simulated result that is predicted by the CHEMKIN-PRO software to validate the accuracy of the ignition delay for the gasoline-biodiesel blended fuel to better understand the fuel ignition characteristics.

5.2 Experimental methods

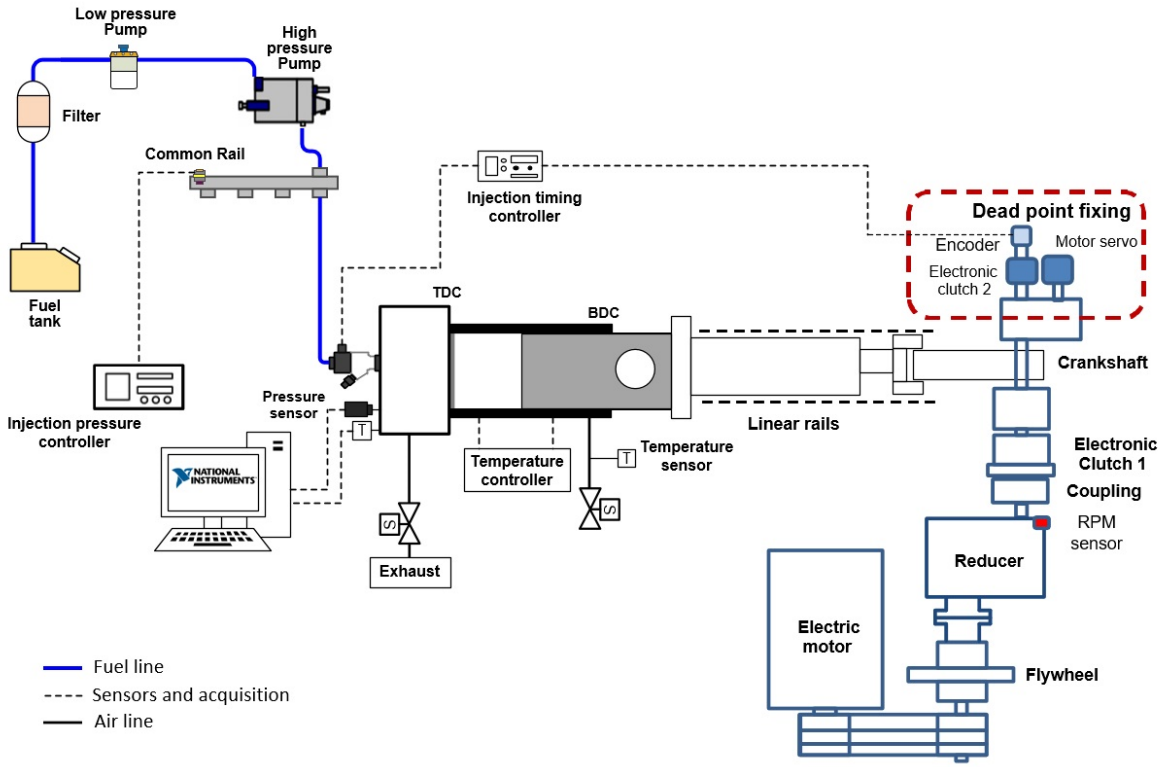

Figure 5.1: Schematic diagram of the RCEM.

The RCEM was installed in a fully instrumented test cell, with all the auxiliary facilities required for its operation and control, as is illustrated in Figure 5.1. This equipment is duplicated single diesel type compression cycle after the combustion process, which is carried out in the environment of high temperature and high pressure. Moreover, to achieve stable intake air conditions, a band heater is equipped on the cylinder wall to maintain a certain temperature. And a supercharger that installed element heater inside supplied the required boost pressure and temperature before going into combustion chamber. The air pressure and

temperature were adjusted within the supercharger. The advantages of making fundamental investigation of HCCI combustion in a RCEM, rather than in a reciprocating engine, arise through the simplification of the mechanical system. Furthermore, there is no previous cycle, which could reduce effects of residual gas and lubrication oil that can be ignored and more detailed about the RCEM is given in the section 3.2.

5.3 Ignition delay calculation

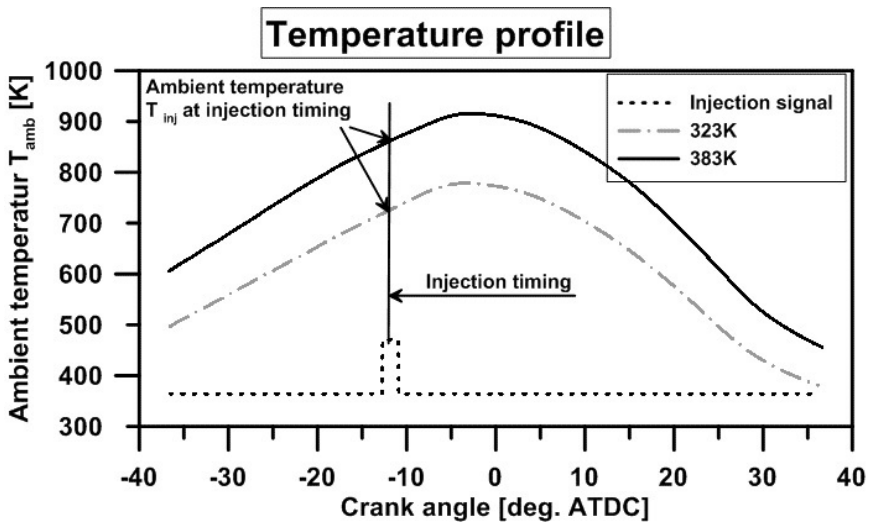

Figure 5.2. Ambient temperature profile in the cylinder during the combustion and expansion stroke.

In this study, the blended fuels were injected into the RCEM cylinder under 800 bar injection pressure at 13-degree crank angle before the top dead center (TDC). The compression ratio (CR) of the RCEM was fixed as 11. The ambient gas temperature at the start of the blended fuel injection T_{inj} was calculated from the state equation, with in-cylinder pressure and volume history measured during the compression stroke. If there was no heat loss during the combustion stroke, the temperature in the cylinder at TDC was found to be 845 K by using the adiabatic process equation. This value was much higher than that calculated from the state equation (775 K). It can be concluded that the heat was lost from the cylinder wall while the piston moves towards TDC. Since the experiment was performed with a crank speed of 200 rpm, it took a long time for completing one cycle, causing heat to be lost to the surroundings. Figure 5.2 shows the ambient gas temperature profiles in the cylinder, T_{amb}, for different intake temperatures. The ambient gas temperature for the injection timing, T_{inj}, was varied from 720

K to 850 K. The test conditions of the gasoline-biodiesel blended fuels for the auto-ignition measurement are shown in Table 5.1.

Table 5.1: Test conditions of the gasoline-biodiesel blended fuels for ignition measurement.

Fuel	GB5, GB10, GB15, GB20
Intake gas temperature [K]	323-383
Injection pressure P_{inj} [bar]	800
Injector specification	Seven holes, nozzle-hole diameter 0.090 mm
Equivalence crank speed [rpm]	200
Compression ratio	11
Premixed gas reactants	Air
Equivalence ratio	0.3
Injection timing t_{inj} [deg. ATDC]	13
Ambient gas temperature at start of injection T_{inj} [K]	720-850
Ambient gas pressure at start of injection [bar] P_{inj}	19

Figure 5.3 shows the details concerning the auto-ignition delay, combustion phasing, and control signal of the injector. The auto-ignition delay is defined as the time (or crank angle) interval between the start of injection and the start of combustion [1] [2]. The start of injection was determined by measuring the solenoid injector current where an additional delay was taken into consideration, which is identified as the physical ignition delay due to physical operation of the injector. This was determined through a suitable calibration. In this study, the injection delay was measured to be 0.36 ms [108]. The start of combustion was determined by responding to the heat release rate (HRR). The first-state ignition timing is determined as the time at the first HRR peak, which is achieved through a low-temperature reaction (LTR). Auto (total) ignition timing is determined as the time after the HRR exceeding more than 20 J/deg. (after first-state HRR) due to a high-temperature reaction (HRT) [109].

The HRR was calculated using Eq. (1), which was derived by Heywood [2]. Here, dQ/dq is the HRR, *k* is the ratio of the specific heats depending on the gas component, and Cp/Cv was taken as 1.35 for the heat release analysis due to the compression ignition condition.

Additionally, p, V, and Θ are used to represent the instantaneous in-cylinder pressure, volume, and crank angle, respectively.

$$\dot{Q}_\theta = \frac{dQ}{d\theta} = \frac{1}{k-1}\left(V\frac{dp}{d\theta} + kp\frac{dV}{d\theta}\right) \quad (1)$$

The heat release is defined by the total amount of heat released by combustion and heat lost from the cylinder walls. Since the heat transfers to the walls, the heat release is always lower than the heat released by combustion in isolation.

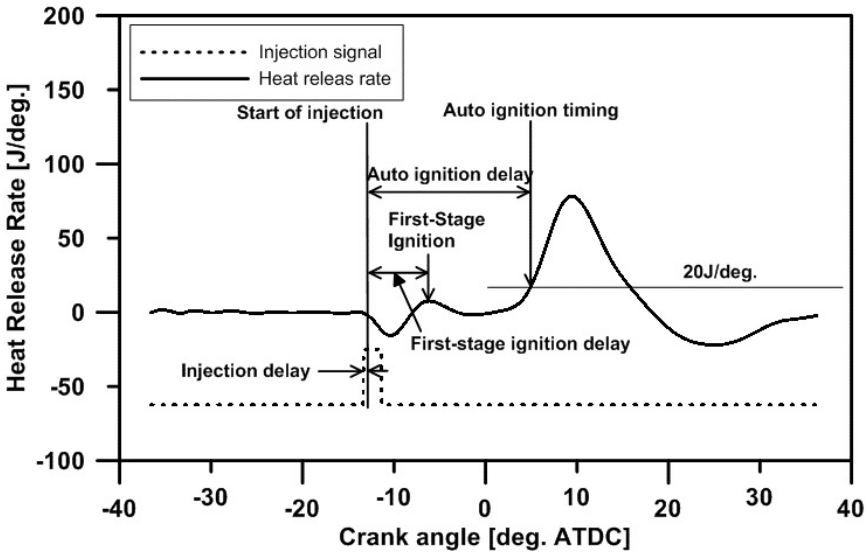

Figure 5.3: Definition of the auto-ignition delay.

5.4 Chemical kinetics calculations and validation

5.4.1 Chemical kinetics calculations

In this study, a numerical simulation of the gasoline-biodiesel blended fuel was performed by using the closed homogeneous reactor model in the CHEMKIN-PRO software to compute the auto-ignition time with biodiesel fraction, temperature, pressure, and equivalence ratio.

Creation of the gasoline and biodiesel elementary reaction schemes

In the PCI concept, combustion is much more sensitive to fuel chemistry. Therefore, the five-component surrogate consisting of toluene, 1-hexene, iso-hexane, iso-octane, and n-heptane from Lawrence Livermore National Laboratory (LLNL) with 1389 species and 5935

reactions was used to represent gasoline fuel. To determine fraction of different compositions for experimental gasoline, Surrogate Blend Optimizer from the Reaction Workbench [33] was used to find model-fuel mixtures that satisfied specific properties of experimental gasoline. The three-component surrogate consisting of methyl decanoate, methyl-9-decenoate, and n-heptane from LLNL with 3299 species and 10806 reactions was used to represent biodiesel fuel. The composition of both surrogates is presented in Table 5.2 and Table 5.3. However, the elementary reaction schemes of gasoline and biodiesel mixtures have not been investigated. Therefore, elementary reaction schemes for the gasoline-biodiesel mixture were created and merged using reaction workbench software. In the biodiesel model, some reactions that duplicated those of the gasoline model were removed because the gasoline scheme represented the basic scheme. Then, the reactions for biodiesel that were not found in the gasoline model were combined with those in the gasoline model to create the final reaction scheme with 4285 species and 15246 reactions.

Table 5. 2: Composition of the gasoline surrogate.

Model fuel components	Representing chemical class	Mole %
Toluene	Aromatics	43
1-Hexene	Alkene	14
Iso-Hexane	Iso-Alkane	10
Iso-Octane	Iso-Alkene	26
n-Heptane	n-Alkane	8

Table 5.3: Composition of the biodiesel surrogate.

Model fuel components	Representing chemical class	Mole %
Methyl-decenoate	Methyl ester	25
Methyl-9-decenoate	Methyl ester	25
n-Heptane	n-Alkane	50

5.4.2 Validation

After the gasoline-biodiesel elementary reaction schemes were established by using the Reaction Workbench, these were validated with the original reaction schemes of gasoline and

biodiesel to determine the accuracy of the blended gasoline-biodiesel model. The amounts of gasoline and biodiesel were varied to compare with the gasoline-biodiesel model and the original gasoline model or the original biodiesel model. For comparison of the gasoline model case, the amount of gasoline was 100% and biodiesel was 0% in the gasoline-biodiesel model. The first stage and total ignition delay are represented by the line 1 and the line 2, respectively. Using the original gasoline model, the first-state and total ignition are represented by the line 3 and the line 4, respectively. The results from the two models are close to each other. For comparison of the biodiesel model case, the amount of biodiesel was 100% and gasoline was 0%. The first stage and total ignition delay are denoted by the line 5 and the line 6, respectively. Using the original biodiesel model, the first-state and total ignition are depicted by the line 7 and the line 8, respectively. The results from the two models are also close to each other. Therefore, it can be concluded that the ignition delays predicted by the gasoline-biodiesel model for both gasoline and biodiesel were in good agreement with the original gasoline model and the original biodiesel model, as shown in Figure 5.4.

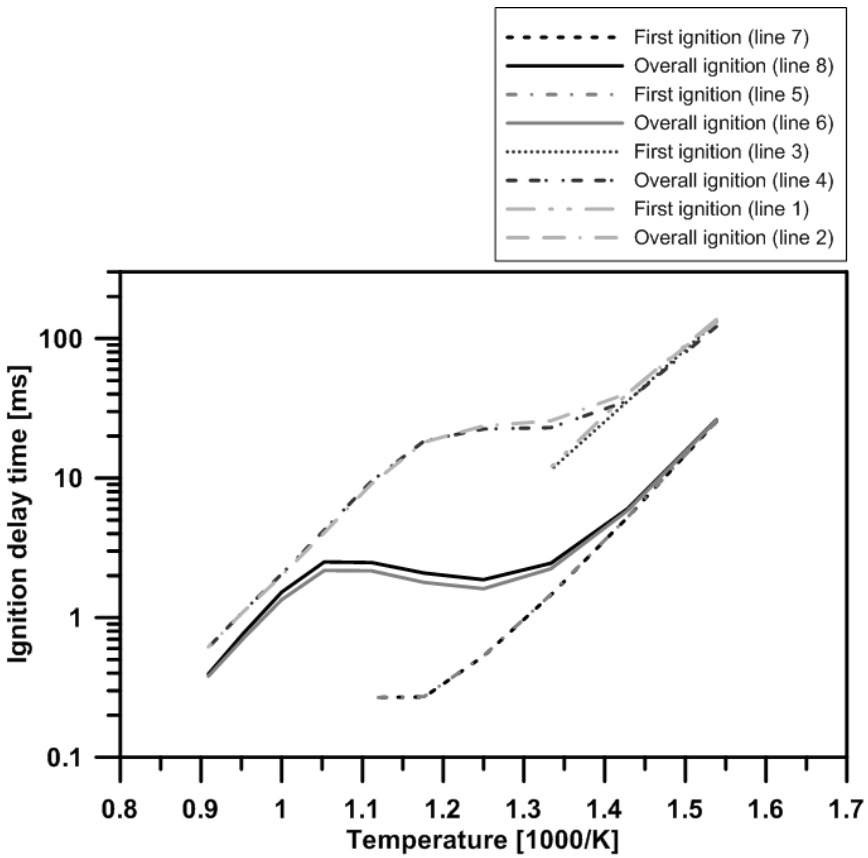

Figure 5.4: Comparison of the ignition delay time between the gasoline-biodiesel model and LLNL's model or Vanhove's model at 650-1100 K, 20 bar, and stoichiometric ratio.

5.5 Pressure trace

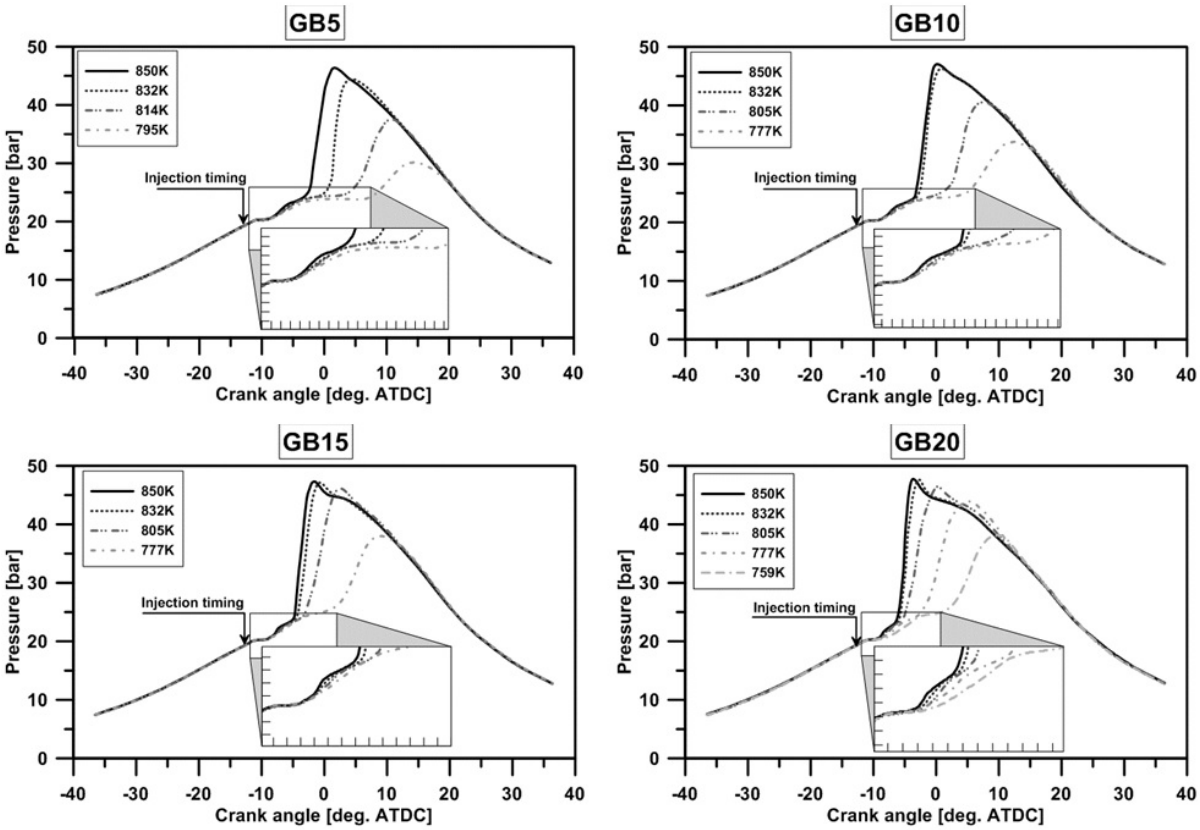

Figure 5.5: Temporal change in pressure with in-cylinder temperature.

The RCEM can behave like a diesel engine which can auto-ignite the combustible mixtures under easily controlled conditions and a cleaner environment than the traditional IC engine with an appropriate turbulence effect during the spray and combustion. The RCEM also gives direct auto-ignition measurement. Figure 5.5 shows the RCEM in-cylinder pressure traces of the four blended fuels for various ambient temperatures at injection timing T_{inj} and CR = 11. The blended fuels were injected at 13° CA deg. ATDC. The combustion of each blended fuel will start after certain time duration. Firstly, adiabatic mixing process took places. Then the blended fuel was atomized, vaporized, mixed with air inside a combustion chamber. The pressure slightly reduces due to lower temperature of the blended fuel which can be observed in magnified region. Then pressure starts to slightly increase again at end of adiabatic mixing process because of the exothermic reaction chemistry at low-temperature region. This period depends on the physical ignition delay. The combustion actually occurs after certain times of chemical delay, when the in-cylinder pressure rises so fast. In general, the in-cylinder pressure increased, and combustion phasing advanced with the increase of T_{inj}. The increase of

T_{inj} also causes the pressure peak to become higher as the temperature increases the reaction rate. For example, it is clear for GB05 that the increase of T_{inj} from 795 K to 850 K led the pressure peak to increase from 30 bar to 47 bars, and combustion phasing advanced approximately 10^{o} deg.CA. During T_{inj} ranging from 720-850 K, every blended fuel exhibited both low-temperature reactions (LTRs) and high-temperature reactions (HTRs). The phenomenon of LTR can be observed more clearly from the HRR curves.

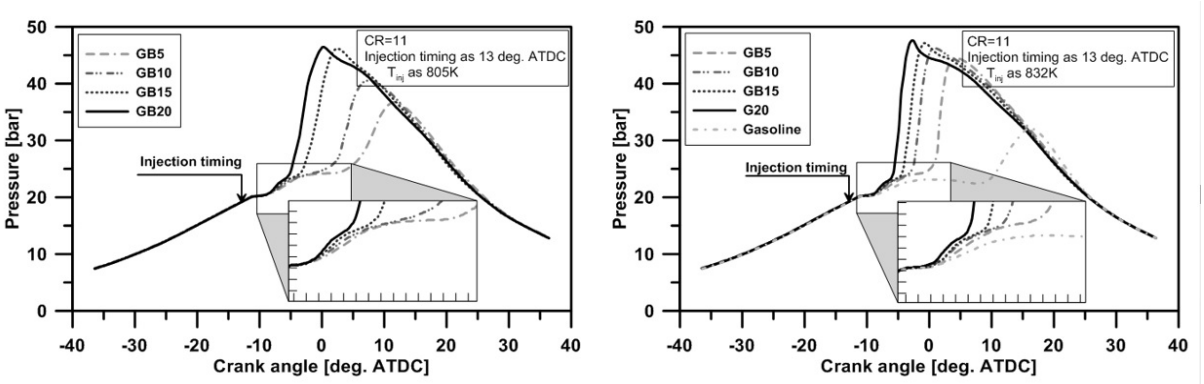

Figure 5.6: Temporal change in pressure with biodiesel fraction.

A clear representation of the influence of biodiesel fraction on combustion phasing can be seen in Figure 5.6, which was compares with the pressure time-histories obtained experimentally for the four different gasoline biodiesel blended fuels at CR=11 and T_{inj} equal to 805 K or 832 K. The test fuels are denoted as GB5, GB10, GB15, and GB20 have 5%, 10%, 15%, and 20% biodiesel by volume, respectively. The four fuels showed significantly different combustion phasing at the same test conditions. Generally, the increase of the biodiesel fraction causes combustion phasing to be more advanced, as can be clearly seen in both cases in Figure 5.6. The reason for the advance lies in the addition of biodiesel, which has a higher cetane number with respect to pure gasoline. A blended fuel with a greater biodiesel fraction results a higher cetane value in the fuel. Combustion phasing was advanced due to the reduced chemical delay of the blended fuel. Pure gasoline has the lowest cetane number, leading to a longer ignition delay, so it showed the latest combustion phasing compared to the blended fuels. In the 805 K case, the pressure peak of GB20 was at TDC and the pressure peak of GB5 was 13 CA deg. ATDC, but the gasoline misfired due to the ignition delay being too long. As far as low-temperature reaction concerns, the higher biodiesel reaction allows the higher-pressure peak.

5.6 Heat release rate

The heat release rate was derived from pressure trace data captured by the pressure sensor at the combustion chamber. Figure 5.7 shows the HRR of the four blended fuels for various Tinj and CR = 11. These data provided insight into the effect of the temperature on the thermal ignition behavior in a diesel-like combustion system. Here all blended fuels produced a two-stage ignition profile, a phenomenon that is commonly observed in diesel combustion systems. The HRR increased with the increase of Tinj. The maximum peak of HRR became higher for every blended fuel as the Tinj was increased to 850 K. But as Tinj reduced more, the HRR of the blended fuel became lower due to the reaction rate between the fuel and oxygen was affected by the ambient temperature. The increase of Tinj accelerated the reaction rate, causing an increase in the heat release rate of all the blended fuels. Also, the increasing Tinj slightly increase the peak of HRR at low-temperature reaction. For each tested fuel, two HRR peaks were observed because of the LTR and the HTR. The fact of two HRR peaks helped to clearly identify the existence of the LTR.

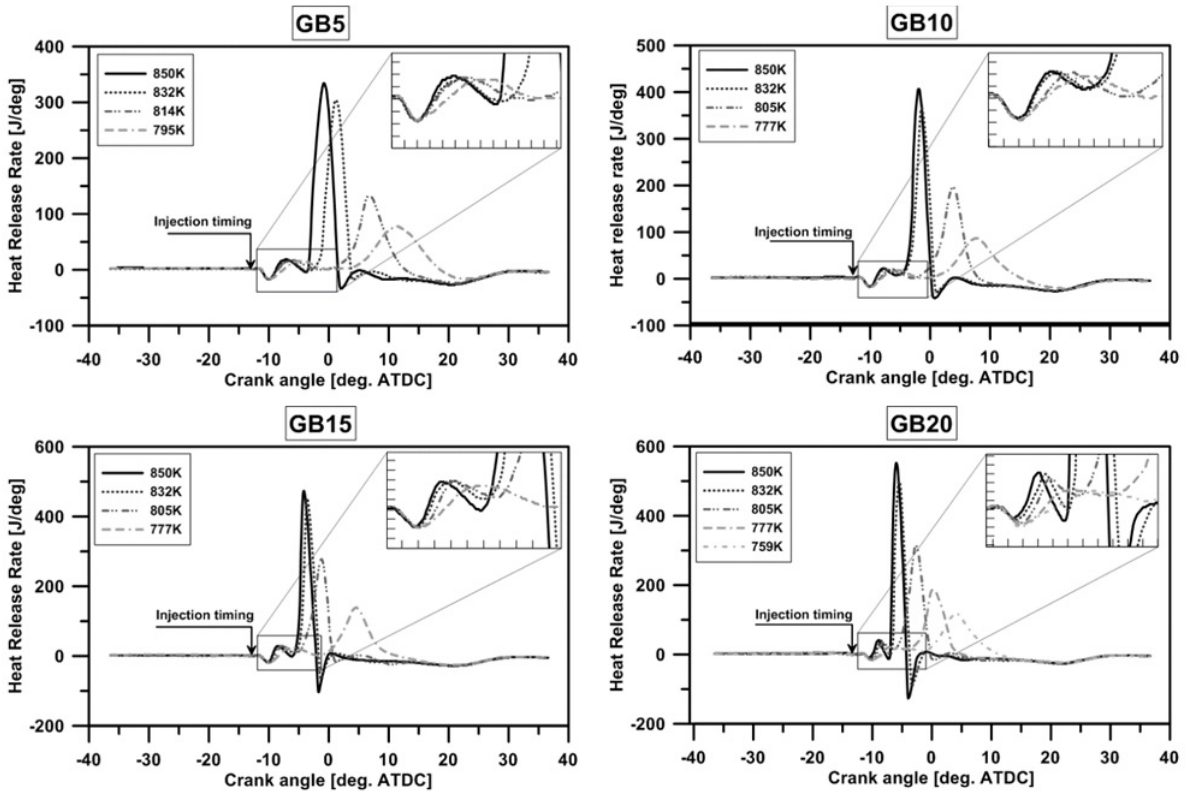

Figure 5.7: Temporal change in heat release rate with in-cylinder temperature.

Figure 5.8 shows a comparison of the heat release rate development for GB5, GB10, GB15, GB20, and pure gasoline at T_{inj}=805 K or 832 K and CR=11. Comparing GB5, GB10, GB15, GB20, and pure gasoline, it was a clear that increasing the biodiesel fraction increases

the magnitude of the maximum peak of HRR, and the appearance of the heat release shifted to earlier times. The Figure 5.8 also indicates that the effect of the biodiesel fraction on the low-temperature HRR and high-temperature HRR was sensitive to fuel type. The magnitude of the low-temperature HRR profile increased slightly with the increasing biodiesel concentration. It can be seen in magnified region in the Figure 5.8. At T_{inj} = 832 K, the appearance of the heat release of gasoline is later than the other fuels due to the long ignition delay of neat gasoline. When T_{inj} decreased to 805 K, the heat release of gasoline disappears due to misfire, thus the ignition delay is too long. In both cases, GB20 showed the highest peak of HRR and neat gasoline showed the lowest peak of HRR.

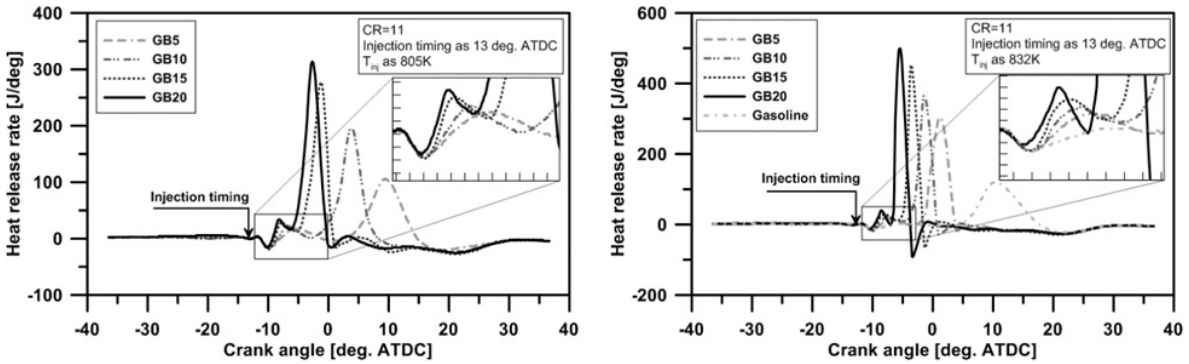

Figure 5.8: Temporal change in the heat release rate with biodiesel fraction.

5.7 Ignition behavior

The auto-ignition period is the duration of time between start of injection and start of combustion played in two stages and carried out with reference to the pressure trace. The pressure trace data was recorded by pressure sensor to HRR to investigate the timing of first ignition and auto-ignition. The first-stage ignition delay is counted from the starting of injection to the onset of first-stage ignition due to exothermic reaction chemistry at low-temperature regimes. The first-stage ignition delays almost related to physical delay while the fuel is atomized, vaporized, mixed with air and raised to self-ignition temperature. The physical delay ends at the onset of first-stage ignition due to exothermic decomposition of Keto-Hydroperoxide species. The transition point marks both of the start of first-stage ignition and end of physical delay. The auto-ignition timing is time at the HRR exceedingly more than 20 J/deg due to exothermic reaction chemistry at high-temperature regimes, it depends on the temperature of the surroundings.

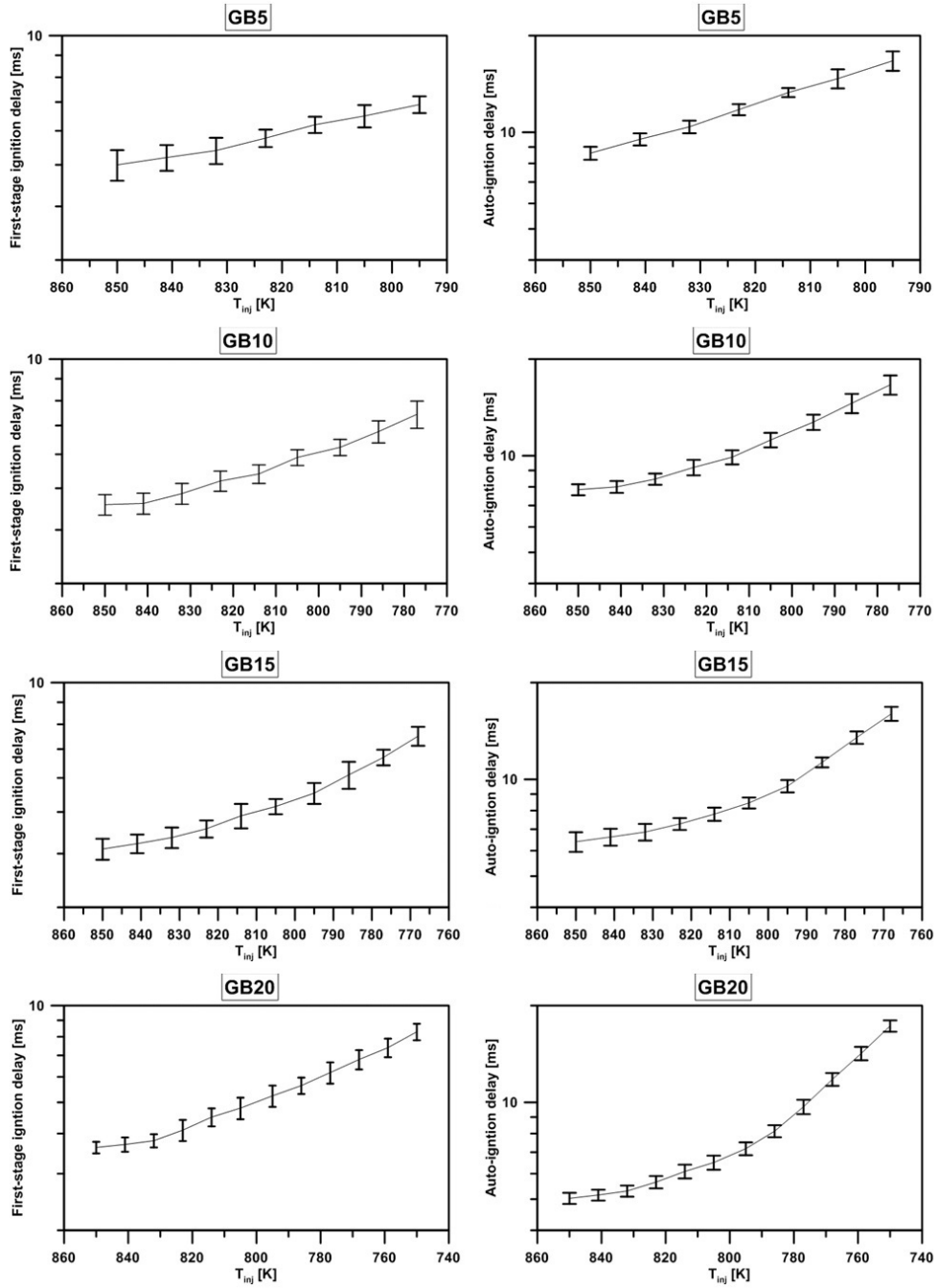

Figure 5.9: First-stage ignition delay, auto-ignition delay at varying ambient temperature for GB5, GB10, GB15, and GB20.

Ten experiments were performed for every case, the first-stage delay and the auto-ignition delay were observed by analyzing HRR. The first-stage delay and auto-ignition delay for GB5, GB10, GB15, and GB20 were measured by the RCEM depicted in the Figure 5.9. In this graph, both of the first stage and auto-ignition delays were shown over ambient temperature at injection timing T_{inj}, and error bars indicate total absolute uncertainty, which was calculated

using standard deviation formulas. The first stage and auto-ignition delays increased with the increase of T_{inj} due to the higher temperature improving the ignition conditions.

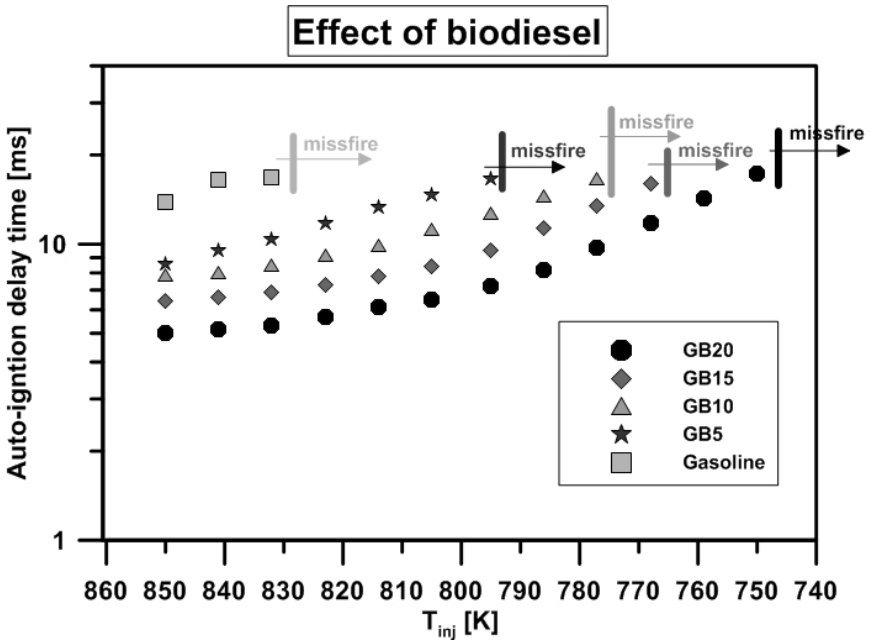

Figure 5.10: Effect of the biodiesel fraction on auto-ignition.

Figure 5.10 shows comparison of the auto-ignition delay for GB5, GB10, GB15, GB20, and neat gasoline with a T_{inj} range of 720-850 K. In every case, the blended fuel with a higher biodiesel fraction showed a shorter auto-ignition delay and misfired at a lower T_{inj}. The misfiring was observed at ambient temperature at injection timing lower than 795 K, 785 K, 765 K, 750 K, and 832 K for GB5, GB10, GB15, GB20, and neat gasoline, respectively. A blended fuel with a higher biodiesel fraction showed a lower misfiring temperature. This reason relied on the higher cetane number of biodiesel fuel. The blended fuels having higher biodiesel fractions, meaning they have a high cetane number and hence, a reduced auto-ignition delay will be observed. According to the results, it is clear that auto-ignition was improved significantly at a low mixture temperature by adding a small amount of biodiesel.

5.8 Simulation and comparison to the experimental investigation

5.8.1 Effects of the biodiesel fraction on the chemical delay of the blended fuel

To investigate the effect of the biodiesel fraction on the chemical delay of blended fuel, biodiesel fractions varying from 20% to 80% were simulated and compared to pure gasoline and pure biodiesel at a stoichiometric air-fuel ratio at 20 bar and a temperature range of 650-

1100 K using the CHEMKIN PRO software. The ignition delay in the simulation is defined by a peak in OH concentration. In Figure 5.11, the ignition delay decreases with the increase of the biodiesel fraction in the gasoline-biodiesel blended fuel. In particular, the influence of biodiesel on the auto-ignition delay becomes more effective when the biodiesel fraction is lower than 20%.

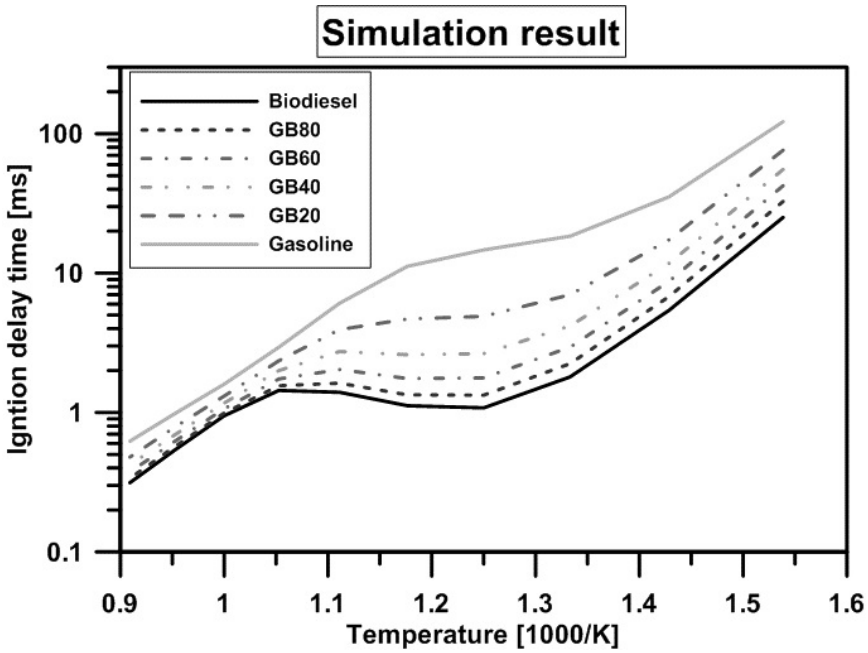

Figure 5.11: Effect of the biodiesel fraction on the chemical delay of the blended fuel.

5.8.2 Experimental and predicted chemical ignition delay for the blended fuel at the RCEM condition

In this study, a closed homogeneous reactor model in CHEMKIN PRO is used to calculate the chemical delay of the gasoline-biodiesel blended fuels which covered a range of the experiment. Therefore, there are some assumptions used in predicting ID. First, after the blended fuel was sprayed into the combustion chamber, the mixture was assumed to fully evaporate before auto-ignition occurs in the RCEM environment and becomes a homogeneous mixture. [110] [111]. Second, a temperature and equivalence ratio of the bulk air-fuel mixture in the RCEM for CHEMKIN kinetic modeling was determined by using the progress of the combustion process in the φ- T plane illustrated in Figure 5.12 [112]. According to the Figure 5.12, ambient temperature can be expected to exert a large influence on the equivalence ratio at the start of ignition. For an O2 concentration of 21% and ambient temperature of 900 K, the mixing process first begins as an adiabatic process. Then, the mixture temperature increases to

820 K, and the equivalence ratio decreases to approximately 1.7. At this point, the path departs from the adiabatic mixing path because low-temperature heat release occurs. Thoo et al. [13] determined the temperature and equivalence ratio at this point for the operating conditions of the bulk air-fuel mixture for kinetic modeling in order to compare the experimental ignition delay taken in the IC engine and the simulated ignition delay using CHEMKIN. The RCEM was designed to be similar to a single-cylinder diesel engine with a direct injection strategy, so the Figure 5.12 was also used to determine the operating conditions for the CHEMKIN model in this study.

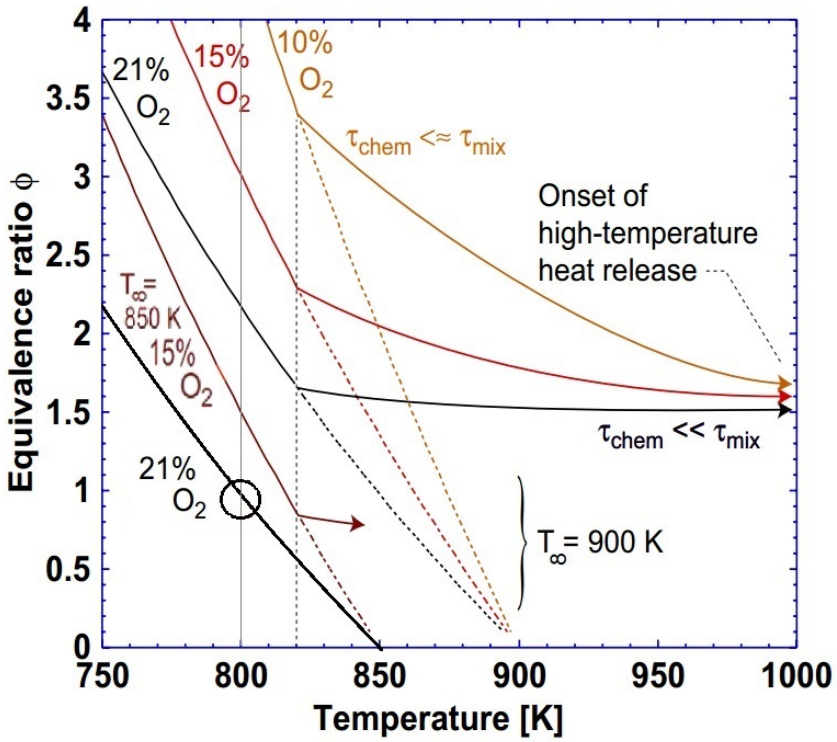

Figure 5.12: The path of a fuel parcel in the φ-T plane corresponding to an adiabatic mixing process followed by low-temperature heat release (Ref. [112]).

To compare between simulation and experimental results taken on the RCEM, only chemical delay from the auto-ignition (experimental total) ignition delay was compared to simulation result at the T_{inj}=850K case. In this case, the in-cylinder temperature is approximately 850 K. Auto-ignition delay of the gasoline biodiesel blended fuel is divided into physical and chemical processes. The chemical delay (ID_{chem}) was calculated by subtracting the physical delay (ID_{phys}) from auto-ignition delay. The physical delay defines as the time interval between the start of combustion and the start of first-stage ignition. The physical delay

depends on engine design and operating condition as well as fuel properties. Viscosity is a key parameter, governing the physical delay during combustion process. If the fuels have low viscosity, the physical delay of the fuels is short and vice versa. To determine chemical delay of gasoline biodiesel blended fuel, as discussed above heat release occurs due to exothermic decomposition of keto-hydroperoxide species at low-temperature reaction to detect the physical delay, the transition point marks end of physical delay. According to the figure 8, after physical delay ends, heat release rate rises again at about 4 deg.CA after start of injection for all blended fuels due to almost same physical delay. The same operating condition and a slight difference of biodiesel fraction, so physical property of the blended fuels is also not varied too much in terms of viscosity. The physical delay only depends on fuel viscosity, so physical delay is almost closer to each other. Therefore, the physical delay was estimated independent of the change in fuel properties for small different biodiesel fraction. In T_{inj}=850K case, the chemical delay of all blended fuels was estimated to be 4 deg.CA corresponding to 3.3 ms.

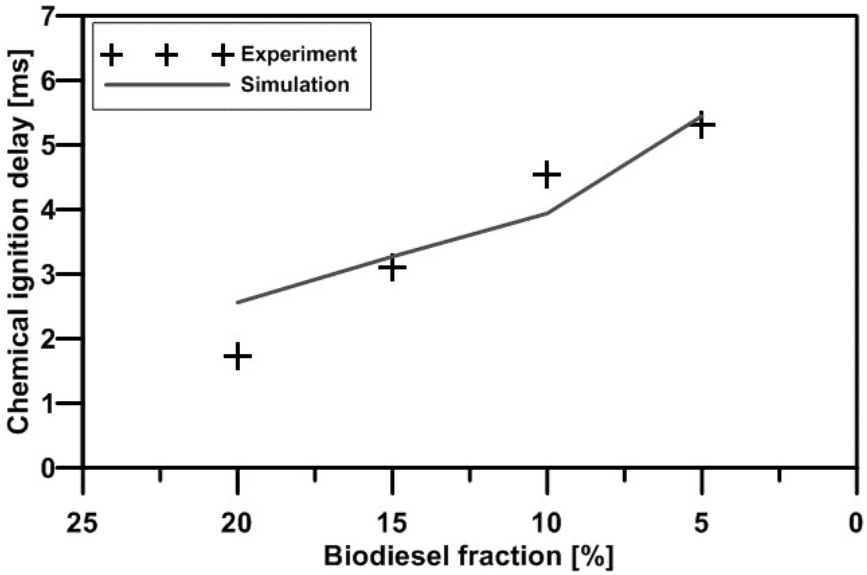

Figure 5.13: Experimental and predicted delay for biodiesel-gasoline blended fuels with an initial temperature of 800 K and mixture equivalence ratio of 1.0 under pressure of 19 bar.

In this case, the adiabatic mixing path takes place in the RCEM which could be shifted to match this temperature value was shown in the Figure 5.12. The equivalence ratio of the mixture is estimated to be 1. The predictive pressures corresponding to cylinder pressures during the ignition delay for the RCEM loads was 19 bar equal to pressure at injection timing. Here, the value is adopted in the kinetic modelling. The mixture temperature at this equivalence ratio is 800 K. The influence of biodiesel fraction on chemical delay can be seen in Figure 5.13.

The chemical delay decreased with increase of biodiesel fraction from 5% to 20% in the both experimental and simulated cases. According to the Figure 5.13, the simulated results of ignition delay were close to the experimental results.

5.9 Summary

In this chapter, an experiment and simulation on the RCEM were used to measure the ignition delay of the four gasoline-biodiesel blended fuels and pure gasoline. Every example fuel was first tested by changing T_{inj}, and the results were compared to each other to investigate the effect of T_{inj} and the biodiesel fraction on auto-ignition. Then, a new reaction mechanism was developed for the gasoline-biodiesel blended fuel model. Subsequently, validation and simulation were implemented by using the CHEMKIN PRO software. Based on the comparisons of pressure trace, heat release rate, and auto-ignition delay for every case, from the experimental and simulated results, conclusions are drawn as follows:

1. At a testing temperature range of 720-850 K, all blended fuels showed both low-temperature reaction and high-temperature reaction. Therefore, the first stage and total ignition delay were observed at both the low-temperature regime and high-temperature regime, respectively.

2. When increasing the ambient temperature at injection timing T_{inj}, the auto-ignition delay was greatly reduced for the four blended fuels.

3. The ignition delay is significantly affected by changing the biodiesel fraction. This change is more effective with a small amount of biodiesel, which promotes a shorter ignition delay and reduces the requirement of intake temperature. So, it improves the low-load and cold-start auto-ignition characteristics of GDCI combustion strategies.

4. From analyzing the pressure trace and HRR curve, the results reveal that changing the biodiesel fraction from 5% to 20% slightly affected the pressure trace and HRR curve for the blend fuels.

5. Comparing the experimental and simulated results, the ignition delay simulated by using the new fuel model is in good agreement with the experiment, which illustrated the accuracy of this study.

6 Effects of the operation parameters on ignition characteristics of GB20 in a constant volume chamber

The GB20 combined from 20 % biodiesel and 80 % gasoline showed the excellent potential for engine fuel application due to utilizing superior lubrication ability, renewables, environmental friendliness, high ignitability from the biodiesel and high volatility from the gasoline. However, there has been no quantitative evaluation of ignition and combustion characteristics for the GB20 spray combustion by the optical investigation, yet. In this work, we performed a comprehensive study focused on the lift-off length and ignition delay of the GB20 in a constant volume chamber under a wide range of experimental conditions simulating engine operating conditions. The GB20 was injected into the combustion chamber under different conditions: gas density (5 kg/m^3 and 15 kg/m^3), ambient temperature (800 K-1200 K), and oxygen content (10 % - 21 %). The single-hole injector with a 0.2 mm diameter is used to inject the fuel sample at various injection pressures (30 MPa - 130 MPa) and injection durations (400 μs – 3500 μs). The ignition delay and lift-off length were determined via broadband chemiluminescence imaging, which was obtained using a high-speed camera. A self-written LabVIEW code was made to separate and smoothen the flame from background noise in the image processing. As a result, the ignition delay and lift-off length heavily depend on the operating conditions. The increase of ambient temperature, ambient gas density, or oxygen concentration significantly decreases the ignition delay and lift-off length. The injection parameters, including the injection pressure and injection duration, also influence the air-fuel mixing process, thus changing the local ambient temperature and local air-fuel ratio, resulting in increasing/decreasing the ignition delay and lift-off length. The ambient temperature is lower than 1000 K for the gas density of 5 kg/m^3 and 900 K for the gas density of 15 kg/m^3 at an oxygen concentration of 10 %, the lift-off length result disappears due to the very few soot particles formation under the deficient oxygen condition.

6.1 Optical arrangement

The emission of light during the combustion process was imaged at high speed to obtain the spray combustion information. The broadband chemiluminescence technique is applied to determine where and when combustion takes place in the combustion chamber. The effectiveness of the method has been presented and demonstrated in many previous studies [31] [32]. Figure 6.1 illustrated the optical arrangement, and Table 6.1 listed the camera settings for

the broadband chemiluminescence method in this work. One 600 nm optical short-pass filter was used to remove the effects of later soot incandescence and any species emitting in the high wavelength range while collecting other radicals (e.g., CH*, C2*).

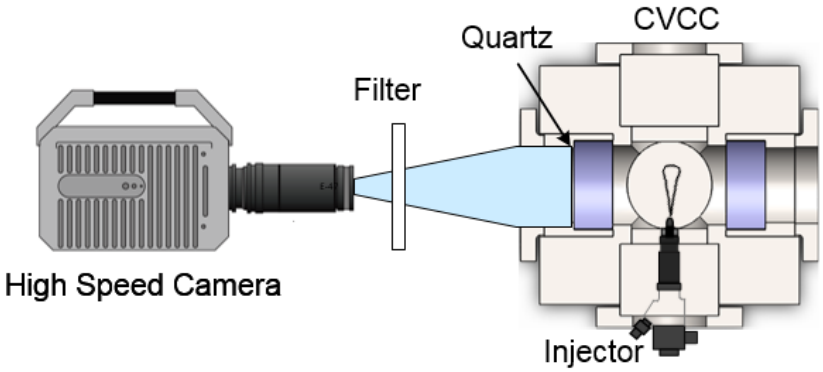

Figure 6.1: Optical arrangement for the broadband chemiluminescence technique.

Table 6.1: Camera specifications.

Camera	Photron SA1.1
Lens	AF Micro-Nikkor 60mm f/2.8D
Frame rate	20000 fps
Optical filter	600 nm Shortpass
Exposure time	50 µs
Resolution	512x256
Scale	0.196 mm/pixel

6.2 Effect of injection pressure and injection duration

As discussed earlier, the broadband chemiluminescence images were utilized to obtain the high-temperature ignition process of fuel samples under diesel engine-like conditions. Figure 6.2 exhibits the flame propagation for the GB20 at an ambient temperature of 900 K, density of 15 kg/m^3, the injection pressure of 50 MPa, and various oxygen concentrations of 21 %, 15 %, and 10 %. The displayed sequence of flames starts at ignition timing for the oxygen concentration of 21 % and ends soon after the ignition for the oxygen concentration of 10 % in chronological order. The same time-based image sequence helps to understand the ignition process and obtain the ignition information effortlessly. In each image, the flame was colored following intensity and bounded in the orange line is to emphasize the high-temperature reactivity zone, while the background is blue color and the injector nozzle situated right side. The difference in oxygen concentration exerts a significant effect on ignition in specific

conditions. In general, the reduction in oxygen concentration remarkably prolongs the ignition delay. The first bright spots appeared at 0.3 ms, 0.5 ms, and 0.9 ms for oxygen concentrations of 21 %, 15 %, and 10 %, respectively. The appearance of the first bright spot points out the ignition timing, and it retarded with a decrease in oxygen concentration. The main reason for this phenomenon is that the lower oxygen concentration provides a lesser amount of oxygen, resulting in reducing collisions between fuel particles and oxygen reactants. Therefore, the reaction rate is decreased and hence lengthens the ignition delay.

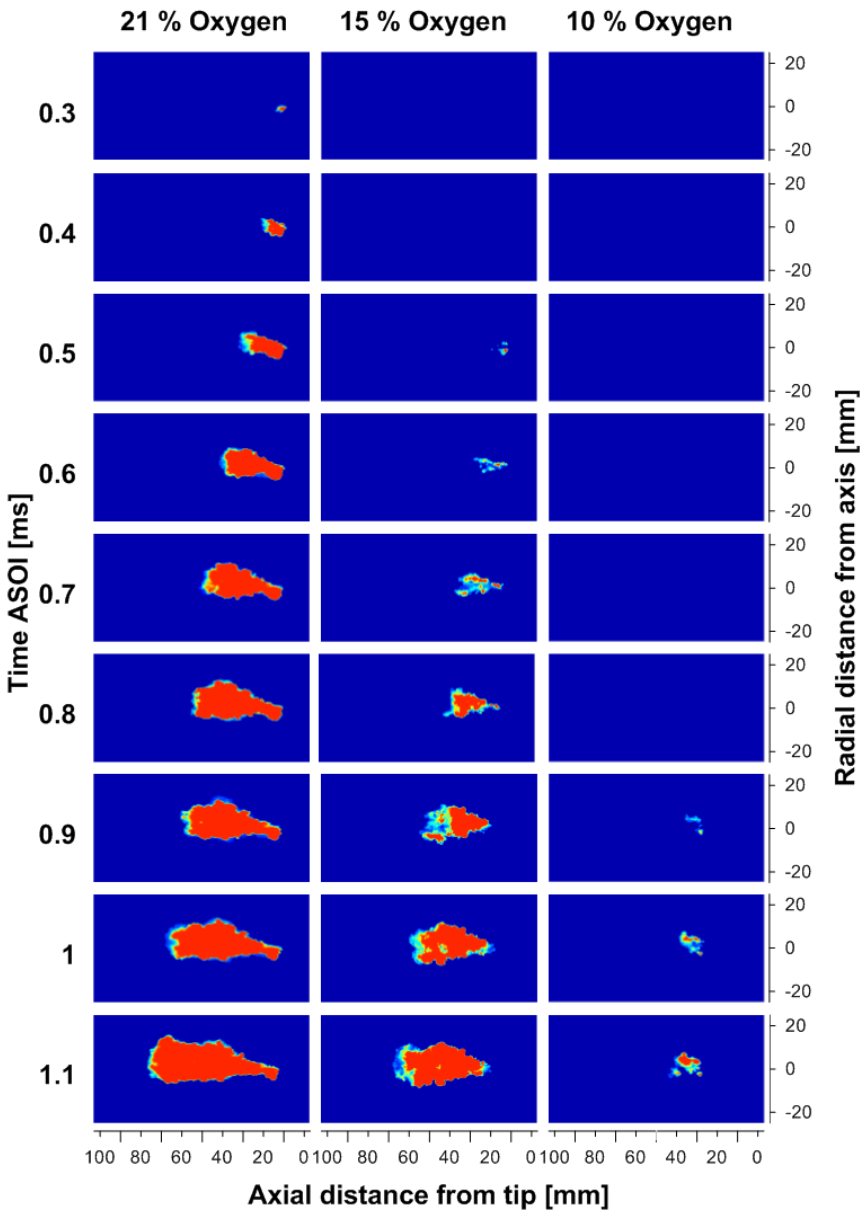

Figure 6. 2: Time sequence of flame images for oxygen concentrations of 21 %, 15 %, and 10 % at the ambient temperature of 1000 K, density of 15 kg/m^3, and injection pressure of

6.2.1 Ignition delay

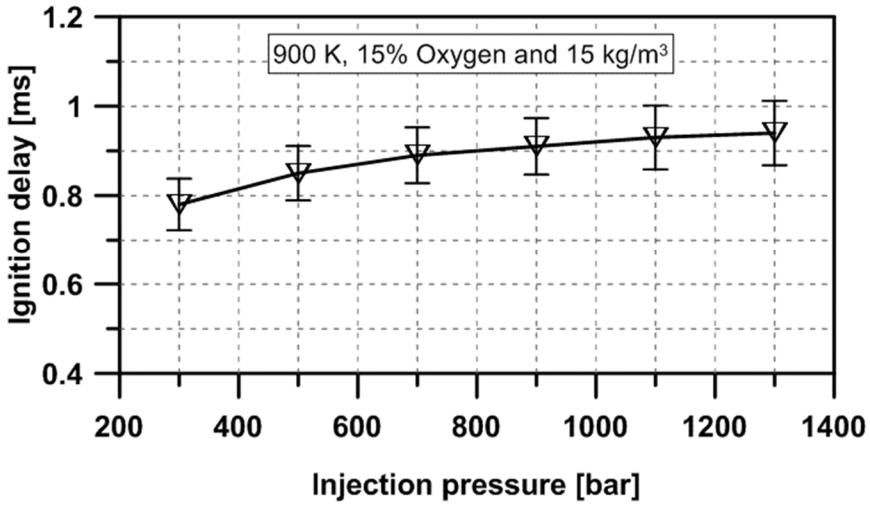

Figure 6.3: Relation between ignition delay and fuel injection pressure for GB20 blend under 900 K, 15 kg/m^3, and 15 % O_2.

Figure 6.3 shows that the higher injection pressure slightly increased the ignition delay for GB20 under the density of 15 kg/m^3, temperature of 900 K and oxygen of 21 %. The higher injection pressure promotes break-up and droplet formation, therefore generating more droplets with a smaller size. Evaporation of fuel is accelerated to become more homogeneous, resulting in the extension of the premixed spray zone and the decline in the air-fuel mixture temperature. The lower local temperature diminishes the rate of conversion of fuel to products of combustion, leading to the lower pre-flame reaction rate. On the other hand, the decrease in the ignition delay with the reduction of injection pressure is that a limitation of the fuel mass is atomized, vaporized, and mixed with air inside the combustion chamber to reach the critical extent of the reaction during the adiabatic mixing process. It makes the air-fuel mixture more quickly to meet the ignition temperature, for which reason the ignition delay is shortened. In the tested condition, the ignition delay for GB20 increases from 0.78 ms to 9.4 ms with the growth of injection pressure from 30 MPa to 130 MPa.

Figure 6.4 shows the relationship between the ignition delay and the injection duration under the ambient gas temperature of 900 K, the density of 15 kg/m^3, and oxygen concentration of 15 %. In this experiment, the injection duration rises from 400 µs to 3500 µs while maintaining the injection pressure at 50 MPa. It is clearly seen from Figure 6.4 that the rise in injection duration increases the ignition delay from 0.67 ms to 0.85 ms. This can be recognized as reasonable due to the longer injection duration produces a massive amount of the

combustible mixture inside the spray zone, cooling the ignition site; hence, combustion chemical reactions are promoted later. However, the ignition delay remains constant when the injection duration is over 1500 μs. The fuel added after this time does not affect the ignition since the start of combustion has already started.

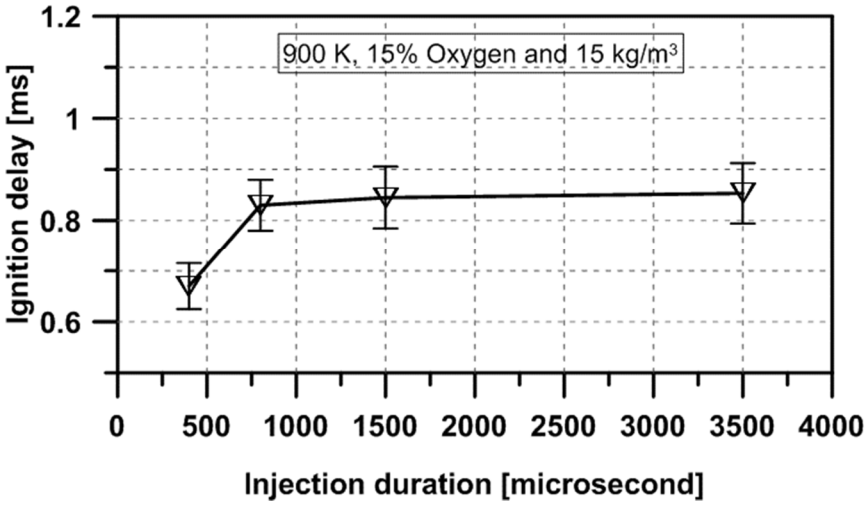

Figure 6.4: Relation between ignition delay and injection duration for GB20 blend under 900 K, 15 kg/m^3, and 15 % O_2.

6.2.2 Lift-off length

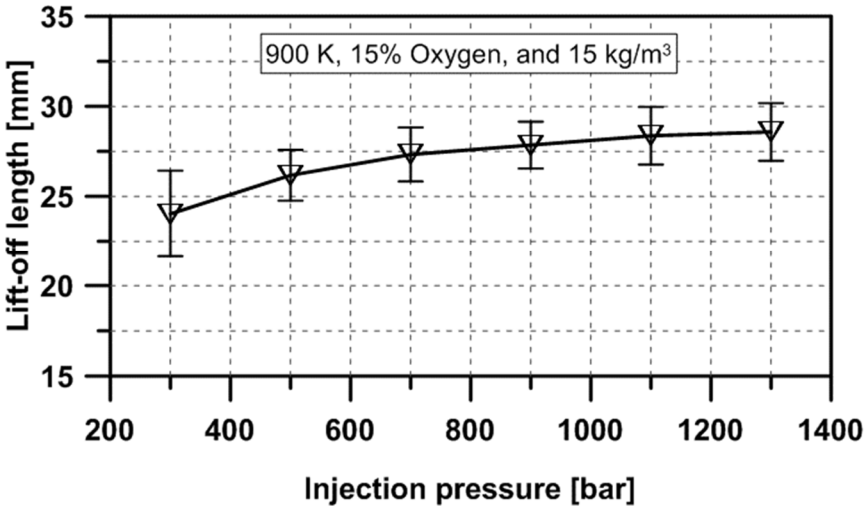

Figure 6.5: Relation between lift-off length and fuel injection pressure for GB20 blend under 900 K, 15 kg/m^3, and 15 % O_2.

The lift-off length is an essential parameter of spray combustion and determined by the broadband chemiluminescence technique. The lift-off length reaches a quasi-steady state

shortly after it appears at a location downstream, which is called the steady lift-off length. Figure 6.5 shows the measurement of the quasi-steady lift-off length at the gas ambient condition as 900 K, 15 kg/m^3, and 15 % O_2 for various injection pressures. Visualization results show that the lift-off length has a strong dependence on injection pressure; the lift-off length is longer from 24.1 mm to 28.6 mm correspondingly with the increase in injection pressure. Because the higher injection pressure generates higher spray velocity at the nozzle exit and momentum of the droplets in the first instants of the injection. The mixture of air and fuel is propagated downstream at higher speed, thus increasing the lift-off length. The results have a generally reasonable agreement with experiment and modeling conclusions, which investigated the effects of injection condition on diesel spray combustion using diesel engines or constant volume vessels [113] [114]. The error bars and lift-off lengths are average values from each data cluster. The error bars representing the standard deviation of the lift-off length are quite low (lower than 10 %), which emphasizes that the stable condition in the CVCC was made to secure high repeatability of the measurements.

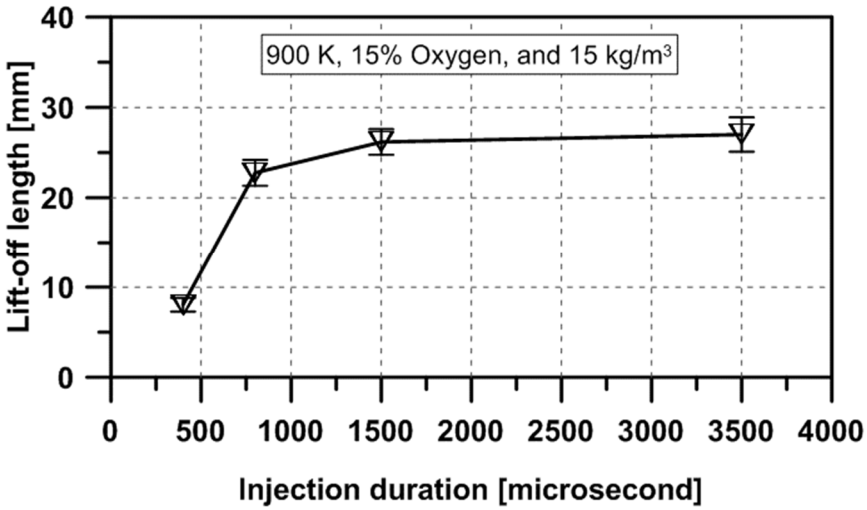

Figure 6.6: Relation between lift-off length and injection duration for GB20 blend under 900 K, 15 kg/m^3, and 15 % O_2

Figure 6.6 gives the lift-off length of the GB20 under the effect of injection duration at an injection pressure of 50 MPa and gas ambient condition of 900 K, 15 kg/m^3, and 15 % O_2. The result shows that lift-off length increases from 8.1 mm to 27 mm with an increase of injection duration. The main reason is that the increase in ignition delay gives more time for combustion flame to travel downstream, which can result in an increasing lift-off length. The remarkable point is that the lift-off length declines abruptly with the decrease of the

injection duration in a range of 400 μs-800 μs. A plausible explanation is a rapid drop in fuel droplet momentum due to the incompletely opening injector. The time for the opening injector is too short, so the nozzle was not opened fully. Fuel packages are not be provided maximum kinetic energy and do not continue to be injected by the injector when the injection has ceased; as a result, the droplet momentums and decay of concentration decrease sharply.

6.3 Effect of the temperature and density

6.3.1 Ignition delay

Two different ambient gas densities as 5 kg/m^3 and 15 kg/m^3 have experimented to explore the effect of ambient gas density on ignition delay under the full temperature range from 800 K to 1200 K and three different oxygen concentrations of 10 %, 15 % and 21 % depicted in Figure 6.7 a, b, and c respectively in this study. As shown in Figure 6.7, the ignition delay of combustion sprays for GB20 has an exponential dependence with ambient temperature and densities and is consistent with the literature and previous studies [113] [114]. The results were also compared with pure diesel to clearly demonstrate the advantages of the fuel blend. The ignition information for pure diesel was gathered from the experiments of Yinjie Ma et al. [31] and plotted on the graphs by the solid black line. All tested conditions, the GB blend has a similar trend with pure diesel but significantly longer ignition delay, and it is the potential for extending and enhancing the mixing process. We found that at lower than 900 K and 10 % oxygen, the combustion produces very low soot emission, so the combustion flame did not appear on the combustion images. It means that the soot formation from the GB blend is less than soot from pure diesel and again demonstrated its ability to reducing soot emissions. The ignition delays for GB20 are longer than that for pure diesel are average approximately 0.22 ms, 0.4 ms, and 0.67 ms under ambient oxygen concentration of 21 %, 15 %, and 10 %, respectively. The higher ambient temperature helps to accelerate the rate of reaction. Hence, the ignition delay of both fuels has a significant decrease with the rise of the heat from 800 K to 1200 K. The gas density is also one of the driving parameters besides the gas temperature and the oxygen concentration to predict the ignition delay. An increase in the gas density increases the collision energy and collision frequency of gas molecules. The higher intensity of molecular collisions leads to the rise of the rate of the chemical reaction. Therefore, the higher density causes a significant decrease in ignition delay in the full experimental temperature range of 800 K-1200 K.

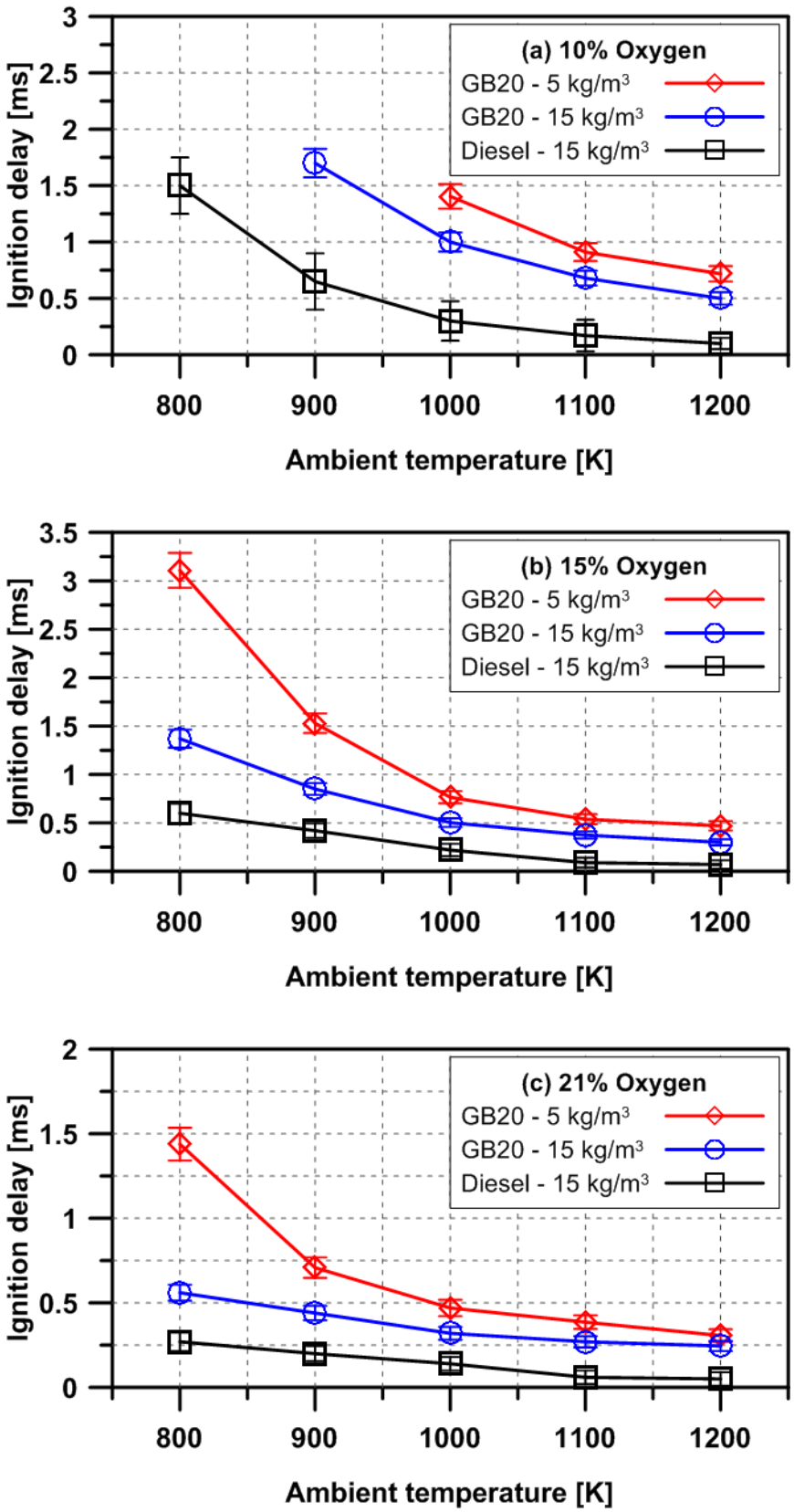

Figure 6.7: Ignition delay of GB20 blend for three different oxygen concentrations under temperature range of 800 K-1200 K in comparison with pure diesel.

6.3.2 Lift-off length

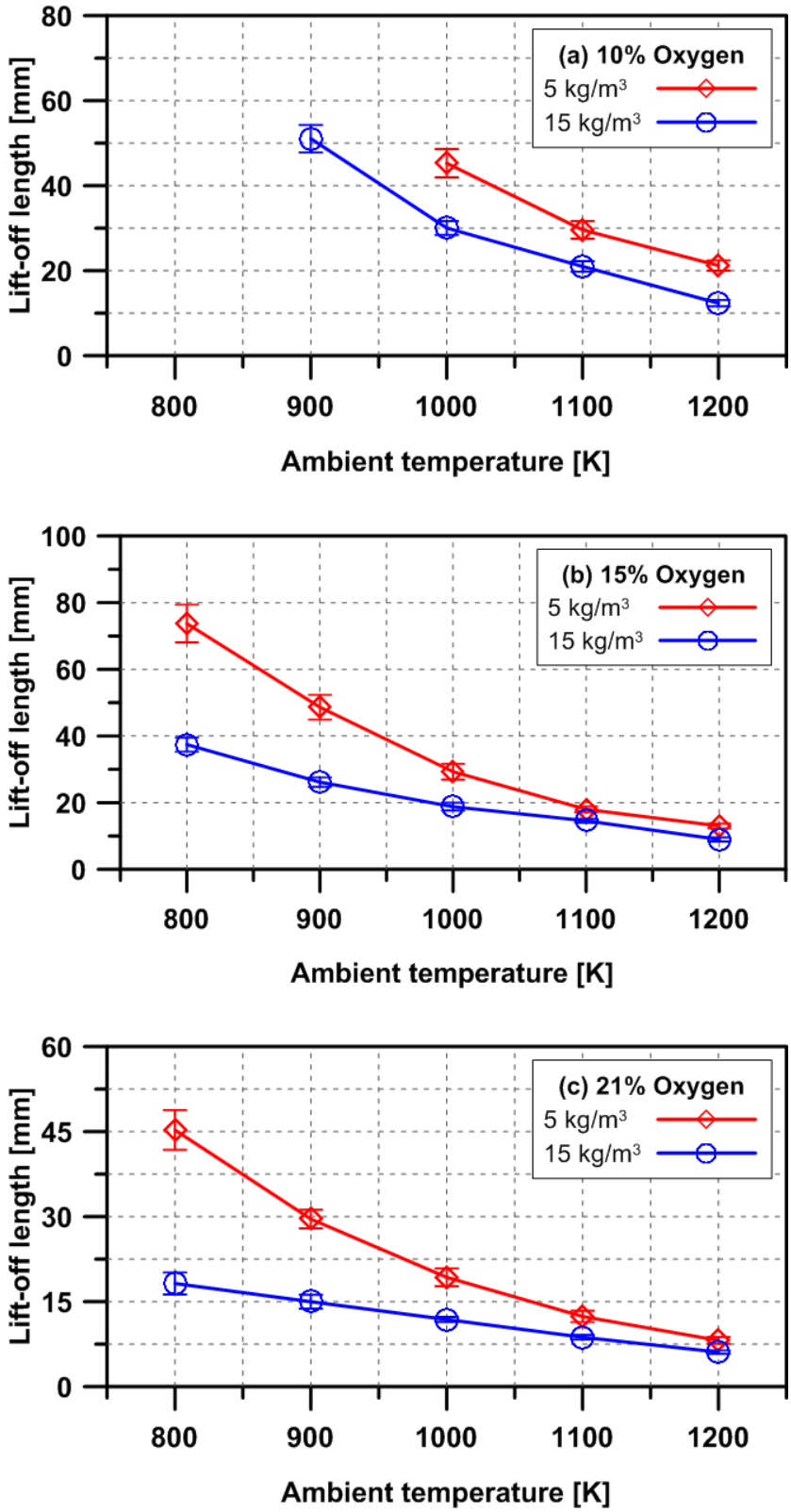

Figure 6.8: Lift-off length of GB20 blend for three different oxygen under temperature range of 800 K-1200 K, injection duration of 1500 µs, and injection pressure of 50 MPa.

Figure 6.8 quantifies the lift-off length for two different ambient gas densities (5 kg/m^3 and 15 kg/m^3) under a wide temperature range (800 K – 1200 K) and three oxygen concentrations of 10 %, 15 % and 21 %. The ambient gas density of 15 kg/m^3 presents a significantly shorter lift-off length than 5 kg/m^3 in the experimental temperature range. This phenomenon is due to the higher ambient density that actively resists the evolution of the spray. So spray development in the direction of the spray axis is slow and causes the shorter lift-off length. Additionally, the decrease in the ignition delay reduces the time of spray flame traveling

6.4 Effect of oxygen content

6.4.1 Ignition delay

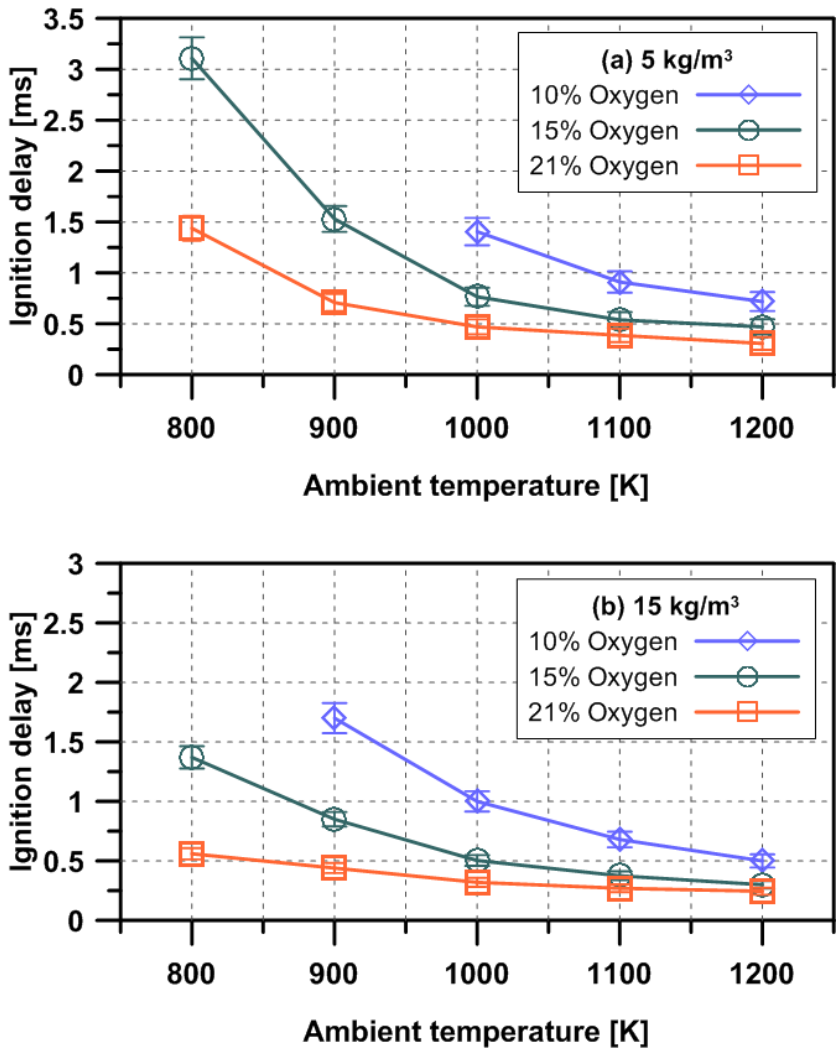

Figure 6.9: Ignition delay of GB20 blend for various oxygen concentrations under two different ambient densities of 5kg/m^3 and 15 kg/m^3, injection pressure of 50 MPa, and injection duration of 1500 µs.

Figure 6.9 shows the ignition delay under a variation of oxygen concentrations from 10 % to 21 %, representing a wide range of EGR. An oxygen concentration of 21 % represents a standard engine condition (without EGR), and an oxygen concentration of 10 % deputizes for a high rate of EGR up to approximately 50 %. Based on these observations, the ignition delay of the GB20 has a strong connection with oxygen content and shows the later ignition timing with the decrease of oxygen content. The leaner situation diminishes the local equivalence ratio inside the spray area and makes the mixture reaching the flammability limit slower.

6.4.2 Lift-off length

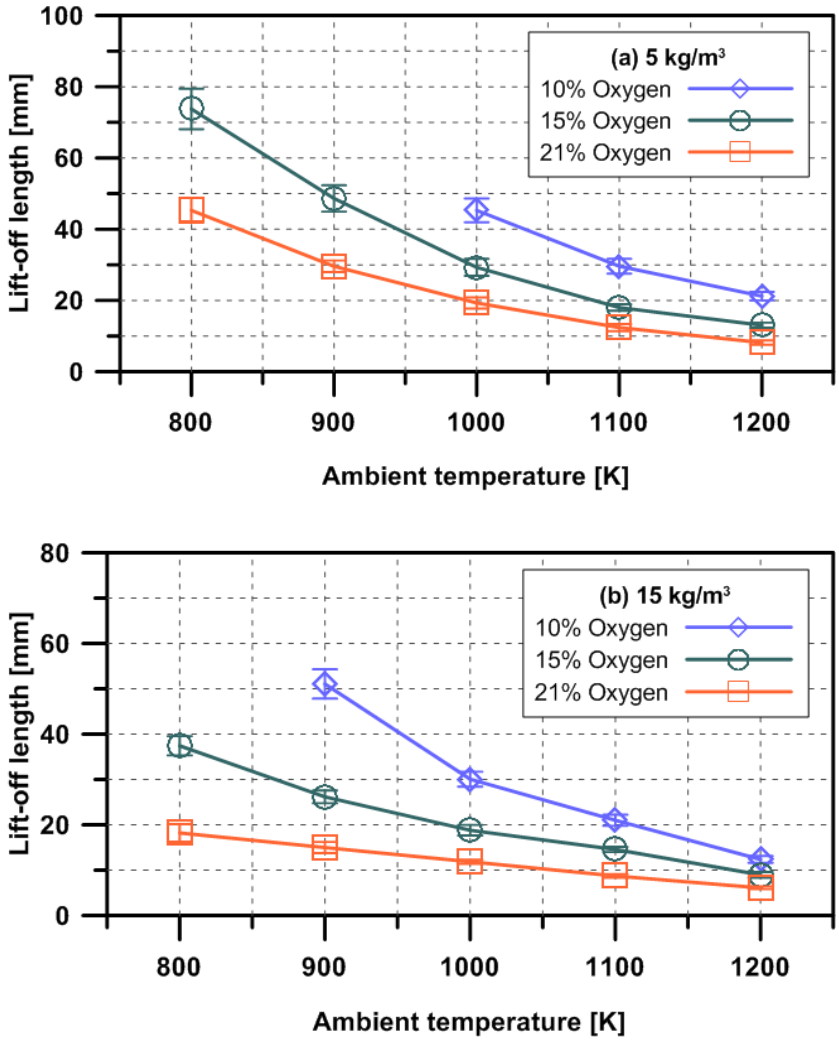

Figure 6.10: Lift-off length of GB20 blend for various oxygen concentrations under two different ambient densities of 5kg/m^3 and 15 kg/m^3, injection pressure of 50 MPa, and injection duration of 1500 µs.

Figure 6.10 shows that the lift-off length for the GB 20 blend presented the same tendency with the ignition delay and reduced significantly with the decrease of oxygen concentration. It is due to the longer ignition delay extends the time of spray flame traveling downstream, leading to an increase in the lift-off length. The remarkable point is that when the ambient temperature is lower than 1000 K for the gas density of 5 kg/m^3 and 900 K for the gas density of 15 kg/m^3 at an oxygen concentration of 10 %, the lift-off length result disappears. A probable reason for this disappearance is that a little number of soot particles can be formed from a deficient oxygen condition. So, there was no visible luminosity from soot emission in the spray area in this case. Therefore, it was difficult to detect anything using the broadband chemiluminescence technique.

6.5 Summary

In this chapter, the CVCC was used to do optical investigation for effects of the operating parameters on ignition delay and lift-off length of the GB20 blend under a wide range of diesel-relevant conditions. Following observations, the main conclusions can be obtained as follows:

1. The ignition delay and lift-off length were measured experimentally for GB20 at various conditions in this study. From experimental observations, both the ignition delay and lift-off length have a significant dependence on the operating condition and injection condition. The results are in reasonable agreement with the literature and previous studies.

2. An increase in injection pressure or injection duration produces a higher amount of the combustible mixture that forms inside the spray zone. It cools down the ignition site, thus decreasing the local temperature during the adiabatic mixing process. Therefore, the ignition delay and lift-off length tend to increase.

3. The ignition delay and lift-off length of combustion sprays have an exponential decrease with ambient temperature and density. It is because the higher ambient temperature helps to accelerate the rate of reaction. The higher gas density also causes an increase in the collision of molecules, thus decreasing ignition delay and lift-off length.

4. The ignition delay and lift-off length of the GB20 are positively related to oxygen content and markedly reduced with the increase of oxygen content. High oxygen concentration helps to speed up the equivalence ratio and makes reaching the flammability limit faster. The decrease in oxygen concentration produced a shorter ignition delay, thus reducing the lift-off length. The remarkable point is that when the ambient temperature is lower than 1000 K for the gas density of 5 kg/m^3 and 900 K for the gas density of 15 kg/m^3 at an oxygen concentration of 10 %, the lift-off length result disappears. A probable reason for this disappearance is the tiny amount of soot particles.

7 Conclusion

This thesis intended to measure the ignition delay, flame lift of length, and combustion characteristics of gasoline biodiesel blended fuels. Almost studies before, the authors used engine as experimental tool to investigate them. However, measurements in engine are somewhat difficult to use for model validations due to the confounding effects of the walls and time-varying boundary conditions. Reliable measurements of ID are especially difficult to acquire in an engine at LTC conditions. At this condition, the ID has a strong influence on combustion-phasing and small differences can swing the engine between knocking and misfires. This high sensitivity prevents making reliable measurements of ID for different speed and load conditions. Also, it is costly and difficult to set up optical measurement in engine. Therefore, ignition delay of gasoline-biodiesel was measured using RCEM and CVCC. The both systems can solve the problems mentioned above. Besides, systems have advantage such as well-controlled (or no) flow interaction, powerful tool for high-load, low-temperature spray combustion measurements and easy to set up optical technique. The ignition delay measurement for the two systems were relatively close for the range of conditions tested. However, the ignition delay for the CVCC was found to be significantly lower compared to the RCEM as showed in Figure 7.1. The probable reasons for the difference, first reason is impingement which cools down the ignition site, thus increasing ignition delay in RCEM. Another reason is existence of NOx due to pre-combustion reducing ignition delay in CVCC. Last reason is higher flow rate of fuel is cooling down injection location, thus also increases ignition delay in RCEM.

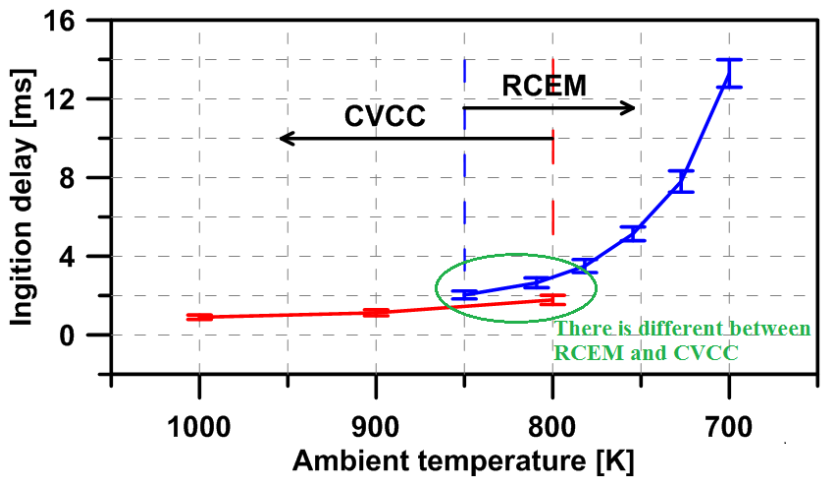

Figure 7.1: Ignition delay of GB20 under different conditions measuring from CVCC and RCEM.

In addition, the gasoline-biodiesel reaction mechanism with 4285 species and 15246 reactions was developed to predict the chemical ignition delay of the blended fuels using the CHEMKIN PRO software. Based on the experimental and simulated results, several main conclusions can be drawn as follows:

- After the gasoline-biodiesel reaction mechanism is successfully created by merging the five-component surrogate represented gasoline fuel and three-component surrogate represented biodiesel fuel. The model was validated to ensure the accuracy of the blended gasoline-biodiesel model. Then ignition calculation is performed using Chemkin Pro software for different biodiesel blended fuels. As simulated results, the biodiesel addition with a high cetane number is useful to advance chemical delay of its blends with gasoline. The influence of biodiesel on the auto-ignition delay becomes more effective when the biodiesel fraction is lower than 20%. At low-temperature range (lower than 850 K), all gasoline biodiesel blended fuels presented both first-stage ignition and second stage ignition due to low-temperature reaction and high-temperature reaction, respectively.

- In this work, two different two different measured technologies were used to determine ignition delay of gasoline biodiesel blended fuels as based-on pressure trace and based-on luminosity. The experimental results showed that the ignition delay presented similar trends for both pressure and luminous approaches. However, the pressure ignition delay is always a little longer than the luminous ignition delay. This difference can increase or decrease depending on the mixing process and the period of ignition delay. These results also agree with the previous researches and elucidated the effect of gasoline-biodiesel blend ratios on ignition delay, lift-off length, combustion phasing, and heat release rate.

- Under low-temperature conditions, the GB blend with a higher biodiesel content reduced the chemical delay, leading to the advanced combustion phasing. The gasoline shows the maximum peak of HRR because of the extension of the mixing process that results in a more substantial mass of air-fuel mixture before the start of combustion. The 750 K case, biodiesel addition significantly advanced the combustion phasing; it confirmed its capacity to help the cold start and prevent the misfiring at low-engine load. However, over 60% biodiesel ratio, the combustion phasing is not different so

much. Almost experiments showed that the ignition delay decreases with an increase in biodiesel content due to the higher cetane number. However, at 900 K the content of biodiesel is more top than 60 %; the ignition delay becomes slightly longer with the increases of biodiesel due to the significant rise in physical delay in total ignition delay.

- The lift-off length increased with an increase in biodiesel fraction under gas temperature conditions as 800 K and 900 K because of very high viscosity and surface tension of biodiesel. Differently, the lift-off length tends to decrease with the rise in biodiesel concentration (less than 60 % biodiesel) at 750 K case. Because the sharp reduction of ignition delay leads to reducing the time for movement of combustion flame at the downstream area, thus decreasing lift-off length.

- Effect of small amount of biodiesel on auto ignition and combustion characteristics was tested in the RCEM at a temperature range of 720-850 K shown that all blended fuels showed both low-temperature reaction and high-temperature reaction. Therefore, the first stage and total ignition delay were observed at both the low-temperature regime and high-temperature regime, respectively. When increasing the ambient temperature at injection timing T_{inj}, the auto-ignition delay was greatly reduced for the four blended fuels. The ignition delay is significantly affected by changing the biodiesel fraction. This change is more effective with a small amount of biodiesel, which promotes a shorter ignition delay and reduces the requirement of intake temperature. So, it improves the low-load and cold-start auto-ignition characteristics of GDCI combustion strategies. Comparing the experimental and simulated results, the ignition delay simulated by using the new fuel model is in good agreement with the experiment, which illustrated the accuracy of this study.

- The GB20 combined from 20 % biodiesel and 80 % gasoline with superior lubrication ability, renewables, environmental friendliness, high ignitability from the biodiesel and high volatility from the gasoline was tested in the CVCC at various conditions. From experimental observations, both the ignition delay and lift-off length have a significant dependence on the operating condition and injection condition. An increase in injection pressure or injection duration produces a higher amount of the combustible mixture that forms inside the spray zone. It cools down the ignition site, thus decreasing the local

temperature during the adiabatic mixing process. Therefore, the ignition delay and lift-off length tend to increase.

- The lift-off length is proportion with ignition delay. The increase in ignition delay increase lift-off length because time for flame travels downstream is longer, thus increasing lift-off length as presented in Figure 7.2.

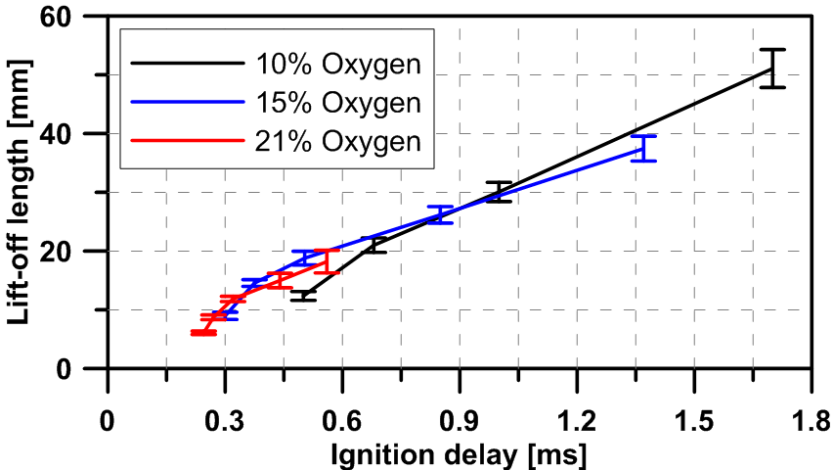

Figure 7.2: Relationship between ignition delay and lift off length of GB20

- The ignition delay and lift-off length of combustion sprays have an exponential decrease with ambient temperature and density. It is because the higher ambient temperature helps to accelerate the rate of reaction. The higher gas density also causes an increase in the collision of molecules, thus decreasing ignition delay and lift-off length. The ignition delay and lift-off length of the GB20 are positively related to oxygen content and markedly reduced with the increase of oxygen content. High oxygen concentration helps to speed up the equivalence ratio and makes reaching the flammability limit faster. The decrease in oxygen concentration produced a shorter ignition delay, thus reducing the lift-off length. The remarkable point is that when the ambient temperature is lower than 1000 K for the gas density of 5 kg/m^3 and 900 K for the gas density of 15 kg/m^3 at an oxygen concentration of 10 %, the lift-off length result disappears. A probable reason for this disappearance is the tiny amount of soot particles.

- This experimental study provides experimental data for the mapping of ignition delay; it is vitally important to control the internal combustion engines for obtaining high performance with gasoline biodiesel blended fuels.

References

[1] Richard Stone and Jeffren K. Ball, Automotive Engineering Fundamentals, Warrendale, USA: SAE Order No, R-199, 2004.

[2] John B. Heywood, Internal combustion engine fundamentals, McGraw-Hill Education: New York, USA, 1988.

[3] Willard W. Pulkrabek, Engineering Fundamentals of the internal combustion engine, Prentice Hall Upper Saddle River, USA: New Jersy 07458, 1997.

[4] Gautam T Kalghatgi, "The outlook for fuels for internal combustion engines," *International Journal of Engine Research,* vol. 15, no. 4, pp. 383-398, 2014.

[5] Charles J. Mueller, André L. Boehman, and Glen C. Martin, "An experimental investigation of the origin of increased NOx emission when fueling a heavy-duty compression ignition engine with soy biodiesel," *SAE international,* vol. 01, no. 1792, p. 28, 2009.

[6] Reed Hanson, Derek A. Splitter, and Rolf Reitz , "Operating a heavy-duty direct-injection compression-ignition engine with gasoline for low emissions," *SAE Technical Paper,* vol. 01, no. 1442, p. 12, 2019.

[7] National Research Council, Technologies and approaches to reducing the fuel consumption of medium-and heavy-duty vehicles, U.S: National Academies Press, 2010.

[8] Leif Hildingsson, Gautam T. Kalghatgi, Nigel Tait, and Bengt Johansson, "Fuel Octane Effects in the Partially Premixed Combustion Regime in Compression Ignition Engines," *SAE Technical Paper,* vol. 01, no. 2648, p. 12, 2009.

[9] L. Pesant, L. Forti, and N. Jeuland, "Effect of Fuel Characteristics on the Performances and Emissions of an Early-injection LTC/Diesel Engine," *SAE Technical Paper,* vol. 01, no. 2408, p. 9, 2008.

[10] Chang-MingGong, KuoHuang, Jing-Long Jia, Yan Su, Qing Gao, and Xun-JunLiu, "Improvement of fuel economy of a direct-injection spark-ignition methanol engine under light loads," *Fuel,* vol. 90, no. 5, pp. 1826-1832, 2011.

[11] Jinhua Wang, Zuohua Huang, Chenglong Tang, and Jianjun Zheng, "Effect of hydrogen addition on early flame growth of lean burn natural gas-air mixtures," *International Journal of Hydrogen Energy,* vol. 35, no. 13, pp. 7246-7252, 2010.

[12] Sage L. Kokjohn, Reed M. Hanson, Derek A. Splitter, and Rolf D. Reitz , "Experiments and Modeling of Dual-Fuel HCCI and PCCI Combustion Using In-Cylinder Fuel Blending," *SAE International Journal of Engines,* vol. 01, no. 2647, p. 51, 2009.

[13] Wei JetThoo, ArmanKevric, Hoon KiatNg, SuyinGan, PaulShayler, and AntoninoLa Roccab, "Characterisation of ignition delay period for a compression ignition engine operating on blended mixtures of diesel and gasoline," *Applied Thermal Engineering,* vol. 66, no. 1-2, pp. 55-64, 2014.

[14] Yu Chao, Wang Jian-xin, Wang Zhi, and Shuai Shi-jin, "Comparative study on gasoline homogeneous charge induced ignition (HCII) by diesel and gasoline/diesel blend fuels (GDBF) combustion," *Fuel,* vol. 106, pp. 470-477, 2013.

[15] Shuaiyng Ma, Zunqing Zheng, Haifeng Liu, Quanchang Zhang, and Mingfa Yao, "Experimental investigation of the effects of diesel injection strategy on gasoline/diesel dual-fuel combustion," *Appllied Energy,* vol. 109, pp. 202-212, 2013.

[16] Dong Hana, Andrew M.Ickes, Stanislav V.Bohac, Zhen Huang, and Dennis N.Assanis, "HC and CO emissions of premixed low-temperature combustion fueled by blends of diesel and gasoline," *Fuel,* vol. 9, pp. 13-19, 2012.

[17] Reed M. Hanson, Sage L. Kokjohn, Derek A. Splitter, and Rolf D. Reitz, "An Experimental Investigation of Fuel Reactivity Controlled PCCI Combustion in a Heavy-Duty Engine," *SAE international journal of engines,* vol. 01, no. 0864, 2010.

[18] Binbin Yang, Mingfa Yao, Wai K.Cheng, Yu Li, Zunqing Zheng, and Shanju Lia, "Experimental and numerical study on different dual-fuel combustion modes fuelled with gasoline and diesel," *Applied Energy,* vol. 113, p. 722–733, 2014.

[19] Scott Curran, Vitaly Prikhodko, Kukwon Cho, C. Scott Sluder, James Parks, Robert Wagner, Sage Kokjohn, and Rolf D. Reitz, "In-cylinder fuel blending of gasoline/diesel for improved efficiency and lowest possible emissions on a multi-cylinder light-duty diesel engine," *SAE Technical Papers,* vol. 01, no. 2206, 2010.

[20] Xiangang Wang, Zuohua Huang, Olawole AbiolaKuti, Wu Zhang, and Keiya Nishida, "An experimental investigation on spray, ignition and combustion characteristics of biodiesels," *Proceedings of the Combustion Institute,* vol. 33, pp. 2071-2077, 2011.

[21] Xiangang Wang, Olawole Abiola Kuti, Wu Zhang, Keiya Nishida, and Zuohua Huang , "Effect of injection pressure on spray flame characteristics and combustion of biodiesel fuel injected by common rail injection system," *Combustion Science and Technology,* vol. 182, no. 10, pp. 1369-1390, 2010.

[22] Cory A.Adams, Paul Loeper, Roger Krieger, Michael J.Andrie, and David E.Foster, "Effects of biodiesel-gasoline blends on gasoline direct-injection compression ignition (GCI) combustion," *Fuel,* vol. 111, p. 784–90, 2013.

[23] Yanuandri Putrasari, and Ocktaeck Lim, "A study on combustion and emission of GCI engines fueled with gasoline-biodiesel blends," *Fuel ,* vol. 189, p. 141–154, 2017.

[24] Yanuandri Putrasari, and Ocktaeck Lim, "A study of a GCI engine fueled with gasoline-biodiesel blends under pilot and main injection strategies," *Fuel,* vol. 221, p. 269–282, 2018.

[25] Decker, The Use of Synthetic JP-8 Fuels in Military Engines, MI: RDECOM-TARDEC, 2008.

[26] Peter Schihl and Laura Hoogterp, On the Ignition and Combustion Variances of Jet Propellant-8 and Diesel Fuel in Military Diesel Engines, MI: RDECOM-TARDEC, 2008.

[27] Pickett, L. M., Siebers, D. L., and Idicheria, C. A, "Relationship between ignition processes and the lift-off length of diesel fuel jets," *SAE Technical Paper,* 2005.

[28] Siebers, D. L., and Higgins, B., "Flame lift-off on direct-injection diesel sprays under quiescent conditions," *SAE Technical Paper,* 2001.

[29] Jeffrey D. Naber and Dennis L. Siebers, "Effects of gas density and vaporization on penetration and dispersion of diesel sprays," *SAE technical paper,* vol. 02, no. 01, 1996.

[30] Maximilian Malin and Vladimir Krivopolianskii, "Soot Investigation on Fish Oil Spray Combustion in a Constant Volume Cell," *SAE technical papers,* vol. 09, no. 06, 2015.

[31] Yinjie Ma, Sheng Huang, Ronghua Huang, Yu Zhang, and Shijie Xu, "Ignition and combustion characteristics of n-pentanol–diesel blends in a constant volume chamber," *Applied Energy,* vol. 185, p. 519–530, 2017.

[32] Sheng Huang, Peng Denga, Ronghua Huang, Zhaowen Wang, Yinjie Ma, and Hui Dai, "Visualization research on spray atomization, evaporation and combustion processes of ethanol–diesel blend under LTC conditions," *Energy Convers Manage,* vol. 106, p. 911–920, 2015.

[33] Gautam T. Kalghatgi, Per Risberg, Hans-Erik Ångström, "Advantages of Fuels with High Resistance to Auto-ignition in Late-injection, Low-temperature, Compression Ignition Combustion," *SAE International,* Vols. 2006-10-16, p. 14, 2006.

[34] John E. Dec, Wontae Hwang, Magnus Sjöberg, "An Investigation of Thermal Stratification in HCCI Engines Using Chemiluminescence Imaging," *SAE International,* Vols. 2006-04-03, p. 20, 2006.

[35] John E. Dec and Wontae Hwang, "Characterizing the Development of Thermal Stratification in an HCCI Engine Using Planar-Imaging Thermometry," *SAE Intenational,* Vols. 2009-01-0650, 2009.

[36] John E. Dec and Yi Yang, "Boosted HCCI for High Power without Engine Knock and with Ultra-Low NOx Emissions - using Conventional Gasoline," *SAE International,* Vols. 2010-01-1086, 2010.

[37] Adams, "Effects of biodiesel–gasoline blends on gasoline direct-injection compression ignition (GCI) combustion," *Fuel,* vol. 111, pp. 784-790, 2013.

[38] Akhilendra Pratap Singh, Nikhil Sharma, Ramesh Agarwal, and Avinash Kumar Agarwal Editors, Advanced Combustion Techniques and Engine Technologies for the Automotive Sector, USA: Department of Mechanical Engineering and Materials Science, 2018.

[39] Harsh Goyal, Sanghoon Kook, Yuji Ikeda, "The influence of fuel ignition quality and first injection proportion on gasoline compression ignition (GCI) combustion in a small-bore engine," *Fuel,* vol. 235, pp. 1207-1215, 2019.

[40] Yingying Lu , Wenbin Yu and Wanhua Su, "Using Multiple Injection Strategies in Diesel PCCI Combustion: Potential to Extend Engine Load, Improve Trade-off of Emissions and Efficiency," *SAE International,* Vols. 2011-01-1396, 2011.

[41] Gautam T. Kalghatgi, "Partially Pre-Mixed Auto-Ignition of Gasoline to Attain Low Smoke and Low NOx at High Load in a Compression Ignition Engine and Comparison with a Diesel Fuel," *SAE International,* Vols. 2007-01-0006, 2007.

[42] Roger F. Cracknell, David J. Rickeard, Javier Ariztegui, Kenneth D. Rose and Martin Muether, "Advanced Combustion for Low Emissions and High Efficiency Part 2: Impact of Fuel Properties on HCCI Combustion," *SAE International,* Vols. 2008-01-2404, 2008.

[43] Aydek Gökçe Erman, Paul Hellier, and Nicos Ladommatos, "The impact of ignition delay and further fuel properties on combustion and emissions in a compression ignition engine," *Fuel,* 2019.

[44] Miao Yang, Zhiwei Wang, Shuman Guo, Xiaofei Xin, Tian Qi, Tingzhou Lei, and Xiaoyu Yan, "Effects of fuel properties on combustion and emissions of a direct injection diesel engine fueled with n-butanol-diesel blends," *Jounnal of rennewable and sustainable energy,* vol. 9, p. 013105 , 2017.

[45] Kukwon Cho, Eric Latimer, Matthew Lorey, and David J. Cleary, "Gasoline Fuels Assessment for Delphi's Second Generation Gasoline DirectInjection Compression Ignition (GDCI) Multi-Cylinder Engine," *SAE International,* vol. 10, no. 4, pp. 1430-1442, 2017.

[46] Youngchul Ra, Paul Loeper, Rolf Reitz and Michael Andrie, "Study of High Speed Gasoline Direct Injection Compression Ignition (GDICI) Engine Operation in the LTC Regime," *SAE Internaltional,* pp. 2011-01-1182, 2011.

[47] Christopher Kolodziej, Janardhan Kodavasal, Stephen Ciatti, Sibendu Som, Neeraj Shidore, and Jeremy Delhom, "Achieving Stable Engine Operation of Gasoline Compression Ignition Using 87 AKI Gasoline Down to Idle," *SAE International,* Vols. 2015-01-0832, 2015.

[48] Changsheng Yao, Fuyuan Yang, Jinli Wang, Haiyan Huang, Minggao Ouyang, "Injection Strategy Study of Compression Ignition Engine Fueled with Naphtha," *SAE International,* Vols. 2015-01-1797, 2015.

[49] Rothamer, D. A., and Murphy, L, "Systematic study of ignition delay for jet fuels and diesel fuel in a heavy-duty diesel engine," *Proceedings of the Combustion Institute,* vol. 34, no. 2, pp. 3021-3029, 2013.

[50] Caton, P. A., Hamilton, L. J., and Cowart, J. S, "Understanding ignition delay effects with pure component fuels in a single-cylinder diesel engine," *Journal of engineering for gas turbines and power,* vol. 133, no. 3, p. 032803, 2011.

[51] Assanis DN, Filipi ZS, Fiveland SB, Syrimis M, "A Predictive Ignition Delay Correlation under Steady State and Transient Operation of a Direct Injection Diesel Engine," in *Fall Technical Conference* , 1999.

[52] Higgins, B., Siebers, D. L., and Aradi, A., "Diesel-spray ignition and premixed-burn behavior," *SAE Technical Paper,* pp. 0148-7191, 2000.

[53] Lahiri D, Mehta P, Poola R, Sekar R, "Utilization of Oxygen-Enriched Air in Diesel Engines: Fundamental Considerations.," in *ASME Paper No. 97-ICE-72*, New York , 1997.

[54] Hardenberg HO, and Hase, FW, "An empirical formula for computing the pressure rise delay of a fuel from its cetane number and from the relevant parameters of direct-injection diesel engines," *SAE International,* vol. 790493, p. 12, 1979.

[55] P. A. Lakshminarayanan, Yogesh V. Aghav, Ignition Delay in a Diesel Engine, Dordrecht: Springer, 2009.

[56] Shubhra Kanti Das, Kihyun Kim, and OcktaeckLim, "Experimental study on non-vaporizing spray characteris-tics of biodiesel-blended gasoline fuel in a constant vol-ume chamber," *Fuel Processing Technology,* vol. 178, pp. 322-335, 2018.

[57] Peter M. Lillo, Lyle M. Pickett, Helena Persson, Oivind Andersson and Sanghoon Kook, "Diesel spray ignitiom detection and spatial/temporal correction," *SAE International,* vol. 5, no. 3, pp. 1330-1346, 2012.

[58] Jesús Benajes, Raúl Payri, Michele Bardi, and Pedro Martí-Aldaraví, "Experimental characterization of diesel ignition and lift-off length using a single-hole ECN injector," *Applied Thermal Engineering,* vol. 58, no. 1-2, pp. 554-563, 2013.

[59] Michele Bardi, Louis Marie C. Malbec, Gilles Bruneaux, Lyle M. Pickett, Julien Manin, Tim Bazyn, and Caroline L. Genzale, "Engine combustion network: comparison of spray development, va-porization, and combustion in different combustion vessels," *Atomization and Sprays,* vol. 22, no. 10, pp. 807-842, 2012.

[60] Casey Fuller, Ponnuthurai Gokulakrishnan, Michael S. Klassen, Barry V. Kiel, and Richard Roby, "Investigation of the Effects of Vitiated Conditions on the Autoignition of JP-8," *5th AIAA/ASME/SAE/ASEE Joint Propulsion Converence & Exhibit,* no. 4925, 2009.

[61] S Kobori, T Kamimoto, and A. A. Aradi, "A study of ignition delay of diesel fuel sprays," *Int J Engine Research,* vol. 1, no. 1, pp. 29-39, 1999.

[62] Varun Ramesh, Daniel Janecek, David A Rothamer, and Jaal B Ghandhi, "Spray ignition measurements in a constant volume combustion vessel under engine-relevant conditions," in *Internal combustion engines*, Knoxville, 2016.

[63] Dung Nguyen and Damon Honnery, "Combustion of bio-oil ethanol blends at elevated pressure," *Fuel,* vol. 87, no. 2, pp. 232-243, 2008.

[64] Jinwoo Lee and Choongsik Bae, "Application of JP-8 in a heavy duty diesel engine," *Fuel,* vol. 90, no. 5, pp. 1762-1770, 2011.

[65] Lyle M. Pickett and Laura Hoogterp, "Fundamental Spray and Combustion Measurements of JP-8 at Diesel Conditions," *SAE International Journal of Commercial Vehicles,* vol. 1, pp. 108-118, 2009.

[66] Pickett, L. M., Siebers, D. L., and Idicheria, C. A, "Relationship between ignition processes and the lift-off length of diesel fuel jets," *SAE technical paper,* 2005.

[67] L.M. Pickett and D.L. Siebers, "Soot in diesel fuel jets: Effects of ambient temperature, ambient density, and injection pressure," *Combust. Flame ,* vol. 138, p. 114, 2004.

[68] Chomiak and A. Karlsson, "Flame lift-off in diesel sprays," *Proc. Combust. Inst,* vol. 26, p. 1996, 1996.

[69] Siebers, D. L., and Higgins, B, "Flame lift-off on direct-injection diesel sprays under quiescent conditions," *SAE Technical Paper,* 2001.

[70] Wenjun Zhong, Tamilselvan Pachiannan, Zhixia He, Tiemin Xuan, and Qian Wang, "Experimental study of ignition, lift-off length and emission characteristics of diesel/hydrogenated catalytic biodiesel blends," *Applied Energy,* vol. 235, no. 1, pp. 641-652, 2019.

[71] Raúl Payria, F.J.Salvador, Julien Manin, and AlbertoViera, "Diesel ignition delay and lift-off length through different methodologies using a multi-hole injector," *Applied Energy,* vol. 162, no. 15, pp. 541-550, 2016.

[72] Brian Higgins and Dennis L. Siebers, "Measurement of the flame lift-off location on DI diesel sprays using OH chemiluminescence," *SAE International,* vol. 03, no. 0918, p. 17, 2001.

[73] Jamil I. Ghojel and Xuan Thien Tran, "Ignition Char-acteristics of Diesel - Water Emulsion Sprays in a Constant-Volume Vessel: Effect of Injection Pressure and Water Content," *Energy&Fuel,* vol. 24, no. 7, pp. 3860-3866, 2010.

[74] Clément Chartier, Ulf Aronsson, Öivind Andersson, Rolf Egnell, and Bengt Johansson, "Influence of jet–jet interactions on the lift-off length in an optical heavy-duty DI diesel engine," *Fuel,* vol. 112, pp. 311-318, 2013.

[75] Chunde Yao, Jiangtao Hu, Peilin Geng, Junjie Shi, Defu Zhang, and Yusheng Ju, "Effects of injection pressure on ignition and combustion characteristics of diesel in a premixed methanol/air mixture atmosphere in a constant volume combustion chamber," *Fuel,* vol. 206, pp. 593-602, 2017.

[76] J Kittler, J Illingworth and J Föglein, "Threshold Selection Based on a Simple image Statistic, computer vision, graphics, and image processing," *Computer Vision, Graphics, and Image Processing,* vol. 30, no. 2, pp. 125-147, 1985.

[77] J.Kittler, and J.Illingworth, "Illingworth, Minimum error thresholding," *Pattern Recognition,* vol. 19, no. 1, pp. 41-47, 1986.

[78] Reitz, R., and Rutland, C, "Development and testing of diesel engine CFD models," *Progress in Energy and Combustion Science,* vol. 21, no. 2, pp. 173-196, 1995.

[79] Ra, Y., and Reitz, R. D, "A combustion model for multi-component fuels using a physical surrogate group chemistry representation," *Combustion and Flame,* vol. 162, no. 10, pp. 3456-3481, 2015.

[80] Jery Chomiak, Anders Karlsson, "Flame liftoff in diesel sprays," *Symposium on Combustion,* vol. 26, no. 2, pp. 2557-2564, 1996.

[81] ExxonMobil, "Energy and envronment," Copyright 2003-2019 Exxon Mobil Corporation, 2012. [Online]. Available: http://www.exxonmobil.co.uk/corporate/files/news_pub_eo2012.pdf. [Accessed accessed 23 J uly 2013].

[82] International Energy Agency, "Technology road-map: biofuels for transport," Technology road-map: biofuels for transport, 2013. [Online]. Available: http://www.iea.org/publica-t i o n s / fr ee pu bl ic at io ns /p ub li ca ti o n /B io f u el s_ R o ad ma p. pd f. [Accessed 2013].

[83] Tim Steinweg, Barbara Kuepper, Matt Piotrowski, "Palm Oil Biofuels Market May See Shake-Up in 2020, Heightening Leakage Risks," *Chain reaction research,* p. 11, 2019.

[84] Wolfgang Vogel, "UFOP Report on Global Market Supply 2017/2018," Chairman of the UFOP Executive Board, Berlin, 2018.

[85] Masjuki Hj.Hassan and Md. Abul Kalam, "An overview of biofuel as a renewable energy source: Development and challenges," *Procedia Engegy,* vol. 56, p. 39–53, 2013.

[86] Jin Suk Lee, "Experiences, Challenging Issues and Future Prospects on Biodiesel Implementation on Biodiesel Implementation in Korea," Bioenergy Research Center, Daejeon, 2007.

[87] Daniel C. Oren, Syed Wahiduzzaman, and Colin R. Ferguson, "A Diesel Combustion Bomb: Proof of Concept," *SAE international,* vol. 10, no. 1, 1984.

[88] Binbin Yang, Shanju Li, Zunqing Zheng, Mingfa Yao, and Wai Cheng, "A comparative study on different dual-fuel combustion modes fuelled with gasoline and diesel," *SAE Technical Papers,* vol. 01, no. 0694, p. 11, 2012.

[89] Yu Shi and Rolf D.Reitz, "Optimization of a heavy-duty compression-ignition engine fueled with diesel and gasoline-like fuels," *Fuel,* vol. 89, no. 11, pp. 3416-3430, 2010.

[90] Dong Han, Yaozong Duan, Chunhai Wang, He Lin, and Zhen Huang, "Experimental study on the two stage injection of diesel and gasoline blends on a common rail injection system," *Fuel,* vol. 159, no. 1, pp. 470-475, 2015.

[91] Dinh Nam Vu, Shubhra Kanti Das, Kyeonghun Jwa, and Ocktaeck Lim, "Characteristics of auto-ignition in gasoline–biodiesel blended fuel under engine-like conditions," *Journal of automobile engineering,* vol. 233, no. 5, pp. 1352-1364, 2018.

[92] Reed Hanson, Scott Curran, Robert Wagner, Sage Kokjohn, Derek Splitter, and Rolf D. Reitz, "Piston bowl optimization for RCCI com-bustion in a light-duty multi-cylinder engine," *SAE International ,* vol. 01, no. 0380, p. 14, 2012.

[93] Justin Yeh, "Biofuel: An Alternative Energy Source," *Fundamentals of Science and Technological Applications,* 2007.

[94] Zhaoyu Luo, Max Plomer, Tianfeng Lua, Sibendu Som, Douglas E.Longman, S.Mani Sarathy, and William J.Pitz, "A reduced mechanism for biodiesel surrogates for compression ignition engine applications," *Fuel,* vol. 99, pp. 143-153, 2012.

[95] Raúl Payria, Juan PabloViera, Yuanjiang Pei, and Sibendu Som, "Experimental and numerical study of lift-off length and ignition delay of a two-component diesel surrogate," *Fuel,* vol. 158, no. 15, pp. 957-967, 2015.

[96] Dennis L. Siebers, and Brian Higgins, "Flame lift-off on direct-injection diesel sprays under quiescent conditions," *SAE International,* vol. 01, no. 0530, p. 24, 2001.

[97] Lyle M. Pickett, Sanghoon Kook, and Timothy C. Williams, "Visualization of diesel spray penetration, cool-flame, ignition, high-temperature combustion, and soot formation using high-speed imaging," *SAE International,* vol. 01, no. 0658, p. 21, 2009.

[98] Karim Kalti and Mohamed Mahjoub , "Image Segmentation by Gaussian Mixture Models and Modified FCM Algorithm," *The International Arab Journal of Information Technology,* vol. 11, no. 1, pp. 11-18, 2014.

[99] BogusławObara, "Identification of transcrystalline microcracks observed in microscope images of a dolo-mite structure using image analysis methods based on linear structuring element processing," *Computers & Geosciences,* vol. 33, no. 2, pp. 151-158, 2007.

[100] Stephen J. Chapman, MATLAB Programming for Engineers, Boston: Nelson Education Ltd, 2018.

[101] Gautam T. Kalghatgi, Per Risberg, and Hans-Erik Ångström, "Partially Pre-mixed Auto-ignition of Gasoline to Attain Low Smoke and Low NOx at High Load in a Compression Ignition Engine and Comparison with a Diesel Fuel," *SAE International,* vol. 01, no. 23, p. 14, 2017.

[102] Mark Sellnau, Wayne Moore, James Sinnamon, Kevin Hoyer, Matthew Foster and Harry Husted, "GDCI multi-cylinder engine for high fuel efficiency and low emissions," *SAE International Journal of Engines,* vol. 8, no. 2, pp. 775-790, 2015.

[103] Gautam Kalghatgi, "Fuel/engine interactions," *SAE International,* vol. 10, no. 08, p. 272 , 2013.

[104] John E. Dec, Yi Yang, and Nicolas Dronniou, "Boosted HCCI – controlling pressure-rise rates for performance improvements using partial fuel stratification with conventional gasoline," *SAE International,* vol. 01, no. 0897, p. 21, 2011.

[105] Rose, "Exploring a gasoline compression ignition (GCI) engine concept," *SAE International,* vol. 01, no. 0911, p. 16, 2013.

[106] Jorge Marchetti and Zhen Fang, Biodiesel: Blends, Properties and Applications, Energy Science, Nova: Nova Science Publishers, 2011.

[107] Zaman Sajid, Faisal Khan, and Yan Zhang, "Process simulation and life cycle analysis of biodiesel production," *Renewable Energy,* vol. 85, pp. 945-952, 2016.

[108] Sakda Thongchai and Ocktaeck Lim, "The effects of gasoline-biodiesel blends fuels on spray characteristics," *Transactions of the Korean hydrogen and new energy society,* vol. 26, no. 3, pp. 287-293, 2015.

[109] Taku TSUJIMURA, Keita MITSUSHIMA, Ryuichi HATA, Yoshiroh TOKUNAGA, Jiro SENDA, and Hajime FUJIMOTO, "Study on characteristics of auto-ignition and combustion in hydrogen jet with a rapid compression and expansion," *Journal of Environment and Engineering,* vol. 4, no. 2, pp. 395-408, 2009.

[110] San Diego, Reaction Workbench 15141, San Diego, USA: ANSYS Reaction Design, 2016.

[111] Errico, "Simplified and Detailed Chemistry Modeling of Constant-volume Diesel Combustion Experiments," *SAE International,* vol. 01, no. 0954, p. 14, 2008.

[112] Sanghoon Kook, Choongsik Bae, Paul C. Miles, Dae Choi, and Lyle M. Pickett, "The Influence of Charge Dilution and Injection Timing on Low-Temperature Diesel Combustion and Emissions," *SAE Intenational,* vol. 01, no. 3837, p. 23, 2005.

[113] Xiangang Wang, Zuohua Huang, Wu Zhang, Olawole Abiola Kuti, and Keiya Nishida, "Effects of ultra-high injection pressure and micro-hole nozzle on flame structure and soot formation of impinging diesel spray," *Applied Energy,* vol. 88, no. 5, pp. 1620-1628, 2011.

[114] Xiangang Wang, Zuohua Huang, Olawole Abiol, Kutib WuZhang, and Keiya Nishida, "Experimental and analytical study on biodiesel and diesel spray characteristics under ultra-high injection pressure," *International Journal of Heat and Fluid Flow,* vol. 31, no. 4, pp. 659-666, 2010.

Appendices

A. List of Publications

1. **Dinh Nam Vu,** Shubhra Kanti Das, Kyeonghun Jwa and Ocktaeck Lim, "Characteristics of auto-ignition in gasoline–biodiesel blended fuel under engine-like conditions", *Institution of Mechanical engineers*, Volume 233, pp 1-13, 2018.

2. **Dinh Nam Vu,** Ocktaeck Lim, "Experimental study on ignition characteristic of gasoline-biodiesel blended fuel in a constant-volume chamber", *Journal of Mechanical Science and Technology*, Volume 33, pp 5073–5083, 2019.

3. **Dinh Nam Vu,** Ocktaeck Lim, "Ignition and combustion characteristics of gasoline-biodiesel blend in a constant volume chamber: Effects of the operation parameters", *Fuel*, Elsevier, Volume 225, pp. 129-138, 2019.

4. **Dinh Nam Vu,** Myung Taeck Lim and Ocktaeck Lim, "Study on Auto-Ignition Characteristics of Gasoline-Biodiesel Blend Fuel in a Rapid Compression Expansion Machine", 8th International Conference on Applied Energy (ICAE2016), 8-1 October 2016, Beijin, China, *Energy Procedia*, Volume 105, pp 1789-1795, 2017.

5. **Dinh Nam Vu,** Ocktaeck Lim, "soot and ignition investigation on gasoline–biodiesel blended fuel in a constant-volume chamber", 10th International Conference on Applied Energy (ICAE2019), 12-15 August 2019, Västerås, Sweden will be published in Energy Procedia, 2019.

6. Kihyun Kim, **Dinh Nam Vu**, Shubhra Kanti Das, Jaeheun Kim, Ocktaeck Lim, "investigation on the spray development process of gasoline-biodiesel blended fuel sprays in a constant volume chamber", 10th International Conference on Applied Energy (ICAE2019), 12-15 August 2019, Västerås, Sweden will be published in Energy Procedia, 2019.

7. **Dinh Nam Vu,** Ocktaeck Lim, "Piston motion control for a dual free piston linear generator: predictive-fuzzy logic control approach," *Institution of Mechanical engineers*, Under review (Status date 2019-10-06).

B. List of conferences

International conferences

1. **Dinh Nam Vu** and Ocktaeck Lim, 2016 International conference on Advanced Automotive Technology (ICAT), Gwangiu, Korea, 2016.
2. **Dinh Nam Vu** and Ocktaeck Lim, International Conference of Applied Energy (ICAE) 2016, Beijing, China, 2016.
3. **Dinh Nam Vu** and Octaeck Lim, 21st International Conference of Mechatronics Technology (ICMT), Ho Chi Minh, Viet Nam, 2017.
4. **Dinh Nam Vu** and Ocktaeck Lim, International conference on material, machines and methods for sustainable development (MMMS), Da Nang, Viet Nam, 2018.
5. **Dinh Nam Vu** and Ocktaeck Lim, International Conference of Applied Energy (ICAE) 2019Västerås, Sweden, 2019.

Domestic conferences

1. **Dinh Nam Vu** and Ocktaeck Lim, KSAE 2015 Annual Conference and Exhibition, Hwabaek International Convention Center, Gyeongju, Korea, 2015.
2. **Dinh Nam Vu** and Ocktaeck Lim, 2018 KSAE Annual Spring Conference, Bexco, Busan, Korea, 2018.
3. **Dinh Nam Vu** and Ocktaeck Lim, 2019 KSAE Annual Spring Conference, Ramada hotel, Jeju, Korea, 2019.
4. **Dinh Nam Vu** and Ocktaeck Lim, KSAE 2019 Annual Autumn Conference & Exhibition, Hwabaek International Convention Center, Gyeongju, Korea, 2019.

C. Image processing code

```
clear all; close all;
videodata='21%5kg_C001H001S0014';
video=strcat(videodata,'.avi');
vidObj = VideoReader(strcat(video));
foregroundDetector = vision.ForegroundDetector('NumTrainingFrames', 10, 'LearningRate',
0.0002);
point1=true;
Tonglift=0;
vj=0;
soanh=vidObj.duration*10;
pixel=vidObj.height;
chenh=soanh-100;
vc=12;
for k=1:vc
   inputImageOrig = read(vidObj, k+chenh);
   graypic= rgb2gray(inputImageOrig);
   colmap = jet(14);
   graypic_dl=graypic;
   levels = linspace(0,255,15);
   for i=1:pixel
      for j=1:512
         r=((j-256)^2+(i-pixel/2)^2)^0.5;
         if r>240
            graypic(i,j)=0;
            graypic_dl(i,j)=0;
         end
      end
   end
Flamekt = size(graypic);
 [ a, b ]= kittlerMinimimErrorThresholding(graypic);
   for i=1:pixel
      for j=1:512
         if graypic(i,j)<a|j<35
            graypic(i,j)=0;
            Flamekt(i,j)=0;
         else
            Flamekt(i,j)=1;
         end
      end
```

```
 end
  foreground = step(foregroundDetector, graypic);
 se1 = strel('disk',2);
 se2 = strel('disk',3);
 FImage= imclose(imopen(foreground,se1),se2);
 FImage = imfill(FImage, 'holes');
for i=1:pixel
    for j=1:512
        if FImage(i,j)==0
            graypic(i,j)=13;
        end
   end
end
 dl=levels(8);
 for i=1:pixel
    for j=1:512
        if graypic_dl(i,j)<dl
            graypic_dl(i,j)=0;
        end
   end
 end
 foreground_dl = step(foregroundDetector, graypic_dl);
 se1 = strel('disk',2);
 se2 = strel('disk',3);
 FImage_dl= imclose(imopen(foreground_dl,se1),se2);
 FImage_dl = imfill(FImage_dl, 'holes');
for i=1:pixel
    for j=1:512
        if FImage_dl(i,j)==0
            graypic_dl(i,j)=0;
        end
   end
end
meanIntensityValue_dl = mean2(graypic_dl);
firstpoint=true;
if (meanIntensityValue_dl>0.1)
   tdl=k/10*pixel/256;
    for n=1:512
        l=513-n;
        for m=1:pixel
            if (graypic(m,l)>100)&&(firstpoint==true)
```

```
            A(k,3)=n;
            firstpoint=false;
            if (vj<10)
               vj=vj+1;
               Tonglift=Tonglift+n;
            end
         end
         if (graypic(m,l)>100)&&(point1==true)
            point1=false;
            C = {'Ignition delay (ms)';'Igntion distance (mm)';'Lift-off lenght (mm)'};
            B = {tdl;n};
         end

      end
   end
else
   A(k,3)=0;
end
 meanIntensityValue = mean2(graypic);
 A(k,1)=k*1/10*pixel/256;
 A(k,2)=meanIntensityValue;
 graypicsoot=graypic;
 foreground = step(foregroundDetector, graypicsoot);
 se1 = strel('disk',2);
 se2 = strel('disk',3);
 FImagesoot= imclose(imopen(foreground,se1),se2);
 FImagesoot = imfill(FImagesoot, 'holes');
 FImagesoot = bwlabel(FImagesoot,8);
 origin = [33 115];
 xOrigin        = origin(1) ;
 yOrigin        = origin(2);
 Center         = origin(2);
 liqCoreMask    = 1;
 dimIm = size(FImagesoot);
 t2=0.4;
 xpolym = [xOrigin-10 yOrigin/t2 dimIm(2) dimIm(2) (dimIm(1)-yOrigin)/t2];
 ypolym = [yOrigin 0 0 dimIm(1) dimIm(1)];
 mask = roipoly(dimIm(1),dimIm(2),xpolym,ypolym);
 [x,y] = Boundary(FImagesoot, ...
    yOrigin, Center, liqCoreMask, xOrigin, ...
    mask);
```

```
        bwimgsoot = false(dimIm);
        for j = 1:size(x)
           bwimgsoot(y(j),x(j)) = 1;
        end
        b=size(bwimgsoot);
         bb=b(1,1);
         bbb=b(1,2);
         for g = 1:bb
           for f=1:bbb
              if bwimgsoot(g,f)==1
                 bwimgsoot(g-1,f-1)=1;
                 bwimgsoot(g,f-1)=1;

              end
           end
         end
    graypic=graypic/1.15;
    for i=1:pixel
        for j=1:512
           if bwimgsoot(i,j)==1
              graypic(i,j)=255;
           end
        end
    end
        colmap = jet(255);
        imshow(graypic,colmap);
           colbar=colorbar('Ticks',[1,250],...
           'TickLabels',{'Min','Max'});
        colbar.Label.String = 'Intensity';
end
tong=0;
for tp=1:vc
    tong=tong+A(tp,2)*0.1*pixel/256;
end
density=0;
soot=0;
for tp=1:vc
    if (A(tp,3)>45)&&(soot<25)
        soot=soot+1;
        density=density+A(tp,2)*0.1*pixel/256;
    end
```

```
end
function [ optimalThreshold, J ] = kittlerMinimimErrorThresholding( img )
J = Inf * ones(255, 1);
histogram = double(histc(img(:), 0:255)) / size(img(:), 1);
for T = 1:255
    histogram1 = histogram(1:T);
    histogram2 = histogram((T+1):end);
    P1 = sum(histogram1);
    P2 = sum(histogram2);
    if (P1 > 0) && (P2 > 0)
        mean1 = sum(histogram1 .* (1:T)') / P1;
        mean2 = sum(histogram2 .* (1:(256-T))') / P2;
        sigma1 = sqrt(sum(histogram1 .* (((1:T)' - mean1) .^2) ) / P1);
        sigma2 = sqrt(sum(histogram2 .* (((1:(256-T))' - mean2) .^2) ) / P2);
        if (sigma1 > 0) && (sigma2 > 0)
            J(T) = 1 + 2 * (P1 * log(sigma1) + P2 * log(sigma2)) ...
                - 2 * (P1 * log(P1) + P2 * log(P2));
        end
    end
end
[~, optimalThreshold] = min(J);
optimalThreshold = optimalThreshold - 0.5;

end
function [b]=jetBoundary(Yb)
    boundaries = bwboundaries(Yb);
    lenb=[];
    for k=1:length(boundaries)
      lenb(k) = length(boundaries{k});
    end
    [d,nmax] = max(lenb);
    if ~isempty(nmax)
        b = boundaries{nmax};
    else
        b=[1 1; 1 1;];
    end
clear all;
[RGB,map_RGB]  = imread('4.png');
graypic_pic= rgb2gray(RGB);
colmap = jet(255);
Flame = size(graypic_pic);
```

```
 [ a, b ]= kittlerMinimimErrorThresholding(graypic_pic);
   for i=1:256
      for j=1:512
         if graypic_pic(i,j)<a|j<35
            graypic_pic(i,j)=0;
            Flame(i,j)=0;
         else
            Flame(i,j)=1;
         end
     end
   end
imshow(Flame);

function [ optimalThreshold, J ] = kittlerMinimimErrorThresholding( img )
J = Inf * ones(255, 1);
histogram = double(histc(img(:), 0:255)) / size(img(:), 1);
for T = 1:255
   histogram1 = histogram(1:T);
   histogram2 = histogram((T+1):end);
   P1 = sum(histogram1);
   P2 = sum(histogram2);
   if (P1 > 0) && (P2 > 0)
      mean1 = sum(histogram1 .* (1:T)') / P1;
      mean2 = sum(histogram2 .* (1:(256-T))') / P2;
      sigma1 = sqrt(sum(histogram1 .* (((1:T)' - mean1) .^2) ) / P1);
      sigma2 = sqrt(sum(histogram2 .* (((1:(256-T))' - mean2) .^2) ) / P2);
      if (sigma1 > 0) && (sigma2 > 0)
         J(T) = 1 + 2 * (P1 * log(sigma1) + P2 * log(sigma2)) ...
               - 2 * (P1 * log(P1) + P2 * log(P2));
      end
   end
end
 [~, optimalThreshold] = min(J);
optimalThreshold = optimalThreshold - 0.5;
end
```